FABRICATION OF METALLIC TEXTILES ASSISTED WITH POLYMER BRUSHES

YAN KA CHI

M.Phil

The Hong Kong Polytechnic University

2016

The Hong Kong Polytechnic University
Institute of Textiles and Clothing

Fabrication of Metallic Textiles Assisted with Polymer Brushes

Yan Ka Chi

A Thesis Submitted in Partial Fulfillment of the
Requirements for the Degree of Master of Philosophy

July 2015

CERTIFICATE OF ORIGINALITY

I hereby declare that this thesis is my own work and that, to the best of my knowledge and belief, it reproduces no material previously published or written, nor material that has been accepted for the award of any other degree or diploma, except where due acknowledgement has been made in the text.

______________________________ (Signed)

Yan Ka Chi (Name of Student)

To my parents
for their unconditional love, patience and encouragement

To my best friends Pete, Billy and Kam
for always keeping me company

ABSTARCT

Recent advance in wearable electronics results in high demand for high-performance flexible conductors as interconnects, contacts and electrodes. In particular, metal-coated textiles are very suitable for fulfilling these purposes, thanks to the intrinsic flexibility of textiles as well as high conductivity imparted by the surface-deposited metals. However, the metal adhesion and also the washing durability of these metal-coated textiles remain major challenges. Besides, there are still no practical strategies to fabricate high-performance, durable and washable metallic textiles in bulk. Concerning these challenges, in this research, we study the synthesis of highly durable, washable and solution-processable copper-coated textiles. By simply modifying the textile surface with a layer of poly[2-(methacryloyloxy)ethyl]trimethylammonium chloride (PMETAC) brush via a first free radical polymerization, immobilization of catalyst and subsequent electroless copper deposition (ELD) are then carried out to yield a homogeneous and compact copper layer on the textile surface. Here, PMETAC acts as an interfacial layer in-between textiles and the as-deposited copper, therefore providing as-deposited copper with outstanding adhesion to withstand repeated bending and washing cycles. As-synthesized copper-coated cotton fabric has a very promising conductivity, with sheet resistance exhibited from 10^3 to 10^{-1} ohm/sq, depending on the ELD conditions. As-synthesized Cu-cotton yarns also exhibited a very good conductivity with linear resistance measured as ~1.4 ohm/cm, with significant improvements on the yarn tensile properties due to the reinforcement by the as-deposited copper layer. The whole process is highly compatible with the current textile finishing technologies such as pad-dry-cure and hank dyeing. To reduce the fabrication cost imposed by the expensive catalyst used in ELD, an alternative approach to preparing high-performance and durable metallic textile is also proposed by grafting other polymer brushes instead of PMETAC, such as poly(methacrylic acid sodium salt) (PMANa) or poly(acrylic acid sodium salt) (PAANa) via a first free radical polymerization on the cotton fiber surface. Around 30 % cost reduction is estimated when comparing the fabrication method assisted with PMETAC to that with PMANa.

To confirm successful modification on the textile surface, chemistries involved in all polymer brush graftings are confirmed by repeated experiments on silicon wafers, which are then studied by attenuated total reflectance-Fourier transform infrared spectroscopy (ATR-FTIR), X-ray photoelectron spectroscopy (XPS) and water contact angle measurement. Surface morphologies and chemical composition of the as-synthesized copper-coated cotton are characterized by scanning electron microscopy (SEM) and energy dispersive X-ray spectroscopy (EDS), respectively. Finally, potential applications of the copper-coated cotton textiles in electronics are demonstrated by connecting the copper-coated textiles with light-emitting diodes (LEDs) as well as acting as electrodes in the woven-based textile triboelectric generators.

LIST OF PUBLICATIONS

Journal:

1. Casey Yan, Zijian Zheng, ‘The Development of Pad-Dry-Cure Compatible Method for Preparing Electrically Conductive Copper Coated Cotton Woven Fabrics’, *Journal of Fiber Bioengineering and Informatics* **2013**, *6*, 117.

2. You Yu, Casey Yan, Zijian Zheng, ‘Polymer-Assisted Metal Deposition (PAMD): A Full-Solution Strategy for Flexible, Stretchable, Compressible, and Wearable Metal Conductors’, *Advanced Materials* **2014**, *26*, 5508.

3. Xiaolong Wang[†], Casey Yan[†], Hong Hu, Xuechang Zhou, Ruisheng Guo, Xuqing Liu, Zhuang Xie, Zijian Zheng, *Chemistry – An Asian Journal* **2014**, *9*, 2170. († equal contribution)

4. You Yu, Yaokang Zhang, Kan Li, Casey Yan, Zijian Zheng, ‘Bio-Inspired Chemical Fabrication of Stretchable Transparent Electrodes’ *Small* **2015**, DOI: 10.1002/smll.201500529.

5. Libin Liu, You Yu, Casey Yan, Kan Li, Zijian Zheng, ‘Wearable Energy-Dense and Power-Dense Supercapacitor Yarns Enabled by Scalable Graphene-Metallic Textile Composite Electrodes’ *Nature Communications* **2015**, 6, 7260.

Patent:

1. Zijian Zheng, Casey Yan, Lee Cheung Lau, ‘An Electrically Conductive Textile Element and Methods of Producing Same’ HK Patent, Application Number: 15102150.5

Award:

1. Zijian Zheng, Lee Cheung Lau, Casey Yan, ‘Durable, Washable and High-Performance Conductive Textiles’, Silver Award in the 43rd International Exhibition of Inventions of Geneva, **2015**

Magazine Article:

1. Casey Yan, Zijian Zheng, ‘Durable and Washable Conductive Textiles’ in TECHNICAL TEXTILES **2015**

Conference Presentation:

1. Casey Yan, ‘Polymer-assisted Metal Deposition (PAMD) on Textiles for Future Wearable and Washable Textile Electronics’, Textile Summit **2014**, University of Leeds, United Kingdom

Conference Paper:

1. Casey Yan, Zijian Zheng, ‘Fabrication of Highly Durable, Washable and Scalable Conductive Textiles by Polymer-Assisted Metal Deposition’, Textile Bioengineering and Informatics Symposium Proceedings **2014**, 1.

Conference Poster:

1. Casey Yan, Zijian Zheng, Croucher Advanced Study Institute on Printed Electronics **2013** P14: Polymer-Assisted Copper-coated Cotton Fabric for Future Wearable and Washable Textile Electronics

ACKNOWLEDGEMENTS

First and foremost, I would like to express my greatest gratitude to my chief supervisor Prof. Zheng Zijian, Associate Professor at the Institute of Textiles and Clothing, The Hong Kong Polytechnic University, for giving me a chance to explore this exciting field of materials science as well as the opportunity to join his research group. During these years I have acquired broader materials science knowledge under his guidance and enriched with research experience. I would like to further thank him for his inexhaustible patience and constant support throughout my study. Next, I would like to thank Dr. Zhou Xuechang, Dr. Liu Xuqing, Dr. Yu You, Dr. Guo Ruisheng and Dr. Liu Libin for the fruitful discussion and insightful suggestions on my research. Their expertise has constantly motivated me to achieve better. My gratefulness also extends to my colleagues in Prof. Zheng’s group, including Dr. Xie Zhuang, Mr. Niu Liyong, Miss Huang Qiyao, Miss Chen Lina, Miss Ng Sze Wing Miya, Mr. Zhang Yaokang, Dr. Li Kan, Dr. Zhen Hongyu, Mr. Xiao Xiang, Dr. Wei Xiaoling, Dr. Zhou Ruitao, Mr. Chen Chaojian, Dr. Ma Xinlei, Dr. Liu Zhilu and Miss Yip Hoi Shan Kate. I would also like to acknowledge Prof. Hu Youfan and her students Mr. Zhao Zhizhen and Mr. Zhang Han at the Peking University for the valuable discussion on the fabrication of triboelectric generators.

In addition, I would like to acknowledge all the scientific officers and technicians in the Institute of Textiles and Clothing. Without their daily maintenance of the instruments, none of the works can be done. My thanks also extend to Dr. Hardy Lui at the Department of Applied Physics, The Hong Kong Polytechnic University, who has offered a lot of help in the material characterizations. I would also like to thank Miss Wendy Liu at The Hong Kong Baptist University for helping us with the XPS characterizations.

Most importantly, I would like to express my sincerest gratitude to my parents, who have been constantly supporting me all along the way with unconditional love, patience and encouragement. Pursuing a research degree is a commitment. As a textile undergraduate switching to material sciences, it

takes me quite a while to figure out if this is the right path that I should take. I would like to thank my parents for giving me a free will to pursue what I want the most, but not shaping me into whom they want to be. I also owe many thanks to all my best friends for their unfailing support, who always bring me laughers, crazy ideas and precious moments when we are together.

TABLE OF CONTENTS

LIST OF FIGURES

LIST OF TABLES

LIST OF ABBREVIATIONS

ATR-FTIR	Attenuated total reflectance-Fourier transform infrared spectroscopy
CNTs	Carbon nanotubes
CVD	Chemical vapor deposition
EDS	Energy dispersive X-ray spectroscopy
ELD	Electroless metal deposition
ICPs	Intrinsically conducting polymers
PAANa	Poly(acrylic acid sodium salt)
PAMD	Polymer-assisted metal deposition
PI	Polyimide
PMETAC	Poly[2-(methacryloyloxy)ethyl]trimethylammonium chloride
PMANa	Poly(methacrylic acid sodium salt)
PVD	Physical vapor deposition
SAM	Self-assembled mono/multilayer
SEM	Scanning electron microcopy
SI-ATRP	Surface-initiated atom transfer radical polymerization
XPS	X-ray photoelectron spectroscopy

CHAPTER 1: INTRODUCTION

1.1 Background and Challenges

Wearable electronics, the future of portable electronics, are inevitably playing a role in many sectors such as monitoring, display, military, energy harvesting, etc (1-17). Rapid advancement of wearable electronics results in high demand for high-performance flexible conductors as interconnects, contacts and electrodes. Textiles, being daily necessities with ultrahigh flexibility, represent an attractive platform for implementing future wearable electronics (18-27). Ironically, looking at those products available in prototypes or in the market, they are embedded with connecting wires, rigid circuit boards and other kinds of electronic auxiliaries that physically attached on or under the garments. Repeated home laundering of these so-called wearable electronics is not feasible, therefore not recommended.

To date, most of the demonstrated prototypes of wearable electronic textiles are based on the direct integration or attachment of electronic components onto the fabric structure. Neither any true integration into the fiber structures is yet demonstrated. The reason for the lag-behind is due to the increasing challenges in developing high-performance wearable prototypes with stable conductivity, durability, flexibility, washability as well as feasibility of scale production. A number of researches reviewed many synthesizing methods for fabricating electrically conductive textiles, such as yarns synthesized by or incorporated with metal oxide (28-30), intrinsically conducting polymers (ICPs) (31-35), and carbon nanotubes (CNTs) (36-40). Nevertheless, these approaches are not ideal for making electronic textiles, generally because of their inflexibility imposed by chemicals or fabrication processes, chemical instability, expensiveness, hazard to human body and most importantly, the difficulties in scale production with compatible technology in the current textile finishing and garment manufacturing industry.

Among all the conducting materials, metal is considered as the most promising conductor for electronics due to its relative low cost and high conductivity. One common practice to synthesize conductive textiles is to deposit a layer of metal coating on top of the textile surface using various deposition techniques (e.g. physical or chemical vapor deposition and electrochemical plating) (41-43). However, great investment, advanced instrumentation, specialized workforce and precise control on parameters are all required, which impede industrialization in the textile industry. More importantly, the adhesion of the as-deposited metal particles remains another major concern. As the metal particles are only physically attached on the textile substrates, they fall off easily upon repeated cycles of abrasion, bending, stretching and washing. Addressing the goal of achieving wearable electronics which are durable and washable, several attempts on surface-coated metallic textiles have proven to be abortive (44-47).

Recently, grafting of functionalized polymer brushes to modify surface architecture of substrate has provided new insights into novel material surface engineering (48-59). Polymer brushes that covalently tether one end on a surface can not only provide modified functional groups on the substrate surface, but also increase the amount of functional groups to be utilized in the subsequent chemical reactions. Azzaroni et al., first demonstrated the utilization of a cationic poly[2-(methacryloyloxy)ethyl]trimethylammonium chloride (PMETAC) brushes grafted selectively on substrate surface. With the loading of catalytic moieties for subsequent electroless metal deposition (ELD), a robust metal layer was selectively deposited with outstanding adhesion properties (60). In their work, such a polymer layer network introduced in-between the metal layer and the substrate can a) numerously increase the number of sites for catalytic moieties attachment for higher rate of ELD; and b) allow an interpenetrating matrix structure to be established which enables a strong adhesion between the as-deposited metal and the polymer brush layer. In 2010, Liu et al. reported a versatile approach to preparing highly durable conductive cotton yarns by growing PMETAC brushes on cotton fiber surfaces using surface-initiated atom transfer radical polymerization (SI-ATRP) (61), which was the first ever demonstration on grafting of PMETAC brushes on natural textile fibers. Subsequent metal ELD yielded conductive cotton yarns with high electrical stability that could withstand multiple bending, stretching, rubbing and even washing cycles. However, concerning the feasibility of scale production, demonstration from Liu et al. is definitely inappropriate because SI-ATRP suffers a number of drawbacks. Firstly, SI-ATRP cannot be carried out under ambient conditions but requires nitrogen protection. Secondly, SI-ATRP reaction takes up a long period of time which is undesirable and cost ineffective if the process is brought to industrial scale (62, 63). Thus, there is a need to further modify the synthesizing process to replace SI-ATRP in order to allow high throughput in scale production.

Therefore, two major research gaps concerning the fabrication of metallic textiles are summarized as follows:

1) Metal adhesion and the washing durability of the metallic textiles reported in the literature are not addressed most of the time. Therefore, many questions still remain answered for the performance stability of these metallic textiles in routine wear.

2) To date, there are no practical strategies to fabricate high-performance, durable and washable metallic textiles in bulk. Most of the proof-of-concepts of metallic textiles are demonstrated merely on lab-scale. Therefore, a solution to fully address the scale fabrication of metallic textiles for wearable electronics is highly demanded.

In this research, it is proposed that by adopting Liu's strategy, conventional free radical polymerization can be carried out to replace SI-ATRP to graft polymer brushes in-situ so as to eliminate the undesirable condition required during SI-ATRP. Conventional free radical polymerization is a rather simpler chemical reaction to grow polymer chains (64-66) and can be carried out under ambient conditions, which is highly advantageous over other means of polymerizations. Notwithstanding, there are still several difficulties to be dealt with to allow successful migration from lab-scale synthesis to mass production. Firstly, it is the feasibility of conventional free radical polymerization introduced into the reaction process, instead of using SI-ATRP to grow PMETAC brush from the textile fiber surface. Secondly, as conventional free radical polymerization is adopted, the feasibility of producing conductive textiles using currently available textile dyeing and finishing technologies, such as pad-dry-cure and hank dyeing remain to be explored. Thirdly, it is the washing durability of the as-made conductive textile. Though it had been proven that polymer brushes acting as an interfacial layer can provide outstanding adhesion between metal and substrate, it remains unknown if there are any changes in properties of the polymer brushes when free radical polymerization is adopted. Fourthly, for the true migration from lab-scale synthesis to large-scale production, cost of production is also one of the major concerns. As PMETAC can only couple with expensive catalytic moieties for the subsequent ELD, it still remains pessimistic about the cost involved when the whole fabrication is brought to scale production. Therefore, in order to eliminate the expensive chemical species involves in the fabrication, other than the PMETAC brush, possible grafting approaches of polymer brushes such as poly(methacrylic acid sodium salt) (PMANa) or poly(acrylic acid sodium salt) (PAANa) remain to be investigated. Finally, as the ultimate goal of this research is to develop durable and washable flexible metallic textiles intended for electronic purposes, application of as-synthesized metallic textiles in electronic textiles remains another issue to be verified.

1.2 Research Objectives

With the challenges abovementioned, objectives being addressed in this research are:

a) To study the surface modification chemistry on textile surface, particularly the surface modification by covalently grafting of polymer brushes using free radical polymerization.
b) To deposit conductive metal layers onto the polymer-coated textiles.
c) To characterize the metallic textiles including surface morphology and conductivity.
d) To study the physical properties and washing durability of metal-coated conductive textiles.
e) To explore the feasibility of fabricating conductive textiles using currently available textile dyeing and finishing technologies, such as pad-dry-cure and hank dyeing.
f) To demonstrate the potential applications of the as-made conductive textiles in wearable electronics.

1.3 Significance and Impact

Considering the demand for flexible electronics and the market-driven wearable technologies, flexible and washable conductive textiles are of great potential in the foreseeable future. This research mainly focuses on the development of durable, washable, and high-performance conductive textiles, and also the compatible technology for the textile industry to synthesize conductive textiles by surface modification with polymer brushes. This research concludes some practical information that evidences the possible reaction of free radical polymerization to grow polymer brushes on textile substrate. Also, the research output can benefit textile garment industry for the technology transfer for truly scalable fabrication of high-performance conductive textiles using currently available textile finishing technologies, therefore contributing a more practical solution to the mass manufacturing of conductive textiles in the textile industry.

1.4 Outline of the Thesis

In this thesis, thorough literature review on the metallic textiles with special focuses on their fabrication methods and applications in wearable electronics is given in Chapter 2. In Chapter 3, detailed literature review on the surface modification techniques on textiles commonly used by most of the chemists, material engineers and textile technologists is included. Special emphasis has been focused on the deposition of self-assembled mono- or multilayer and also grafting of polymer brushes. In Chapter 4, experimental designs, procedures and the characterization methods are listed. Chapter 5 summaries the results of the fabrication and characterizations of metallic textiles assisted with a cationic polymer brush poly[2-(methacryloyloxy)ethyl]trimethylammonium chloride (PMETAC). Chapter 6 summaries the results of the fabrication and characterizations of metallic textiles assisted with another anionic polymer brush which is poly(methacrylic acid sodium salt) (PMANa) or poly(acrylic acid sodium salt) (PAANa). Chapter 7 summaries some of the preliminary results of the fabrication of textile triboelectric generators using as-synthesized metallic textiles reported in Chapter 6 and 7. Chapter 8 gives a conclusion that sums up all the results reported in this thesis and also provides directions in the future studies.

CHAPTER 2: OVERVIEW OF CONDUCTIVE TEXTILES, THEIR FABRICATIONS AND APPLICATIONS IN WEARABLE TEXTILE ELECTRONICS

2.1 Introduction

Conductive textiles generally refer to fiber or fabric substrates, which are directly drawn, filled, incorporated, laminated and/or surface-coated with conductive materials such as metals and/or their oxides, intrinsically conducting polymers or other advance materials such as carbon nanotubes and graphene. Amongst all the conductive textiles, metallic textiles are particularly one of the most recognized functional textiles in the textile industry due to their intensive applications, particularly in heating garments and also medical garments with bactericidal properties imparted by the metal ions on the textile surface. In this chapter, we will first review a new emerging field of wearable textile electronics and the role of metallic textiles in wearable textile electronics. We will then focus on the fabrication of conductive textiles, with particular focus on the fabrication of metallic textiles by different physical and chemical deposition approaches. Other fabrication methods such as coating with intrinsically conducting polymers and carbon materials are also addressed. Finally, applications of conductive textiles in wearable textile electronics demonstrated in prototypes as reported in the literatures, including fiber-based transistors, wearable sensors, energy storage devices and triboelectric generators are briefly discussed.

2.2 Wearable Textile Electronics

Textiles as one of the necessities in daily living, exhibit themselves in three major structures which include a) woven: yarns of warp and weft directions cross and interweave with one another (67-69); b) knitted: yarn in one set interlocks with loops of the neighboring yarn (70); and c) nonwoven: fibers aligned in certain or random directions bound by chemical bonding or physical entanglement (71). Besides aesthetic functions in fashion and home furnishing, textiles also provide industrial applications such as geotextiles in reinforcement of embankments, composite materials in buildings, medical textiles in implants, wound dressing, rehabilitation as well as protective functions in adverse weather, aerospace and warfare (72-77). As computer and semiconductor electronics are getting more advanced, faster in clock speed and physically smaller in size, more advanced technologies emerged majorly as portable, or even 'worn-on-the-body' electronic gadgets. Well-known examples are Google Glass developed by Google, iWatch developed by Apple and various fitness trackers by Jawbone, Nike, Fitbit etc. Apart from these so-called wearable gadgets, truly wearable electronics have already been well extended to many market-available sports garments, such as adidas miCoach training shirt, which can detect your heart rate while doing physical training. Another example is The North Face Hustle Audio Jacket which features an external joystick pad on the forearm to control your iPod. Such a rise in the technology advancement particularly using textile garment as a platform therefore gives a new emerging field namely textile electronics (1, 2, 7, 18, 19, 78-81). In fact, the earliest idea of textile electronics had already been demonstrated in 1996 by Park et al. who presented the well-known Georgia Tech Wearable Motherboard (GTWM), or the 'Smart Shirt', as the first prototype of wearable electronics (82-83). The as-presented sensor-plugged GTWM can detect human vital signals in a systematical way. Not until recently, electronics integrated into textiles become truly viable especially in the medical and sports sectors. However, most of the wearable electronic garments always attach conventional off-the-shelf electronic devices and components directly onto the clothing (18, 78-84), without the true integration of the electronic devices into the garment itself. Today, many researchers are still under the way to integrate the electronics within fabrics and fibers with ambient production methods. More focuses have been put on the device's performance stability, washing ability, durability and compatibility of the manufacturing process with the current textile manufacturing industry.

2.3 Fabrication of Conductive Textiles

Rapid advancement of wearable electronics results in high demand for high-performance flexible conductors as interconnects, contacts and electrodes. A number of researches reviewed many synthesizing methods for fabricating conductive textiles in the recent decade, such as yarns and fabrics directly drawn or incorporated with metal or metal oxide (28-30), coated with intrinsically conducting polymers (ICPs) (31-35), or carbon nanotubes (CNTs) (36-40). However, as the conductivity of textiles becomes more critical in wearable electronics, plus the advantage of being at a relatively low cost, metallization of textiles become the most attractive strategy to yield conductive textiles. In this section, fabrication methods of metallic textiles are addressed. Other conductive textiles synthesized by coating of intrinsically conducting polymers and also other carbon materials are briefly discussed.

2.3.1 Coating with Metals

Metallic textiles has attracted tremendous attention as they possess not only aesthetic effect in fashion, home furnishing, installations and decorations, they also add value to the conventional textiles industry as well as the emerging field of wearable electronics. Essential criteria for textiles qualified for being as electronic textiles are the ability to conduct electricity and also good adhesion of the conductive materials with textile substrate surface even when they are subject to repeated cycles of bending, stretching and abrasion. Throughout many years of devoted efforts to search for a universal material to durably coat conductive materials on textile surface, metals are found to be the most promising materials that enable true reliability and conductivity. Moreover, they are relatively at lower cost comparing to other conducting materials such as conductive polymers, carbon-based materials such as carbon nanotubes and graphene.

Common metals used to deposit on the textile surface are copper, nickel, silver, aluminum and gold (85-92), in which copper and nickel are found to be the most attractive and promising candidates owning to their high conductance, comparatively low cost, as well as the ease of deposition by various deposition techniques. Many fabrication approaches focusing on textile metallization had been reported in the past decades, which put forward significant progress in the making of metallic textiles. Here we will explore some commonly utilized approaches to preparing metallic textiles, including electrochemical plating, physical vapor deposition, chemical vapor deposition, and electroless metal deposition.

2.3.1.1 Electrochemical Plating

Electrochemical plating is one of the metallization methods to surface deposit metals on a conductive surface, which is utilized particularly in the furnishing industries such as chromium and cadmium plating of mirror-like finish for decoration purpose on bathroom faucets. Metallization by electrochemical plating on textile fibers is also feasible, but seems not promising for robust conductors in textile electronics. Little et al. reported the electrodeposition of gold on Kevlar fibers (93). Their experiment actually involved three steps. They first brought the Kelvar fibers into a conventional Sn^{2+}/Pd^{2+} solution for surface activation. The sensitized Kevlar fibers were then immersed into the nickel electroless bath to carry out electroless nickel deposition on the Kevlar fibers. Finally, they put the nickel-coated Kevlar fibers to electroplate with gold by the thiosulfate procedure. Metallization of Kevlar yarns by conventional Sn^{2+}/Pd^{2+} surface activation coupled with electroless nickel deposition can render the fibers conductive, nickel-coated Kevlar fibers can subsequently serve as cathodes for electrochemical plating of gold. However, as seen in the SEM images shown in Figure 2.1, the adhesion of the nickel is very poor, where many defects and cracks are observed on the fiber surfaces. Even after the electroplating of gold, the SEM image shown in Figure 2.2 reveals that the gold metal layer is not conformal on the fiber surface, indicating that gold metals may easily fall off from the fiber surface. Such poor adhesion is also verified in the conductivity measurement. As depicted in Figure 2.3a, a stable V-I curve is obtained only when the length of the gold-plated Kevlar in measurement is 3.2 cm. When the length of measurement increases up to around 6.5 cm as shown in Figure 2.3b, the gold-plated Kevlar fibers show obvious burn marks as mentioned in the paper, indicating that the electroplated gold is highly uneven on the Kevlar yarn surface.

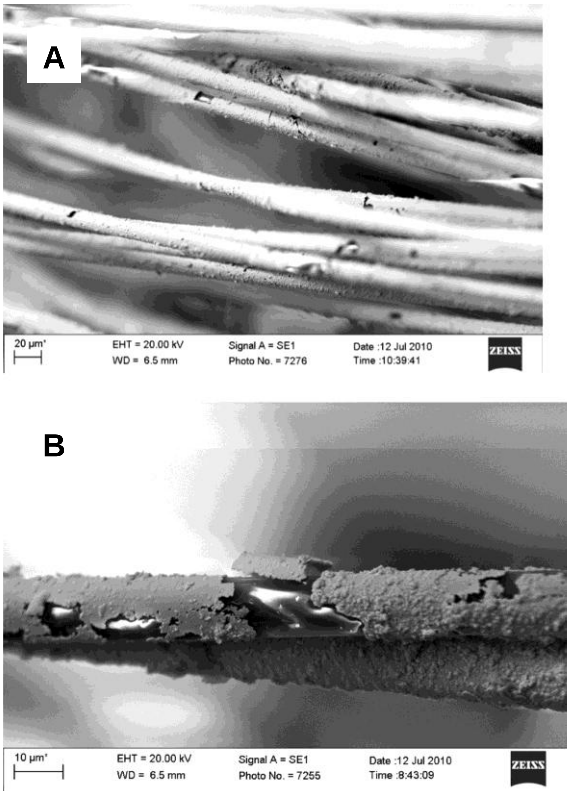

Figure 2.1 SEM image at (A) low and (B) high magnification of Kevlar fibers first coated in the Ni electroless bath, then exposed to ultrasound in H_2O and electroplated with Au via the thiosulfate procedure. (93)

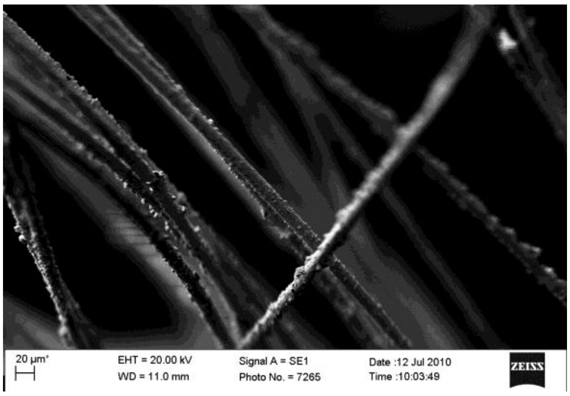

Figure 2.2 High magnification SEM image displaying coatings on Kevlar fibers treated three times with the electroless Ni method, then coated three times with Au via electrodeposition. The coating contained 1.03 g of Ni/Ni_xP_y and 3.68 g of Au per g of fiber. (93)

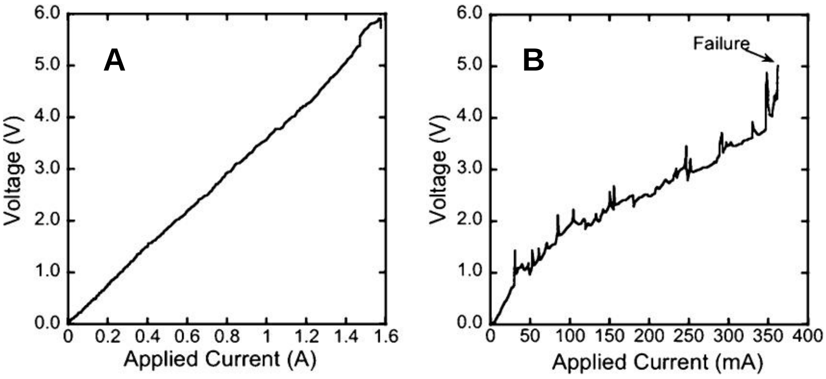

Figure 2.3 Plots of voltage versus current obtained for a 9 cm Kevlar yarn treated three times with the electroless Ni method, then coated three times with Au via electrodeposition. (A) Results from measurements over a yarn distance of 3.2 cm. (B) A point failure at 1.8 W for a distance along the yarn of 6.5 cm. (93)

2.3.1.2 Physical Vapor Deposition (PVD)

Physical vapor deposition (PVD) generally relies on the physical interactions of the deposited materials with the substrate surface. Examples considered as PVD are thermal evaporation and sputtering. Thermal evaporation is already a very well developed technology in the semiconductor industry. In a typical thermal evaporation process, metal source is heated up and evaporated from solid phase to vapor phase under a vacuum condition. The vaporized metal particles are then condensed on the textile surface, forming a layer of metallic coating. Lai et al. demonstrated the fabrication of metalized polyester filaments, by evaporating silver, copper, aluminum and titanium onto the polyester film with a thickness of 12 μm (94). After respective metal evaporation, the metalized polyester film was slit into 0.254 mm width filaments, which were finally combined with another polyester yarn to form conductive yarns.

Besides thermal evaporation, sputtering is also a mature metal deposition technique in the semiconductor industry. Sputtering is a process that utilizes plasma, in which atoms or ions of the targeted materials are knocked off by the bombardment of high kinetic energy electrons or inert ions under a vacuum condition. Those atoms or ions being knocked off are ejected from the target, travel to and condense on the substrate surface to form a thin metal layer. Many research groups applied sputtering technology to obtain copper-, silver-, aluminum- and titanium-coated textiles. Depla et al. conducted an explorative study of making metallic textiles by magnetron sputtering deposition (95). They investigated the deposition of aluminum, copper, titanium as well as some metal oxides such as aluminum oxide and titanium oxide on woven and non-woven textile substrates. Wei et al. also gave a detailed characterization of the copper-coated textiles prepared by magnetron sputtering deposition (96), where they specifically deposited copper with a thickness of 20 nm, 50 nm and 100 nm, respectively, on the surface of polypropylene spun-bonded fabrics.

2.3.1.3 Chemical Vapor Deposition (CVD)

Commonly adopted by the semiconductor industry to fabricate thin films on silicon wafers, chemical vapor deposition (CVD) is a chemical reaction in which the source materials are vaporized to form volatile species, and then diffuse to the substrate surfaces to form a coating. CVD is an alternative approach to deposit metal species on textiles to obtain metallic textiles, in which sophisticated and conformal metal coating is enabled. Conventionally, CVD is equipped with heating elements, which is categorized as thermal CVD. However, the temperature range for thermal CVD can reach few hundred degrees Celsius, which is not suitable for commodity fibers such as cotton. Therefore, plasma-enhanced PVD (PECVD) as a modification to conventional CVD has been realized, by replacing the heating elements in the conventional CVD with electrical discharging unit. The temperature of the reaction can therefore be reduced, and can facilitate the deposition process on commodity textile fibers.

Further modification to the conventional thermal CVD has emerged to a special kind of CVD namely atomic layer deposition (ALD). ALD is a kind of deposition technique to deposit highly precise coating with each layer of one atom thick. In 2013, Kalanyan et al. used ALD to coat non-woven nylon to yield highly conductive tungsten-coated nylon mat (97). Such a tungsten-coated nylon mat was fabricated by exposing the non-woven nylon mat with tungsten hexafluoride (WF_6) and 2 % silane (SiH_4) in an argon atmosphere. The as-synthesized tungsten-coated nylon mat exhibited a high conductivity of 1000 S/cm. Jur et al. further utilized the ALD technique and presented a work of coating zinc oxide on cotton and tungsten on quartz fiber, respectively at 115 ˚C and 200 ˚C with ALD (98). The reported conductivities were highly satisfactory, in which the zinc oxide-coated cotton exhibited ~24 S cm^{-1} while that of the tungsten-coated quartz fiber reached ~1150 S cm^{-1}. In 2014, metal oxide patterns fabricated on the non-woven fiber mat was demonstrated by the same group. They used an extra patterned mask covered on top of the non-woven fiber mat and carried out ALD of zinc oxide (99) (Figure 2.5). However, although ALD process is highly scalable with compatible roll-to-roll equipment, it requires many repeated cycles of gas exposure, which is very low throughput and cost ineffective. Moreover, different from other metallization or deposition techniques, all CVD techniques require highly precise control on the deposition parameters, where many optimizations and also calibration work have to be done prior to the fabrication.

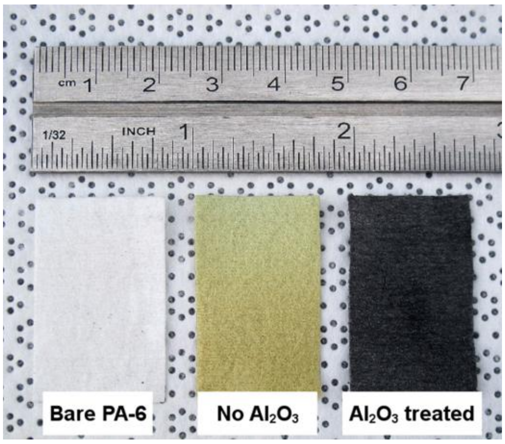

Figure 2.4 Photograph showing nonwoven nylon-6 fiber mats after coating with 100 cycles of W ALD at 140 °C. The sample on the left is not treated with Al_2O_3, resulting in poor tungsten nucleation on the fibers, whereas the sample on the right shows proper W nucleation as a result of pre-treatment with 25 cycles of Al_2O_3 at 140 °C. (97)

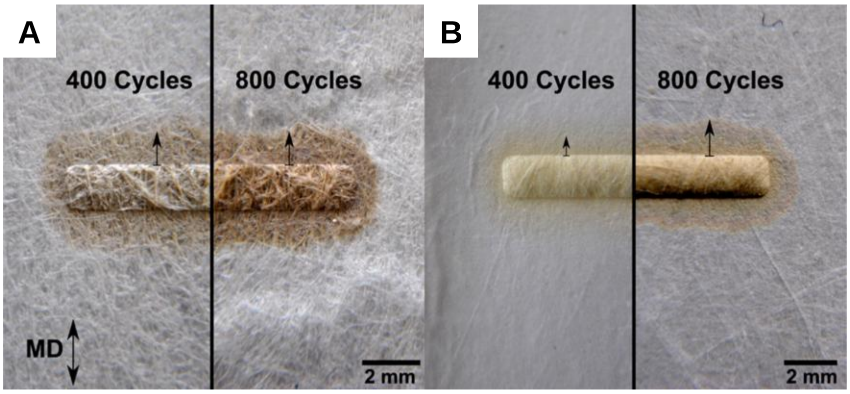

Figure 2.5 ZnO ALD on (A) nylon-6 nonwoven fiber mats cut in the machine direction and (B) polypropylene nonwoven mats. For deposition on nylon, the extent of diffusion under the masked area is the same for 400 vs 800 ALD cycles, whereas for the polypropylene substrate the 800 cycle deposition is more spread out than the 400 cycle sample. For more deposition cycles, precursor diffusion into the polypropylene polymer may extend growth further under the mask region. The images were digitally enhanced to increase contrast by 50 %. (99)

2.3.1.4 Electroless Metal Deposition (ELD)

Among different metal deposition strategies, electroless metal deposition (ELD) is the most preferred method (100-102), because merely metal salt, reducing agent and simple equipment are required without the use of electricity. In addition, ELD is a solution-processable method which does not require vacuum condition. Therefore, it is low-cost and at the same time high-quality and uniform metal layer can be easily obtained. In 2012, Lu et al. had proposed a palladium-free catalytic electroless copper deposition on bamboo fabrics (103). The fabrication process only involved surface modification of the bamboo fiber surface by using thiol groups in 3-mercaptopropyltrimethoxysilane (MPTS) ethanol solution. Copper metal was subsequently deposited on the modified bamboo fabric by ELD using dimethylamineborane (DMAB) as a reducing agent. The preparation process is shown in Figure 2.6. Conductivity of the as-deposited bamboo fabric was reported as about half of the conductivity of bulk copper, which was highly satisfactory. The advantage of this approach is the elimination of expensive palladium as catalyst for activation. However, the adhesion of the copper coatings on the as-deposited bamboo fabric was only addressed by the Scotch tape test, which remained a question about how satisfactory the adhesion was between the as-deposited copper particles and the bamboo fiber substrate when washed with water.

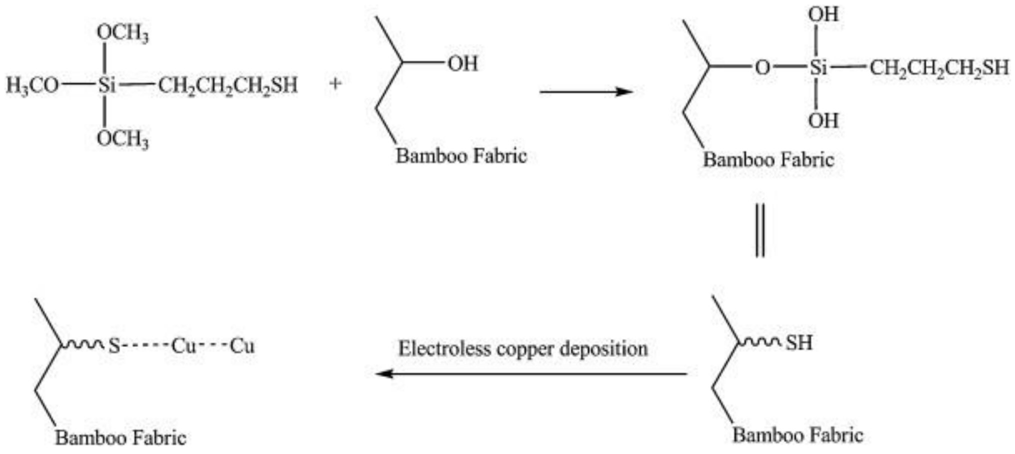

Figure 2.6 Fabrication of copper/bamboo fabric composite. (103)

In 2013, Lee et al. had successfully deposited aluminum metal on the textile surface at room temperature via a solution process, in which aluminum precursor composites were simply decomposed by suitable metallic salts to yield aluminum metal particles on the textile surface (104) (Figure 2.7). The as-made aluminum-coated paper and threads showed excellent electrical properties with sheet resistance of less than 250 milliohm/sq and linear resistance of less than 30 ohm/10 cm, respectively. Though the resultant fabric and thread were packed with densely structured aluminum films with mechanical endurance against bending and folding deformation, the washing ability, still, was not addressed in their investigation.

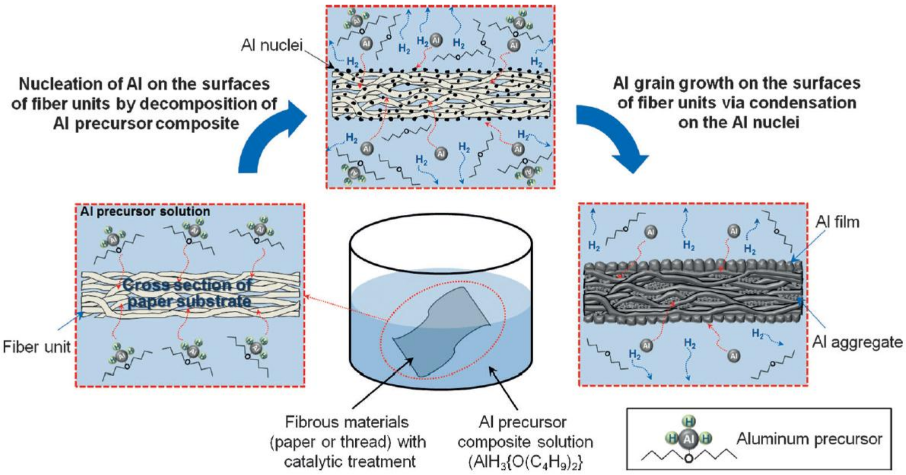

Figure 2.7 Schematic representation of the chemical solution process for fabrication of highly conductive aluminum fibrous materials by immersing the catalytically pre-treated fibrous materials into an aluminum precursor composite ($AlH_3\{O(C_4H_9)_2\}$) solution at room temperature. (104)

Many other research groups had also provided many innovative solutions for possible commercialization of conductive textiles. In 2003, Montazer et al. had immobilized silver nanoparticles on the polyester fabric surface by simply boiling polyester fabrics with silver nitrate, sodium hydroxide and subsequently with ammonia, followed by ELD of silver particles to yield highly conductive silver-coated polyester fabrics (105). The mechanism of silver nanolayer formation on polyester fabric surface is illustrated in Figure

2.8. Such a chemical approach proposed had provided great insights into making silver-coated textile in reduced time and cost, by eliminating the use of expensive noble metal ions for subsequent ELD. They used the by-products such as ethylene and terephthalic acid generated in the polyester alkaline hydrolysis as reducing agents for the reduction of silver ions to form elementary silver. As reported, the electrical resistance of the silver-coated polyester fabric by using optimized recipe was as low as 1.3 ohm/sq. In this work, they had further challenged the washing ability of the silver-coated polyester fabrics. The authors reported that the washed samples exhibited resistances of 120 ohm/sq after two cycles of washing with ammonia at 60 °C for 20 min, which showed a fair stability of the silver nanoparticles adhered onto the fabric surface.

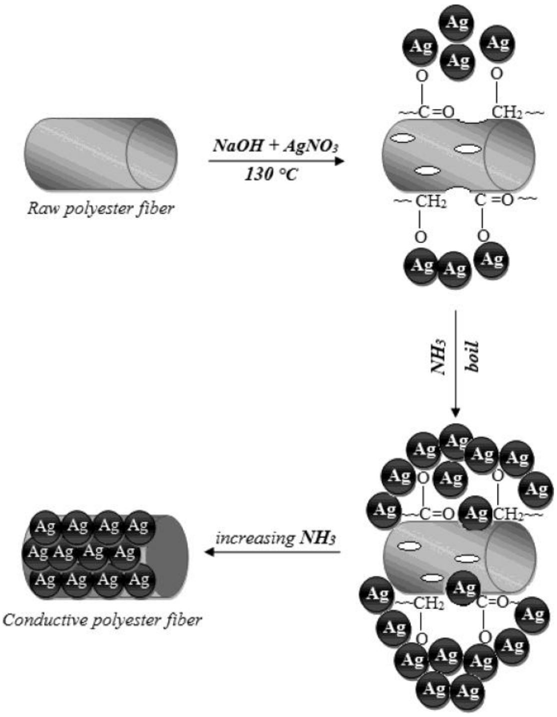

Figure 2.8 Mechanism of silver nanolayer formation on polyester fabric surface. (105)

To address the adhesion problem between the deposited metal and the substrate surface, in 2013, Wang et al. reported the use of poly(dopamine), which was an universal adhesive protein secreted by mussels that could attach to virtually all types of inorganic and organic surfaces, to prepare silver-coated meta-aramid fibers (106). The resultant fibers not only provided high mechanical durability but also anti-bacterial applications. In their experiment, poly(dopamine) was first grafted on the polymetaphenylene isophthamide (PMIA) fibers, followed by electroless silver plating (Figure 2.9). They also eliminated the process of activation by noble metal catalyst, which brought the reaction in a relatively low cost. The electrical resistivity of the silver-coated PMIA fibers was estimated as low as 0.61 milliohm·cm. Though effort had been made in finding a solution for better adhesion of metal particles on textile surface, again, the resistance against washing was not discussed.

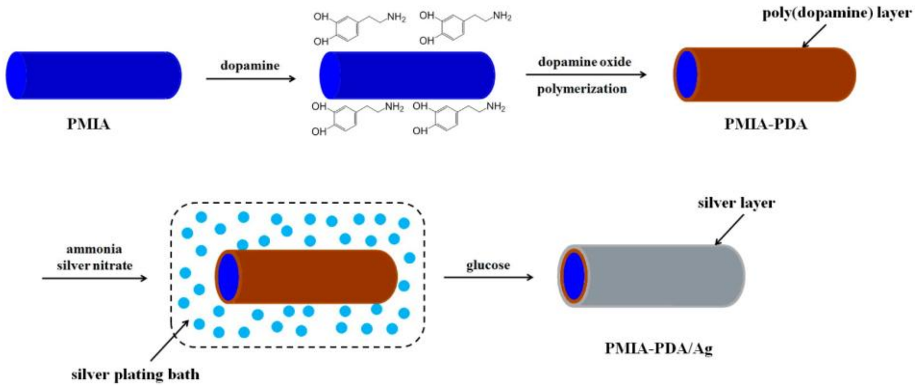

Figure 2.9 Schematic illustration of procedure for the fabrication of PMIA-PDA/Ag composite by poly(dopamine)-assisted electroless silver plating. (106)

With several reviewed literatures about making of metallic textiles, it can be concluded that although the approaches adopted for the deposition of metal on textile surface are found to be innovative, low-cost, scale producible and can result in high-performance conductive textiles, the adhesion between the metal layer and the textile substrate is generally unsatisfactory.

2.3.2 Coating with Intrinsically Conducting Polymers (ICPs)

Intrinsically conducting polymers are the organic polymeric materials with a conjugated system for the conduction of electricity of delocalized electrons. Examples of intrinsically conducting polymers are polypyrrole (PPY), polyaniline (PANI), poly(3,4-ethylenedioxythiophene) (PEDOT) and polythiophene. The direct and easiest way to impart ICPs on textile surface is by in-situ polymerization. In 2011, Hu et al. had demonstrated the inkjet printing of poly(3,4-ethylenedioxythiophene):poly(styrene sulfonate) (PEDOT:PSS), onto polyester mesh fabrics (107). With increased printing numbers of PEDOT:PSS, the average conductivity of the fabric could reach 22 S cm^{-1} with an average PEDOT:PSS thickness of 1.1 µm. The SEM image of the inkjet-printed PET fabric mesh is shown in Figure 2.10.

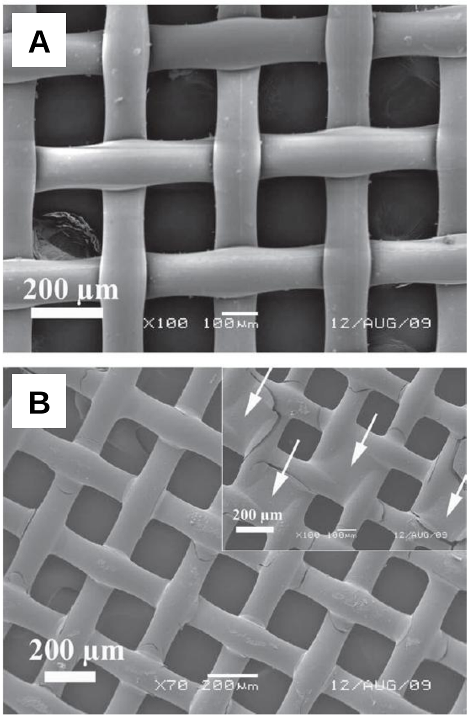

Figure 2.10 SEM images of the PET mesh fabric before (A) and after (B) being inkjet printed with 6 cycles of PEDOT:PSS. The inset is an SEM image taken at a higher magnification for the six-layer PEDOT:PSS PET mesh fabric. Some of the open areas (white arrows) on the fabric are blocked by the PEDOT:PSS film. (107)

2.3.3 Coating with Carbon-based Materials

Recently, carbon materials are gaining much attention due to the discovery of carbon nanotubes with remarkably outstanding properties such as lightweight, high strength, high thermal and electrical conductivity, etc. Incorporation of CNTs into textiles was demonstrated by Hu et al. in 2010. They used a very simple dip-dry method to coat singe-walled carbon nanotubes (SWCNTs) on the cellulose fibers (15). The as-made SWNT-coated textiles exhibited a high conductivity of 125 S cm^{-1} with a sheet resistance of less than 1 ohm/sq. The schematic illustration of the structure of the SWCNT-coated cellulose fiber and also the surface morphology are shown in Figure 2.11.

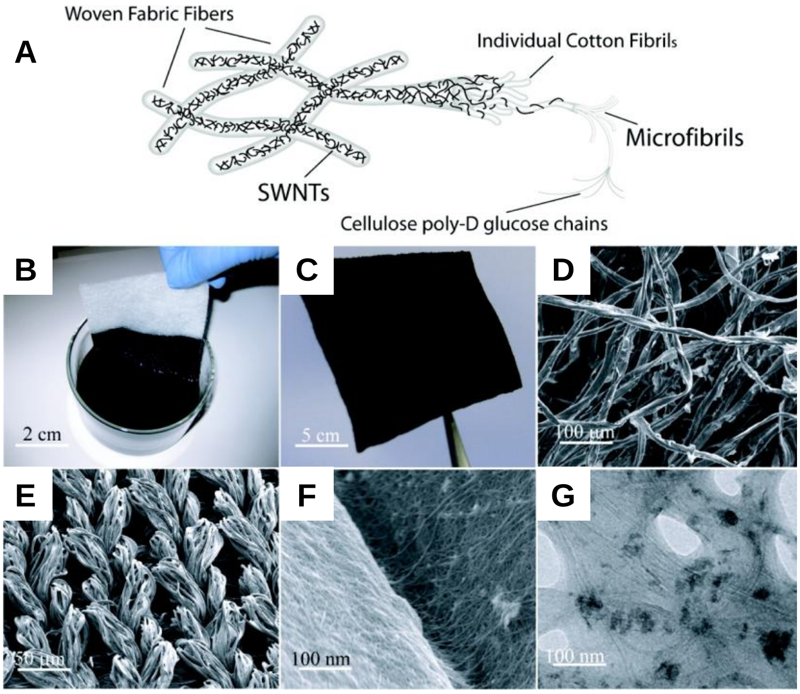

Figure 2.11 Porous textile conductor fabrication. (A) Schematic of SWNTs wrapping around cellulose fibers to form a 3D porous structure. (B) Conductive textiles are fabricated by dipping textile into an aqueous SWNT ink followed by drying in oven at 120 °C for 10 min. (C) A thin, 10 cm × 10 cm textile conductor based on a fabric sheet with 100% cotton and Rs of 4 ohm/sq. (D) SEM image of coated cotton reveals the macroporous structure of the cotton sheet coated with SWNTs on the cotton fiber surface. (E) SEM

image of fabric sheet coated with SWNTs on the fabric fiber surface. (F) High-magnification SEM image shows the conformal coating of SWNT covering and bridging between the fabric fibers. (G) TEM image of SWNTs on cotton fibers. (15)

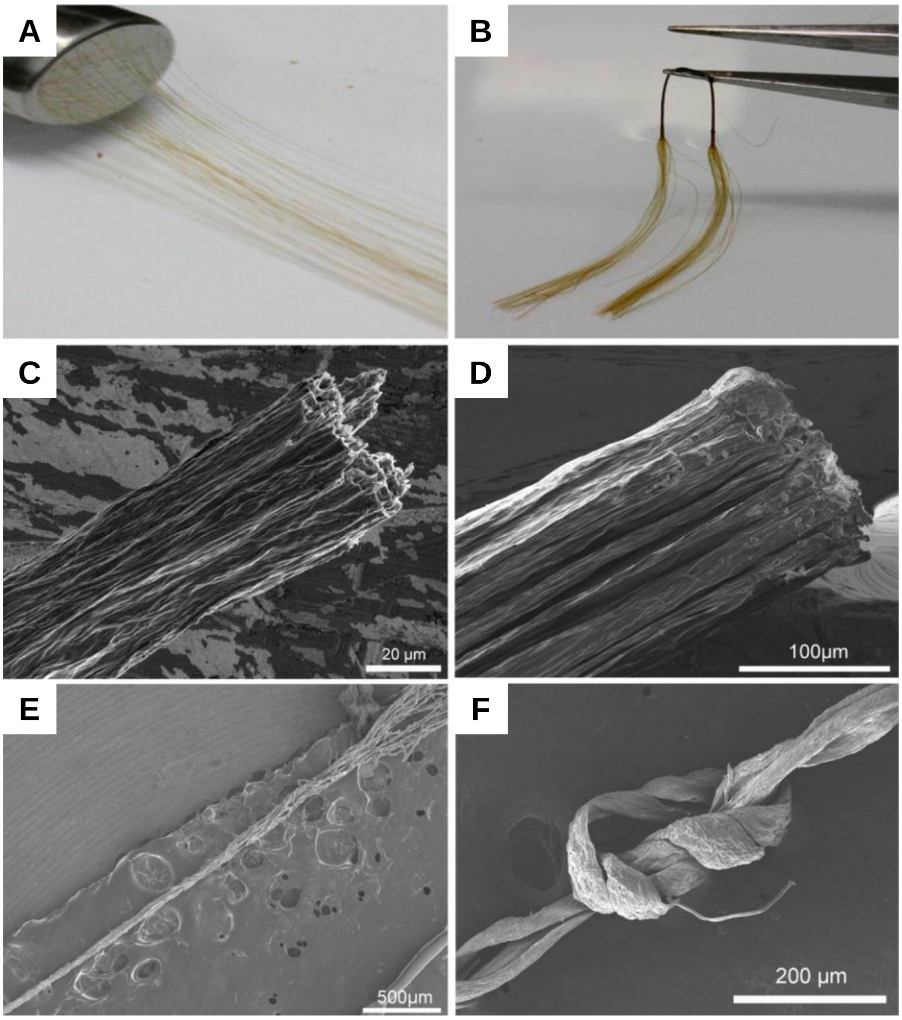

Figure 2.12 Spinning of GO fibers and yarns. (A) Digital image of the formation of gel-state GO yarns produced using a multihole spinneret. As the LC GO is injected into the coagulation bath, GO filaments are being coagulated instantly by the coagulation solution. (B) Dried GO yarn can be easily separated into individual filaments when they are immersed in water. However, the fibers could still maintain their structural integrity in the presence of water. FESEM micrographs of (C) an irregularly shaped GO fiber. (D) A GO yarn composed of many GO fibers. (E) An unwoven GO fiber

yarn. (F) A loosely knotted GO yarn demonstrating the flexibility of the as-prepared GO fibers in an acetone bath. (108)

Other than CNTs, fabrication of graphene-based textiles also attracts tremendous attention. Aboutalebi et al. had reported the fabrication of graphene textile electrodes applied in supercapacitors (108). They used a wet spinning method to produce continuous graphene oxide (GO) fibers from slightly acidic (pH is ~3) liquid crystal (LC) dopants in a pure acetone bath. The proposed wet-spinning strategy by wet spinning can be readily scalable and commercialized in the market (Figure 2.12). The-as-fabricated yarn exhibited high mechanical robustness (Young's modulus in excess of 29 GPa) and high electrical conductivity (2508 ± 632 S m^{-1}).

2.4 Applications of Conductive Textiles in Wearable Textile Electronics

2.4.1 Fiber-based Transistors

Transistors are one of the fundamental building blocks in the field of electronics. Full integration of transistors into garment clothing is one of the goals to be achieved in the next generation of textile electronics. Over the past decades, many researches had demonstrated the feasibility of such revolutionized ideals implemented into textile fibers to enable computerized logics in fibers. In 2003, Lee and Subramanian first reported their successful fabrication of flexible organic field effect transistors (OFETs) printed directly onto fibers without using the conventional lithography techniques (109). In their experiment, they used 250 μm and 500 μm diameter aluminum wires as the gate lines. After depositing a layer of dielectric and evaporating active material pentacene, overwoven wires were placed on top and served as the channel marks for evaporated gold to form as source and drain contact pads. After the removal of the overwoven wires, arrays of transistors were then resulted at each intersection (Figure 2.13). As reported, this fiber-based transistor exhibited a similar performance comparing to the planar transistors. As the entire patterning on the fibers was achieved by only shadowing from the overwoven fibers that covered on the underneath fibers without using high-end lithography techniques, the whole process can be upscale in the semiconductor industry. However, very high precision has to be achieved in making such fiber-based transistors, which is still one of the hurdles hindering mass production in the textile industry as there are no currently available textile manufacturing machineries available for suiting this precise fabrication purpose.

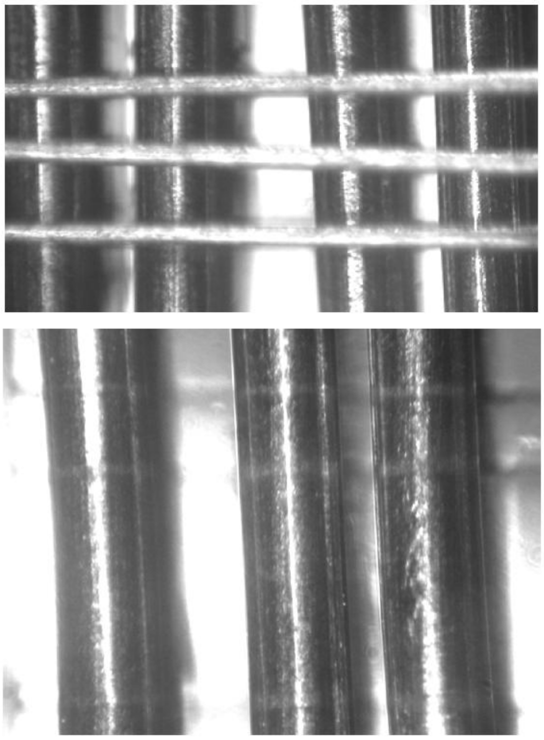

Figure 2.13 (Top) Masking process used to fabricate transistors on fiber. (Bottom) Arrays of 500 × 50 μm transistors formed using weave-based masking. Strips of pentacene are visible between the gold pads. (109)

Despite of the fact that high precision was found necessary in making fiber-based transistors, other fabrication methods of fiber-based transistors flourished after the first demonstration from Lee and Subramanian. Owing to some drawbacks of OFETs which require well-defined gate insulator thickness as well as high operating voltage, later development of fiber-based transistors had been focused on the organic electrochemical transistors

(OECTs). In 2007, Hamedi et al. had delivered a scheme of making fiber-embedded micrometer-sized OECTs by utilizing intrinsically conducting polymer PEDOT:PSS directly coated onto the textile fibers surface (20). In their fabrication scheme as shown in Figure 2.14d, the PEDOT:PSS-coated monofilament nylon fibers of 10 μm diameter were joined together with a solid electrolyte set at the cross point. As the authors suggested, these transistors were denoted as wire electrochemical transistors (WECTs). In 2009, they further improved the transistor designs and reported the fabrication of fiber-based organic electrolyte-gated thin film transistor (TFT) using another intrinsically conducting polymer poly(3-hexylthiophene) (P3HT) (110). In the device fabrication, they first coated the woven fabric mesh with gold layer by evaporation. The upper fibers on top in the woven structures of the fabric mesh acted as a shadow mask to create gold patterns on the lower fibers at bottom as the source and drain contacts. The gold-coated fibers were then unrevealed from the woven fabric and deposited with a thin layer of P3HT. Pure gold wires were then placed perpendicularly to the P3HT-coated fibers, where a junction was created. Finally, the fiber-based organic electrolyte-gated TFT was fabricated by dropping a solid polymeric ionic liquid (IL) at the junction (Figure 2.15c). Later in 2011, Inganäs's group further demonstrated the feasibility of making conductive silk for electrochemical transistors (ECTs) (111), which was the first ever report on the making of fiber-based transistors using natural fibers as substrates.

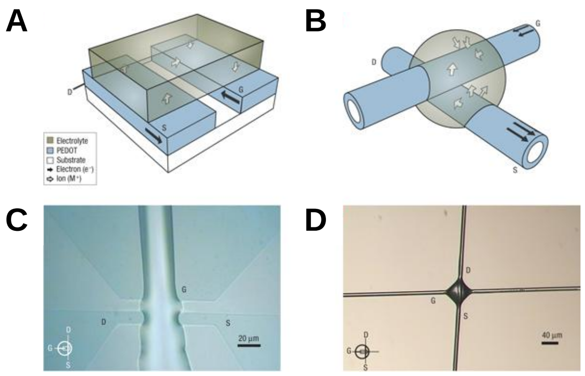

Figure 2.14 (A) Schematic picture of a planar ECT (S: source; D: drain; G: gate). (B) Schematic picture of a wire ECT (WECT). (C) Optical micrograph of a planar micro-ECT (channel width=15 μm). (D) Optical micrograph of a

WECT constructed at the junction of two PEDOT/PSS-coated polyamide monofilaments with 10 μm diameters. (20)

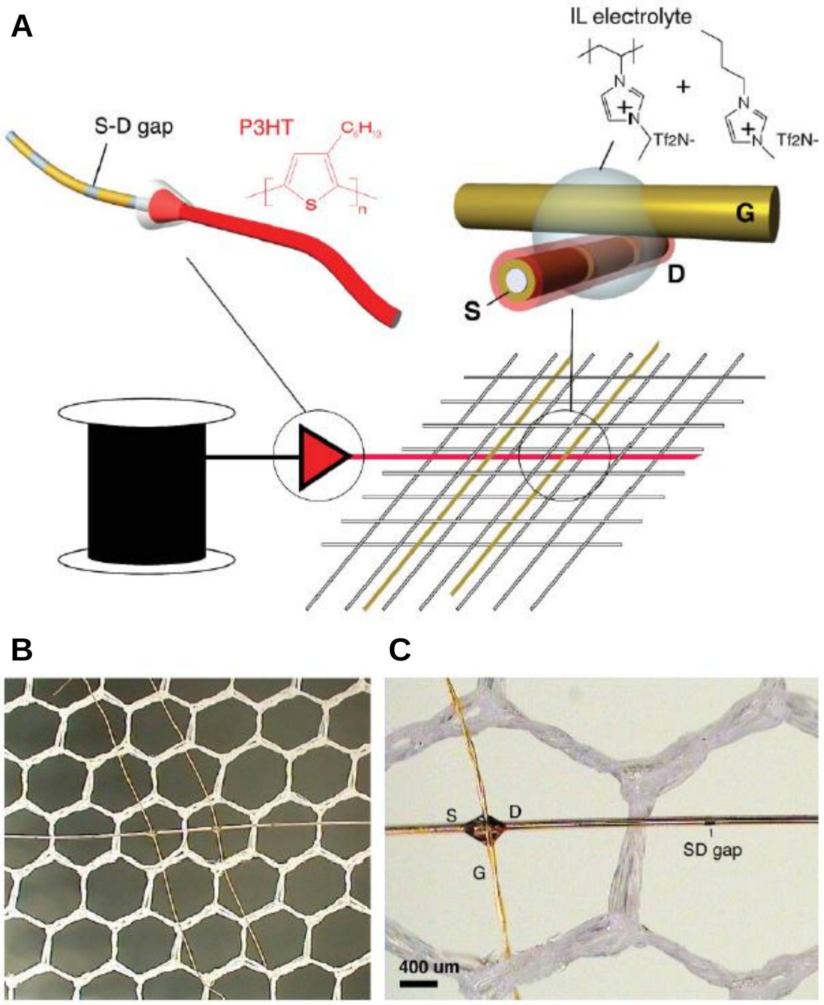

Figure 2.15 (A) Schematics of P3HT coating on top of fibers, with prepatterned source-drain gaps weaving of electrolyte-gated OTFT (top-left). Transistor formed at a fiber junction connected through an IL electrolyte (top-right) and weaving of transistors/devices using different fibers (bottom). (B) Microscopy image of two transistors created along the horizontal fiber, all woven in a tulle. (C) Microscopy image showing a close up of a fiber transistor on the left side, and a visible prepatterned transistor gap at the right side of the horizontal fiber. (110)

2.4.2 Wearable Sensors

Textile-based wearable sensors for monitoring body movement and physiological activities are highly applicable due to their ‘portable’ nature. With continuously expanding populations, the demand of health monitoring system is getting even higher. Till now, applications of electronic textile have been mostly targeted to the medical sectors to monitor patients’ physiological signals, such as heart rate, respiration rate, skin temperatures, movement of muscles as well as brain activities.

Electronic textiles, being very attractive in making wearable sensors, exhibits many advantages like highly flexible, noninvasive and comfort. With integrated electrochemical sensors, textiles can now provide real time monitoring not only an individual’s body conditions, but also threats in the environment. In 2011, Malzahn et al. had demonstrated the making of textile-based wearable sensors on underwater garments using screen printing and stamp transfer approaches (112). The electrochemical sensor printed on the garment can detect heavy metal pollutants and also nitroaromatic explosives in the marine environment. Owing to the ease of the fabrication, such process can be scaled up in production. Also, by using screen printing method, different electrode geometries can be realized with different feature sizes by simply adjusting the pattern sizes on the screen. Later in 2012, Windmiller et al. further developed an alternative approach by using stamp transfer to print electrochemical sensors and biosensors on three-dimensional surfaces (113). Stamp transfer approach overcomes the drawbacks brought by the screen printing, providing a more versatile fabrication methodology for the irregular-shaped electrode patterns (Figure 2.17). Their group made use of the as-made flexible electrodes to successfully fabricate flexible electrochemical biosensors to monitor various physiological analytes. Even though the fabrication is simple, their demonstrations on using stamp for transferring the conductive ink to the textile surface is highly adoptable in the current and textile industry.

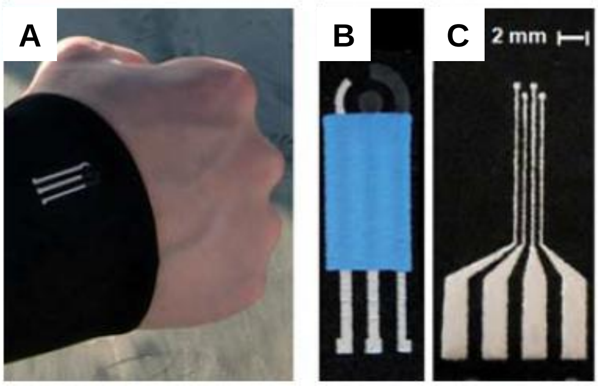

Figure 2.16 (A-C) Screen-printed electrodes on an underwater garment. (112)

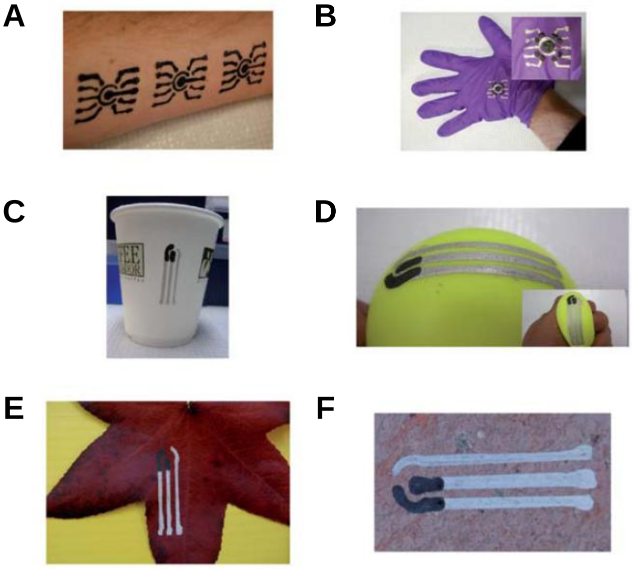

Figure 2.17 (A) Three eight-electrode carbon ink-based arrays stamped on the epidermis for biosensing operation. (B) Eight-electrode array on a nitrile glove. Inset shows the array under flexion of the glove. (C) Three-electrode contingent on a disposable paper cup. (D) Three-electrode contingent on a Neoprene® stress ball. Inset illustrates the resiliency of the electrochemical sensor upon compression of the stress ball. (E, F) Images of three-electrode contingent on a maple leaf and a granite slab, respectively. (113)

Fabrications of fully flexible and tactile capacitive sensor made with conductive fabric electrodes were reported by Viry et al. in 2014 (114). They simply fabricated the pressure sensor by assembling copper/tin-coated fabrics as top and bottom electrodes, which then laminated with a layer of fluorosilicone and encapsulated by two pieces of polydimethylsiloxane (PDMS) (Figure 2.18).

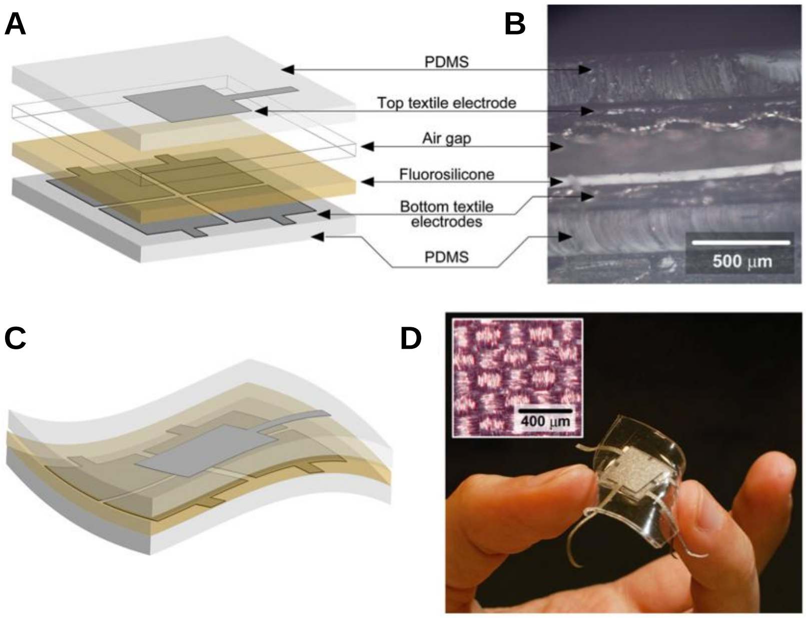

Figure 2.18 Schematic representation and description of the sensor architecture (A) with corresponding cross-sectional view (B). (C, D) Illustration of the flexible sensor. Inset in (D) shows an optical microscopy picture of the conductive textile electrode. (114)

Such a pressure sensor can be regarded as a capacitor. When the contact force is applied on the pressure sensor, the distance between the two conductive fabrics in the device is reduced, while at the same time the capacitance is varied. Owing to the multi-layer architecture, the as-made sensor showed high performances even at very low pressures. As reported, this sensor exhibited remarkable sensitivity with less than 10 mg and 8 μm, which were dictated as the minimal detectable weight and displacement, respectively. Besides normal force that could be detected as other pressure sensors, this capacitive sensor can also detect the contact force in tangential direction, paving the way for the further development of the textile-based sensors that emulate closer to a natural touch system to provide more precise pressure mapping on human body.

Very recently, Lee et al. reported the fabrication of yarn-based capacitive pressure sensor (115). By coating poly(styrene-block-butadien-styrene) (SBS) polymer on the Kevlar fiber surface, subsequently absorption of the silver precursors followed by reduction, high-performance silver-coated Kevlar fibers were obtained which served as the conductive electrodes in the yarn-based capacitive sensors. As reported, the silver-coated Kevlar fibers exhibited a highly satisfactory electrical performance of 0.15 ohm/cm. The fabrication of this yarn-based capacitive pressure sensor is illustrated in Figure 2.19. This yarn-based capacitive pressure sensor was fabricated by two conductive Kevlar fibers where they were coated with a layer of PDMS, and perpendicularly stacked with each other to form a cross point. The as-made sensor showed a remarkably high sensitivity of 0.21 kPa^{-1} in the low pressure region, and fast relaxation time of less than 10 ms.

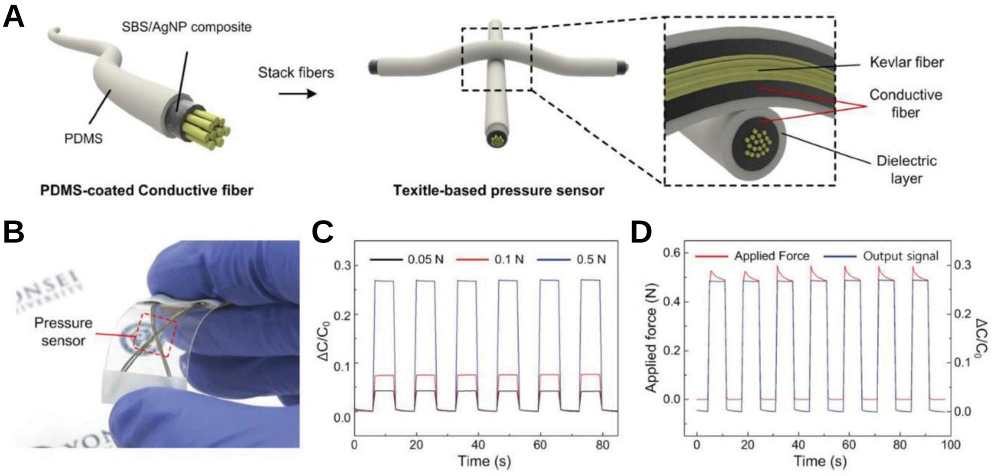

Figure 2.19 (A) Schematic illustration of the fabrication of the pressure sensor. (B) Photograph showing the fabricated pressure sensor on a PET substrate using 2 × 2 conductive fibers. (C) Capacitive response of the pressure sensor for the various applied loads of 0.05, 0.1, and 0.5 N. (D) Response and relaxation curve for the device under repeated application and removal of a 0.5 N load. (115)

2.4.3 Energy Storage Devices

Powering portable electronic devices in wearable electronics are one of the key issues and challenges that require lightweight, long-lasting and stable power output. To date, almost all of the electronic devices rely on the heavy lithium ion batteries, in which they are installed externally as the sole source of electricity. For the realization of truly wearable electronics, many researchers had paid much attention to develop textile-based energy storage, in order to get rid of the disadvantages brought by the conventional batteries.

In 2003, Gui et al. had demonstrated the feasibility of using cotton as a substrate to fabricate textile-based supercapacitors (16). They made use of the mesoporous and water absorbing properties of cotton to act as an interior electrolyte reservoir in the supercapacitors. Some other examples of making yarn-based supercapacitors were demonstrated using carbon materials such as carbon nanotubes and graphene (17, 116). In 2013, Lee et al. had integrated wearable textile battery with solar cells so that it could be recharged by solar energy (117). The device electrodes were fabricated by coating polyester fabrics with nickel in the conventional electroless deposition. The as-made wearable textile battery showed good cycling performance after repeated folding-unfolding actions (Figure 2.20). Later in 2015, Liu et al. demonstrated the making of high-performance supercapacitor yarns (118). The current collectors in the supercapacitors are nickel-coated cotton yarns which were fabricated by polymer-assisted metal deposition (PAMD) (Figure 2.21). The as-made nickel-coated cotton yarns showed a remarkable performance even after of 5000 bending cycles. The nickel-coated cotton yarns were then coated with conductive RGO to yield RGO/Ni-cotton composite electrodes. The final yarn-based supercapacitor was assembled by using two RGO/Ni-cotton composite electrodes, with polyvinyl alcohol (PVA)/LiCl gel as both the electrolyte and separator.

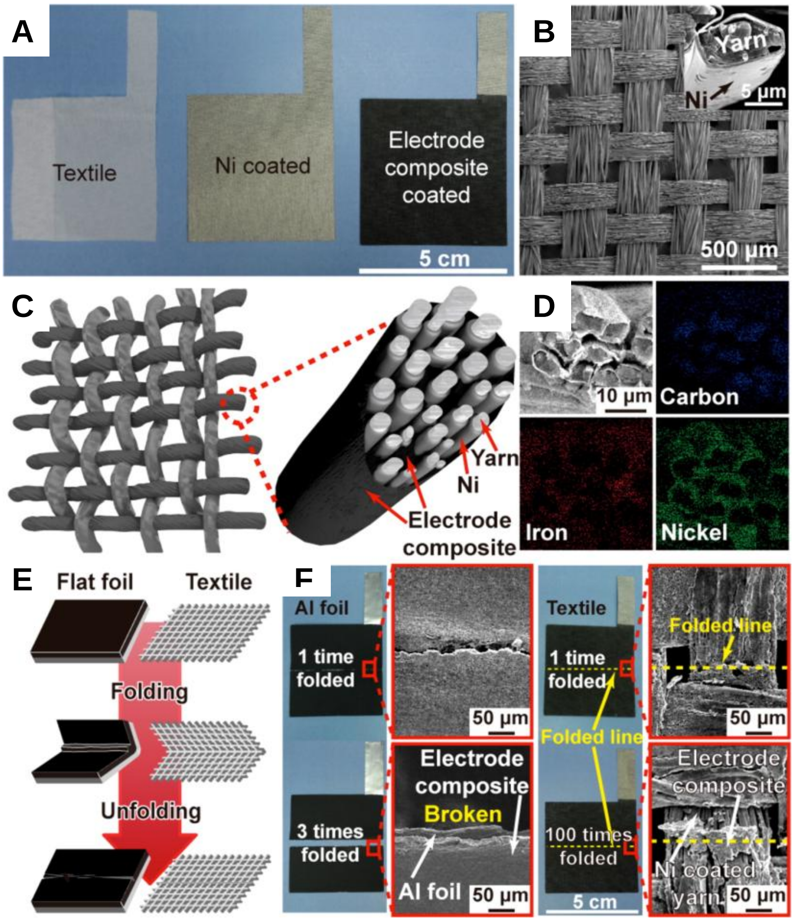

Figure 2.20 Electrode structures of wearable textile battery and its enhanced folding tolerance. (A) Preparation sequence of the active electrode (5 × 5 cm^2). From left to right: bare polyester yarn substrate, Ni-coated textile substrate by electroless deposition method (EDM), and the final electrode after conformal coating of the electrode composite. (B) The morphology of the Ni-coated textile. (Inset) a cross-sectional SEM images of the same Ni coated textile. (C) A schematic illustration of woven battery electrode yarns. A magnified view indicates that each yarn consisting of multiple strands is coated by Ni and battery composite. (D) A cross-sectional SEM image of the composite electrode textile (top left) together with EDS elemental mapping with regard to carbon, iron, and nickel. (E) A schematic comparison between the electrode based on conventional flat metal foil and the textile battery electrode based on the woven yarn during repeated folding tests. (F) Photographs and SEM images comparatively showing distinctive durability between the foil-based conventional electrode and the textile battery electrode (117).

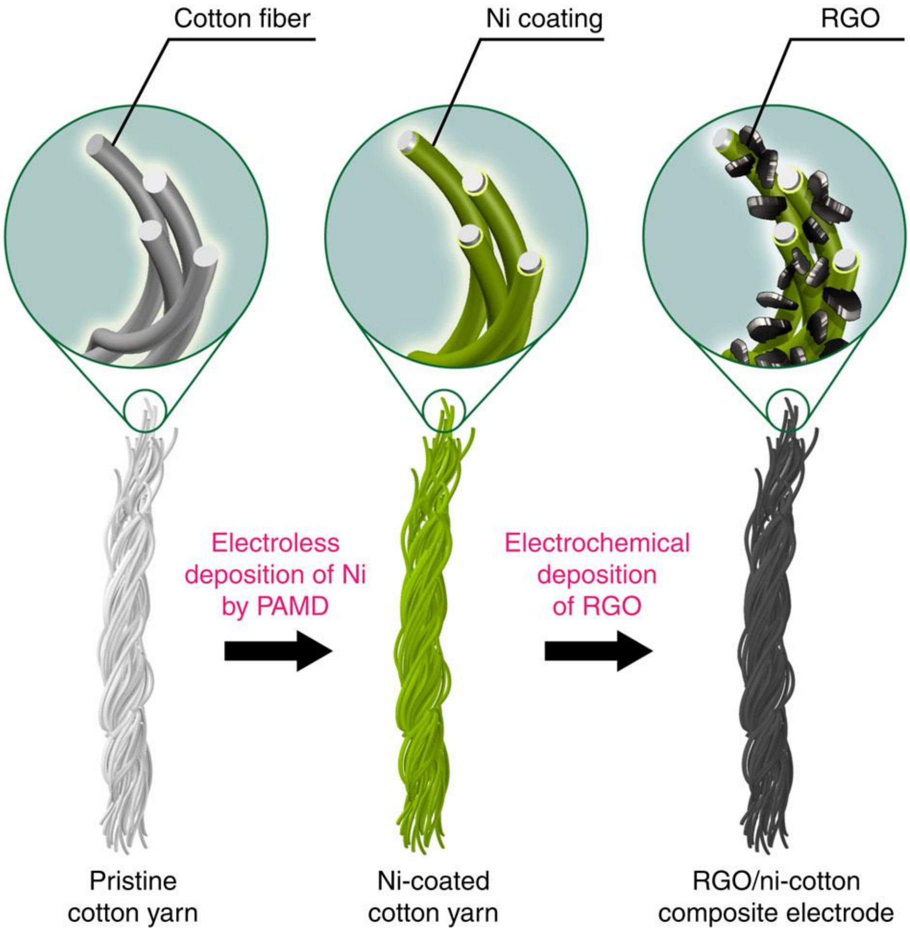

Figure 2.21 Schematic illustration of the fabrication of RGO/Ni cotton yarn composite electrodes. (118)

The performance of the solid-state supercapacitor yarns was shown in Figure 2.22. As shown in the CV curve of the supercapacitor yarn, the shape of the curve at high scan rates was similar to those at low scan rate, indicating that the supercapacitors yarn had a high rate performance and efficient ionic and electronic transports in the electrode materials. The authors also incorporated the supercapacitor yarns in the conventional weaving process to obtain a woven fabric.

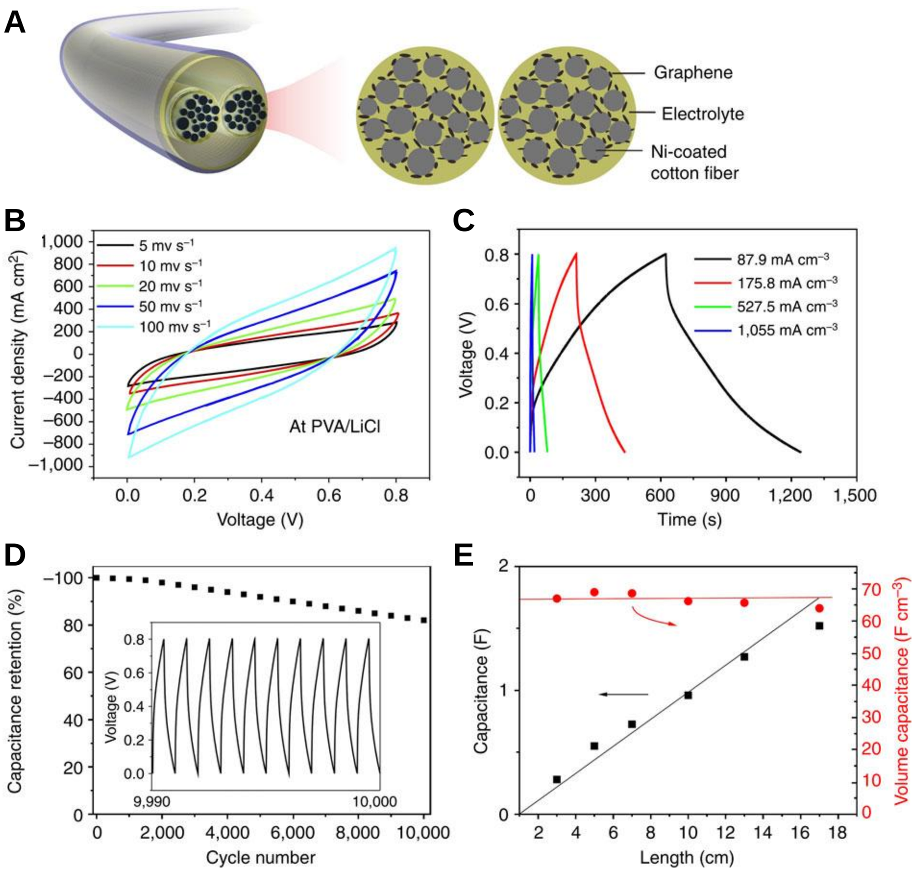

Figure 2.22 (A) Schematic illustration of the structure of one SC yarn. (B) CV curves of the device at scan rates ranging from 5 to 100 mv s^{-1}. (C) GCD curves of the device at different current densities. (D) Cycle life of the device. The inset is the GCD curve from the 9,990th to 10,000th cycle. (E) Device capacitance as a function of the device length. (118)

2.4.4 Triboelectric Generators

In 2012, the first flexible triboelectric generator (TEG) was invented by Fan et al. (119), which was reported as an innovative and effective approach that utilized the distinctively different triboelectric characteristics between two materials to generate an electrical potential. Such a TEG was fabricated by stacking two different polymer sheets which were polyester and polyimide (Kapton) with different triboelectric properties, with metal films deposited on the top and bottom of the assembled structure (Figure 2.23). When the device was subjected to a mechanical deformation, these two different polymer sheets were rubbed against each other. Charge transfer then occurred resulting in the generation of opposite signs of charges distinctively at the surfaces of the two materials. Therefore, an electrical potential was developed. As reported, such a flexible polymer TEG gives an output voltage of up to 3.3 V at a power density of ~10.4 mW/cm^3 (Figure 2.24). They also investigated different device sealing methods and found that they could directly affect the output performance of the triboelectric generator.

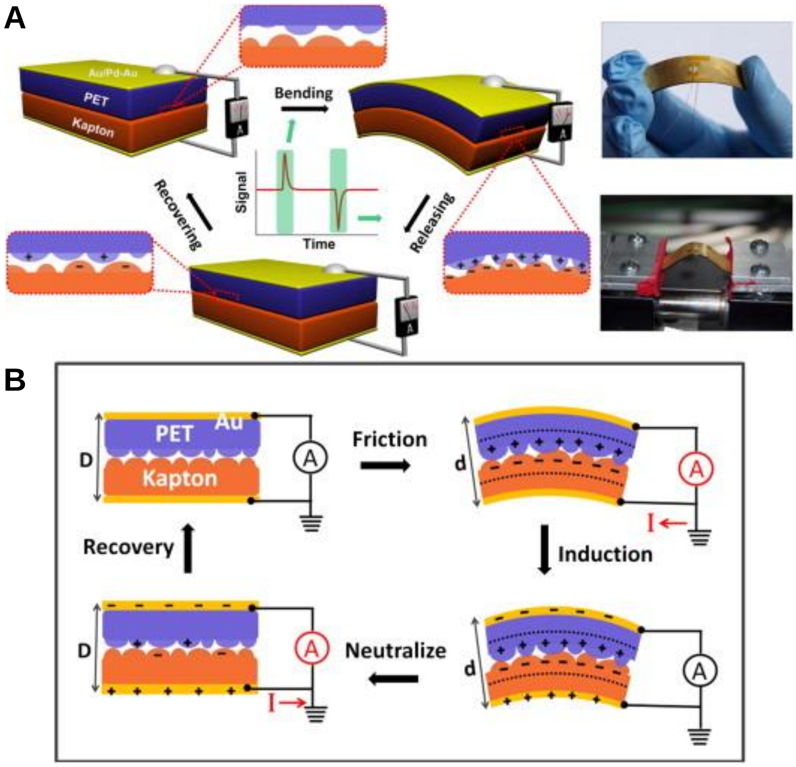

Figure 2.23 Schematic illustrations of the structure and working principle of the triboelectric generator. (A) The structure of an integrated generator in bending and releasing process and related electrical measurement tests. Photographic images of a flexible TEG and mechanical bending equipment. (B) Proposed mechanism of a TEG (see text for details): charges are generated by frictioning two polymer films, which results in the creation of a triboelectric potential layer at the interfacial region (indicated by dashed lines); a mechanical compression results in a change in the distance between the two electrodes (from D to d), thus, under the driving of the triboelectric potential, a change in system capacitance leads to the flow of

current in the external load which drives the flow of the free electrons across the electrodes to minimize the total energy of the system. (119)

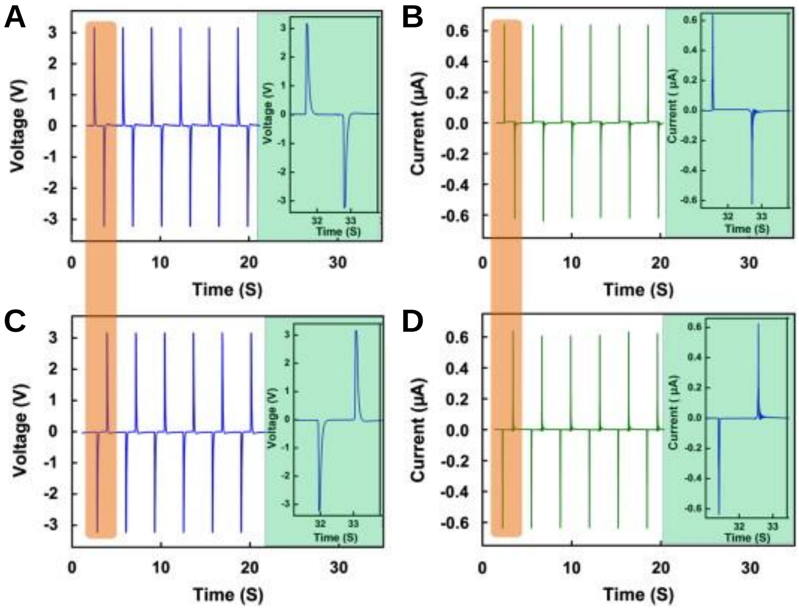

Figure 2.24 Electric output of a typical triboelectric nanogenerator. (A) Open circuit voltage and (B) short circuit current when forward-connected to measurement system. (C) Open circuit voltage and (D) short circuit current when reverse-connected to measurement system. The insets are enlarged views of single signal peak in the voltage and current outputs. Note the forward and reverse connections are defined in reference to the measurement voltmeters for testing if the output signal is truly from the TEG. (119)

Integration of TEG into textile substrates gains high importance in the development of truly wearable TEG. Zhong et al. had later demonstrated a fiber-based generator (FEG) and incorporated this generator into a wireless body temperature sensor system (120). The fabrication of this FBG was simple, which merely consisted of two entangled surface-modified cotton threads. As shown in Figure 2.25a, a cotton thread was coated with a layer of carbon nanotubes (CNTs) while anther cotton thread was coated with both CNTs and polytetrafluoroethylene (PTFE). The mechanism of this FBG with a length of ~9 cm is schematically shown in Figure 2.26a. As reported, the performance of this FEG when connected to an external load of 80 megaohm could have a current output of ~11 nA at a strain value of 2.15 %.

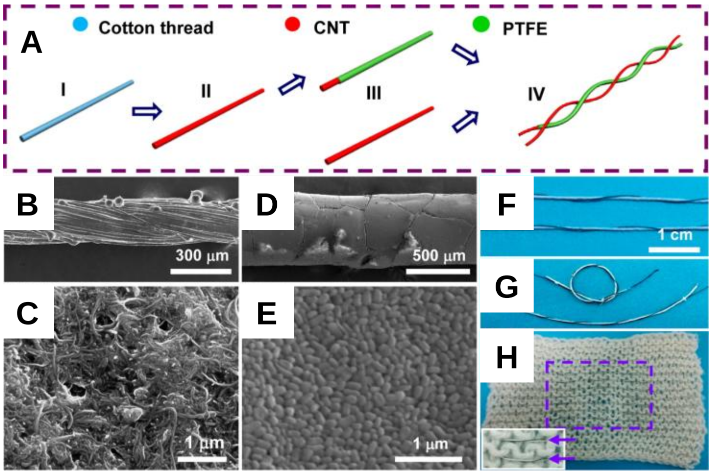

Figure 2.25 Fabrication of fiber-based generator (FBG). (A) Schematic diagram illustrating the fabricating process of an FBG. SEM images of a carbon nanotube coated cotton thread (CCT) with (B) low and (C) high magnification, respectively. SEM images of polytetrafluoroethylene (PTFE) and carbon nanotube coated cotton thread (PCCT) with (D) low and (E) high magnification, respectively. Digital photography of FBGs (F) with linear shape, (G) with curved shape, and (H) woven into fabric. (120)

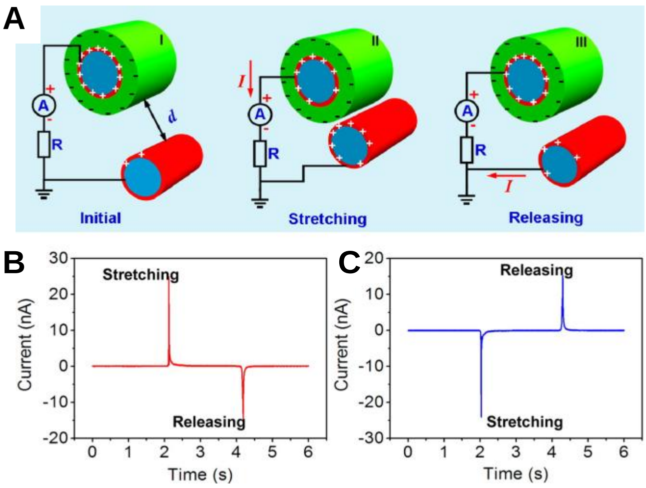

Figure 2.26 Power generation mechanism of the FBG. (A) Schematic diagram illustrating the power generation mechanism of the FBG with an external load of *R* when the device is at (I) the original, (II) stretching, and (III)

releasing states, respectively. The corresponding output current-time curves (B) when forward-connected to the measurement system and (C) when reverse-connected to the measurement system. (120)

2.5 Chapter Conclusion

Conductive textiles are one of the advanced materials, which are highly critical and essential in realizing wearable textile electronics. Particularly, metallic textiles are the most promising in term of their conductivity, low cost and high stability comparing to ICPs and carbon materials such as CNTs. In this chapter, we have reviewed commonly used methods to fabricate metallic textiles, which include electrochemical plating, physical vapor deposition such as thermal evaporation and sputtering, chemical vapor deposition such as atomic layer deposition, and electroless metal deposition. Other methods to produce conductive textiles including the use of intrinsically conducting polymers and carbon materials such as carbon nanotubes and graphene are also reviewed. With vast possibilities of conductive textiles applied in the electronics, demonstrations such as fiber-based transistors, pressure sensors, energy storage devices such as batteries, and triboelectric generators are summarized.

CHAPTER 3: SURFACE MODIFICATIONS OF TEXTILES

3.1 Introduction

Textiles require surface modifications with functional materials, in order to impart extra functionalities to the surface. Surface architecture of textiles, are therefore altered, modified or new functional groups can be introduced to completely change their surface interactions with the surroundings. In this chapter, two common methods for surface modifications of textiles commonly adopted by chemists, material engineers and textile technologists are explored, namely self-assembled mono- or multilayer (SAM) and polymer brush.

3.2 Self-assembled Mono/Multilayer (SAM)

A substrate surface can be modified with new surface functional groups by coating of self-assembled mono/multilayer (SAM). As the name suggests, SAM is a layer of functionalized molecular assemblies spontaneously chemisorbed at the interface until the system approaches equilibrium (121). The first self-assembled layer was demonstrated in 1946 by Bigelow and co-workers (122), who prepared a monolayer of a surfactant on a clean metal surface. However, at that time their discovery and the importance of self-assembly had not been recognized yet until Nuzzo and Allara reported the adsorption of bifunctional organic disulfides on gold surface in 1983 (123). In fact, SAM on the substrate surface not only provides a modified surface chemistry, but also provides new physical properties like wetting and adhesion. Typically, chemicals used to assemble SAM possess a head group at one end and a functional group at the other end. The schematics of SAM formed on the substrate surface is illustrated in Figure 3.1. SAM is deposited by the means of spontaneous chemisorption of head groups of the assembled molecules to the substrate surface by self-assembly, forming a modified layer with functionalized terminal ends protruding away from the substrate surface and interacting with the environment for subsequent chemical reactions.

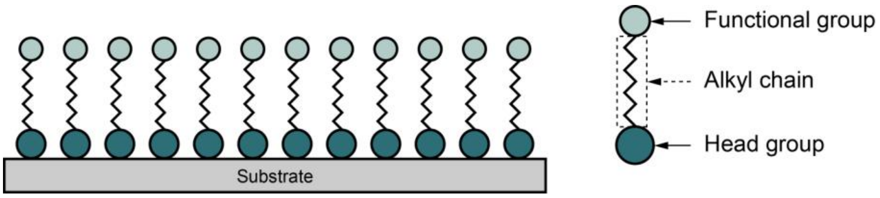

Figure 3.1 Illustration of SAM formation on a substrate surface.

Common chemical species used to fabricate SAM are organosulfur and organosilicon, which are used in modifying metal surface and hydroxylated surface, respectively. Figure 3.2 shows the typical structures of thiol molecule and organosilane molecule. Thiol, one of the sub-groups in organosulfur, has S—H bonding where the sulphur has a high affinity towards metal surface such as gold, silver and copper.

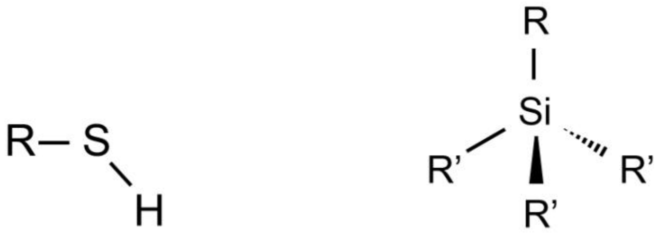

Figure 3.2 Typical structures of a thiol molecule (left) and organosilane molecule (right).

The use of thiol to modify substrate surface had been extensively reviewed by many research groups. However, the use of organosilanes seem rather recognized and attractive, as the only requirement for forming SAM is the presence of hydroxyl groups on the substrate surfaces, which is a lot more common and easier to be achieved by just exposing the substrate to oxygen plasma prior to the surface modifications. Organosilanes are a group silicon containing hydrocarbons, which have chemical structure as shown in Figure 3.2 (right), with R being an alkyl, aryl, or organofunctional group while the R' being methoxy-, ethoxy- or chloro- group. In the past twenty years, much effort had been put in investigating the properties and deposition mechanisms of various organosilanes, to achieve better reproducibility in the monolayer preparation. Common organosilanes are alkyltrichlorosilane and alkyltrialkoxysilane. The former provides a more reactive reaction while the latter is less reactive, however can achieve a multilayer coverage on the substrate surface.

3.2.1 Alkyltrichlorosilane

Alkyltrichlorosilane is one of the families in organosilanes, having a structure of a centre silicon atom bonded with functional group and three chlorine atoms as shown in Figure 3.3. Commonly used alkyltrichlorosilanes are trichlorovinylsilane, (3-bromopropyl)trichlorosilane, trichloro(phenethyl)silane, (3-methacryloyloxypropyl)trichlorosilane, etc (Figure 3.4).

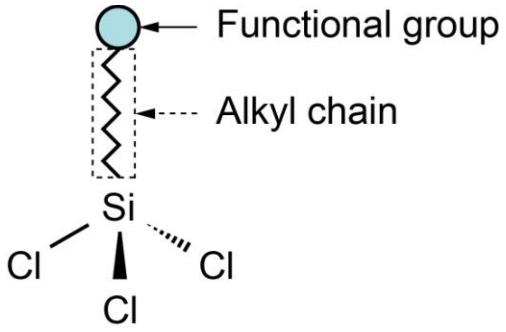

Figure 3.3 Chemical structure of alkyltrichlorosilane.

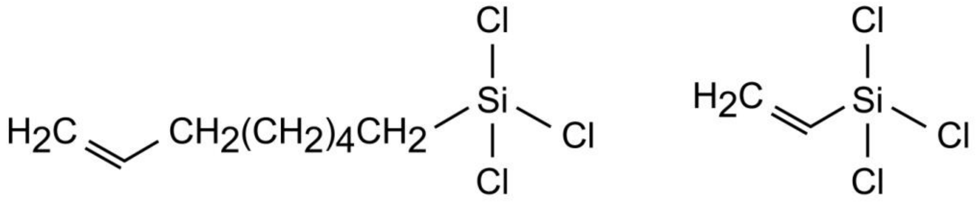

Octenyltrichlorosilane Trichlorovinylsilane

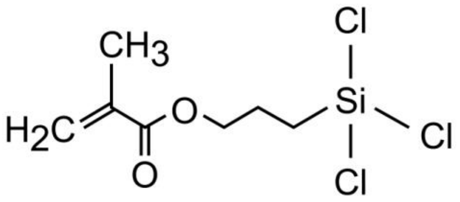

(3-methacryloyloxypropyl)trichlorosilane

Trichloro(phenethyl)silane (3-bromopropyl)trichlorosilane

Figure 3.4 Commonly used trichlorosilanes.

The reaction of trichlorosilanes with substrate of hydroxyl groups on the surface is illustrated in Figure 3.5. When the trichlorosilane molecules get closer to the substrate, hydrolysis is first carried out to form silanols, at the same time releasing hydrochloric acids as by-products. Subsequent covalent grafting of the silanols occurs on the substrate surface where condensation is carried out. Silberzan et al. had first reported on the effect of varying temperature as well as the importance of water traces on self-assembling octadecyltrichlorosilane (OTS) (124). An optimization of the experimental condition in the self-assembly reaction was proposed to get a high quality monolayer. It is worthy to note that successful hydrolysis of trichlorosilane group requires a thin layer of water adsorbed on the substrate surface (125). Other parameter such as solvent selection is also crucial to the quality of the final monolayer. McGovern et al. and Hair et al. verified that a small amount of water is necessary for the silanization, as well as the effect of different solvents on silanization reaction on monolayer quality. According to their report, with suitable solvents such as toluene or benzene, reproducibility of highly dense OTS monolayer can be achieved (126, 127), which can give a relatively higher conformity over the whole substrate surface.

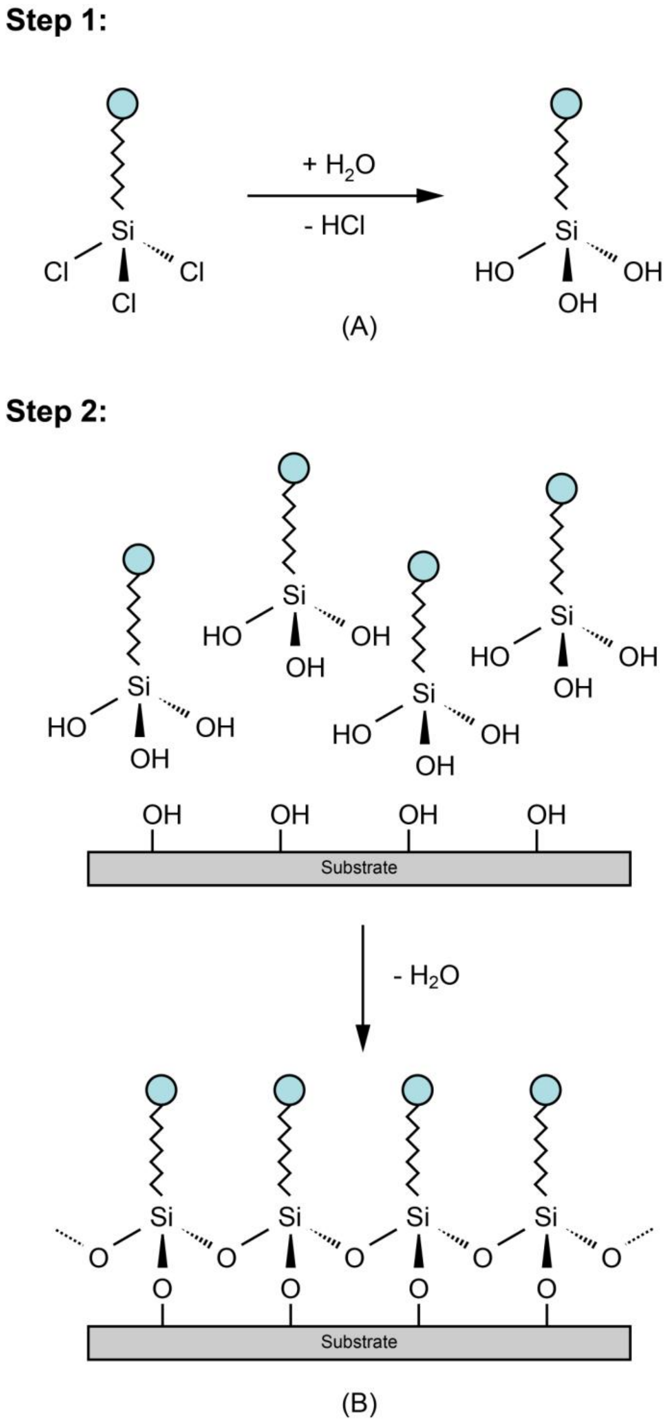

Figure 3.5 Self-assembly of trichlorosilane on substrate. (A) Hydrolysis. (B) Condensation.

3.2.2 Alkyltrialkoxysilane

Alkyltrialkoxysilane is another family of silane coupling agent, which is generally a group of silane that constitutes a structure of a centre silicon atom bonded with one functional group and three alkoxyl groups (Figure 3.6). Commonly used trialkoxysilanes are vinyltrimethoxysilane, (3-bromopropyl)trimethoxysilane, (3-glycidyloxypropyl)trimethoxysilane and (3-aminopropyl)triethoxysilane) (Figure 3.7). For successful chemical deposition of trialkoxysilane on the substrate, hydrolyzed trialkoxysilane is firstly obtained like the one occurs in tricholorsilane. However, the hydrolysis conditions of trialkoxysilanes are quite different from that of tricholorosilane. Trialkoxysilanes hydrolyze stepwise either in acidic or alkaline condition to give the corresponding silanols, which subsequently condense to siloxanes (Figure 3.8). The rate of hydrolysis highly depends on the pH values of the surround medium where the trialkoxysilane is dissolved in, and also the order of trialkoxysilane. The higher the order of the trialkoxysilane, the slower the rate will be the hydrolysis. At a pH of 3-5, dilute solutions are stable for more than a day and consist predominantly of the monomeric silane triol.

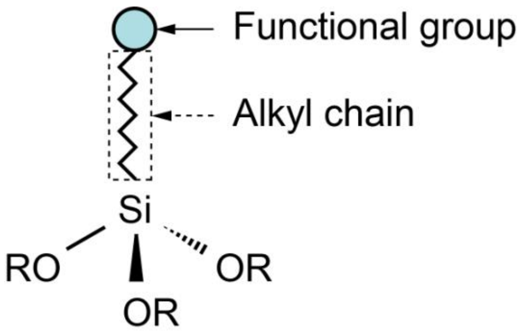

Figure 3.6 Typical structure of an alkyltrialkoxylsilane molecule.

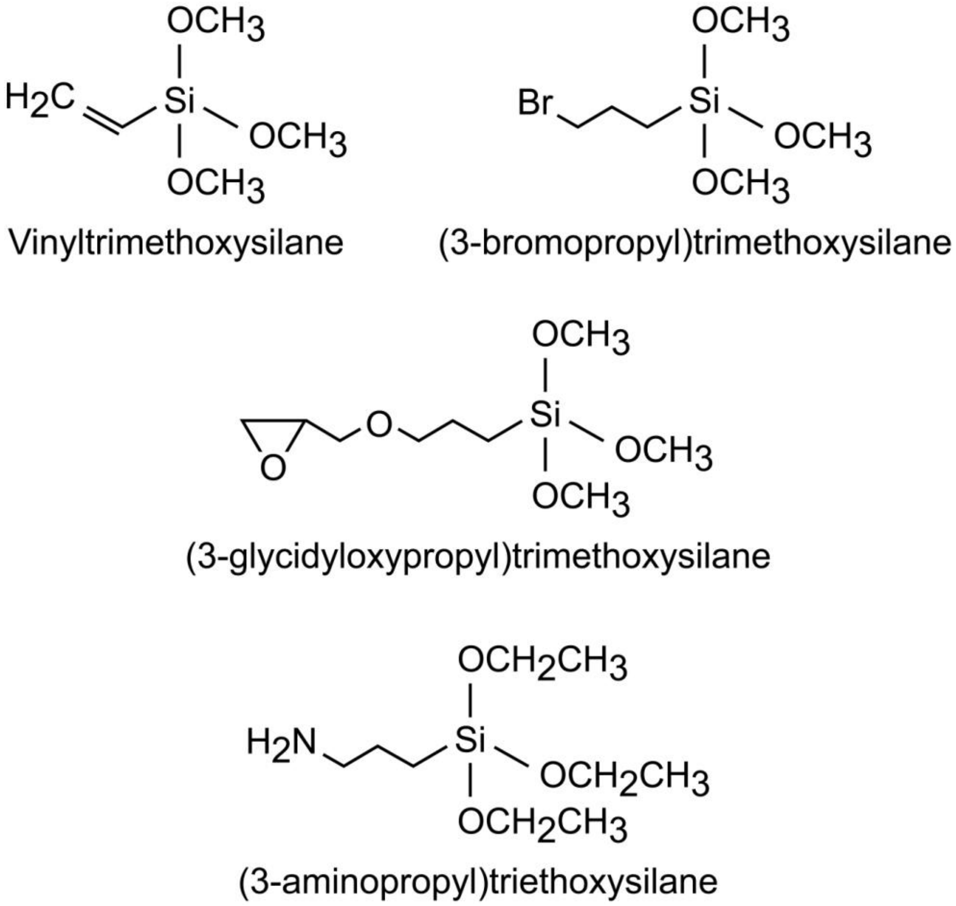

Figure 3.7 Commonly used trialkoxysilanes.

To date, the use of organosilane as self-assembled layer extends to different fields owning to that desirable functional groups that can be introduced into the system, thus changing the bulk behavior of the materials itself. In addition, the ease of fabrication under ambient condition is another advantage. Recent development of organosilane had received considerable attention, especially in electronics, surface superhydrophobicity and bio-sensing (128-132).

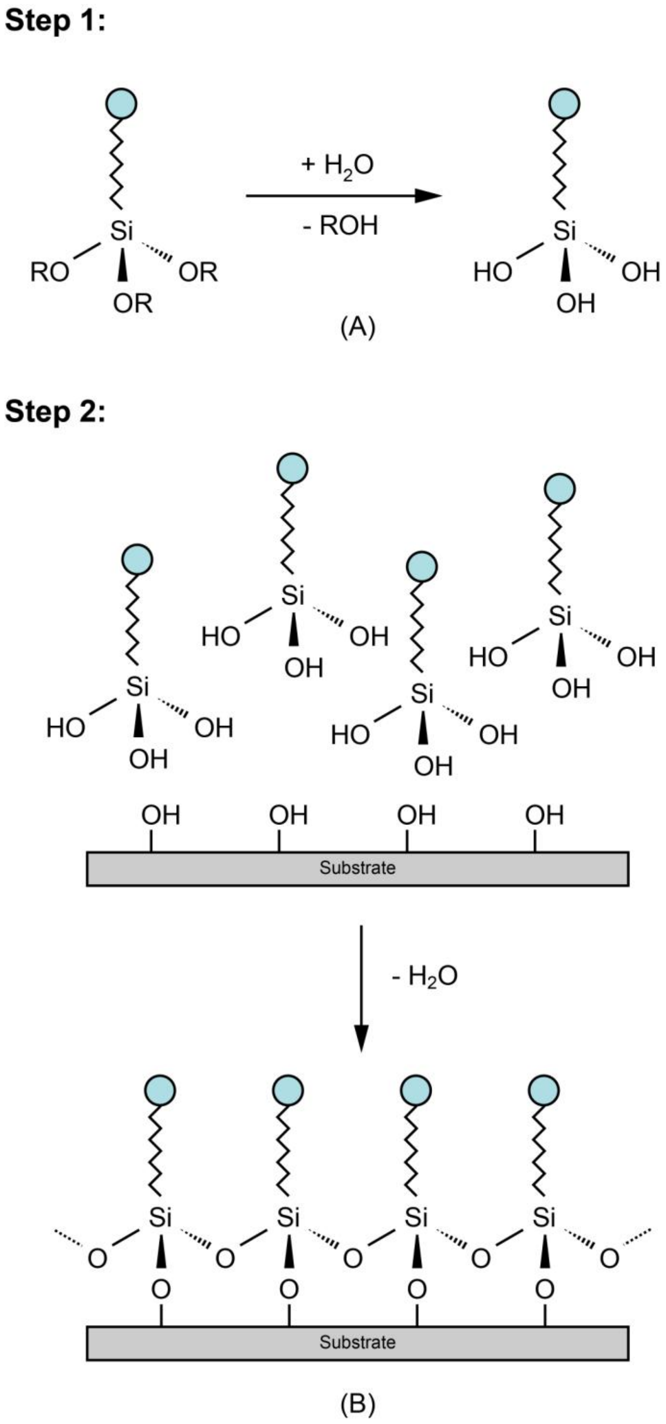

Figure 3.8 Self-assembly of trialkoxysilane on substrate. (A) Hydrolysis. (B) Condensation.

3.2.3 Applications

SAM has gained much attention in modifying the surface architecture, also in the surface modifications of textile materials. The most common known textile modified with SAM is the superhydrophobic effect (with a water contact angle larger than 150°) on the substrate surface, to impart the self-cleaning properties of the fabrics. In 2008, Li et al. reported the fabrication of superhydrophobic cotton fabric and paper by coating with polymethylsilsesquioxane in polycondensation reaction of the hydroxyl between cellulose and the silanol (133). The chemical reaction is illustrated in Figure 3.9.

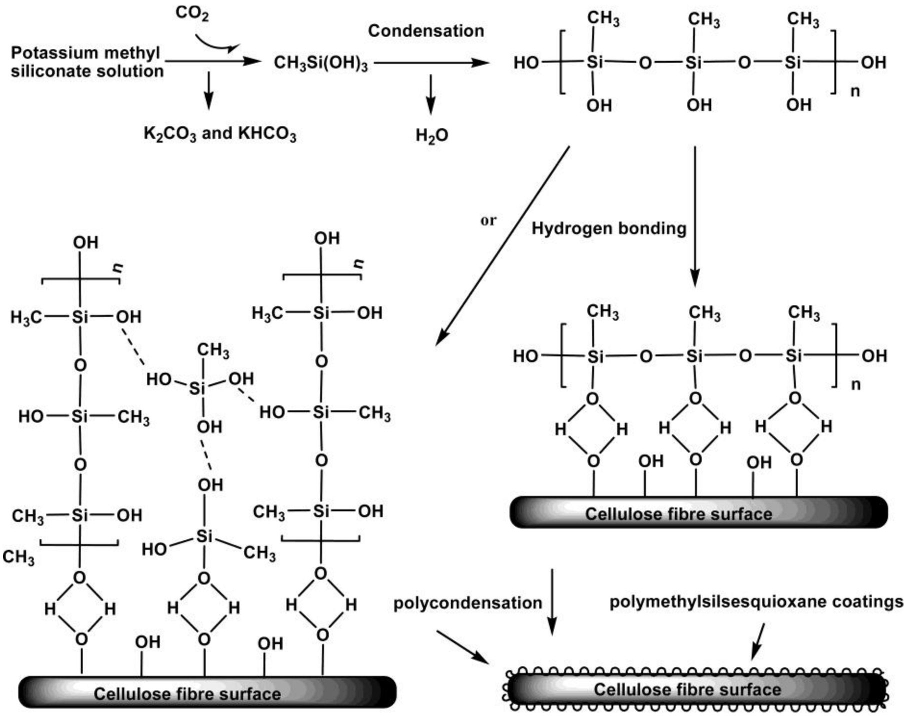

Figure 3.9 The formation of a superhydrophobic polymethylsilsesquioxane coating on a cellulose fiber surface. (133)

In 2013, Guo et al, reported the coating of silver nanoparticles on the cotton fabric surface using the SAM as the modifying layer of the cotton textiles (134). They first modified the cotton fabric surface with a layer of 3-aminopropyltrimethoxysilane. By direct reduction of silver ions with sodium citrate as the reducing agent assisted with microwave irradiation, silver nanoparticles were then coated on the cotton surface.

3.3 Polymer Brush

3.3.1 Overview

Polymer brushes are assemblies of macromolecules chains with one end chemically tethered to a substrate. With sufficiently high grafting density, such chains are forced to induce significant stretching away from the substrate surface (135-137). The morphology of polymer brushes on the substrate highly depends on the grafting density of the polymer brush, in which grafting density highly depends on the synthesis approach adopted, as well as the density and distribution of the SAM molecules.

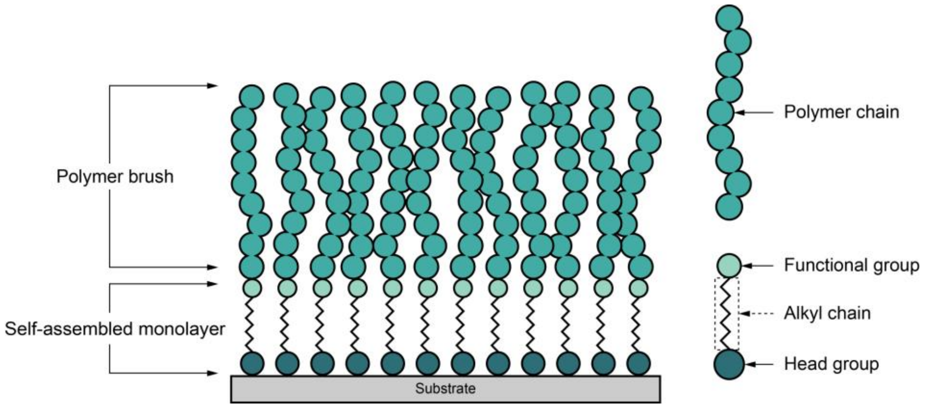

Figure 3.10 Schematic presentation of substrate with deposited SAM and grafted polymer brushes.

At high grafting density, polymer chains are forced to stretched away so as a result of steric repulsion between each other. Brush-like confirmation will be resulted. At low grafting density, polymer chains adopt mushroom or pancake confirmation. Illustration of different morphologies of polymer brush is present in Figure 3.11. Different grafting approach will directly influence the surface features, as well as the physical and chemical properties of the polymer brushes.

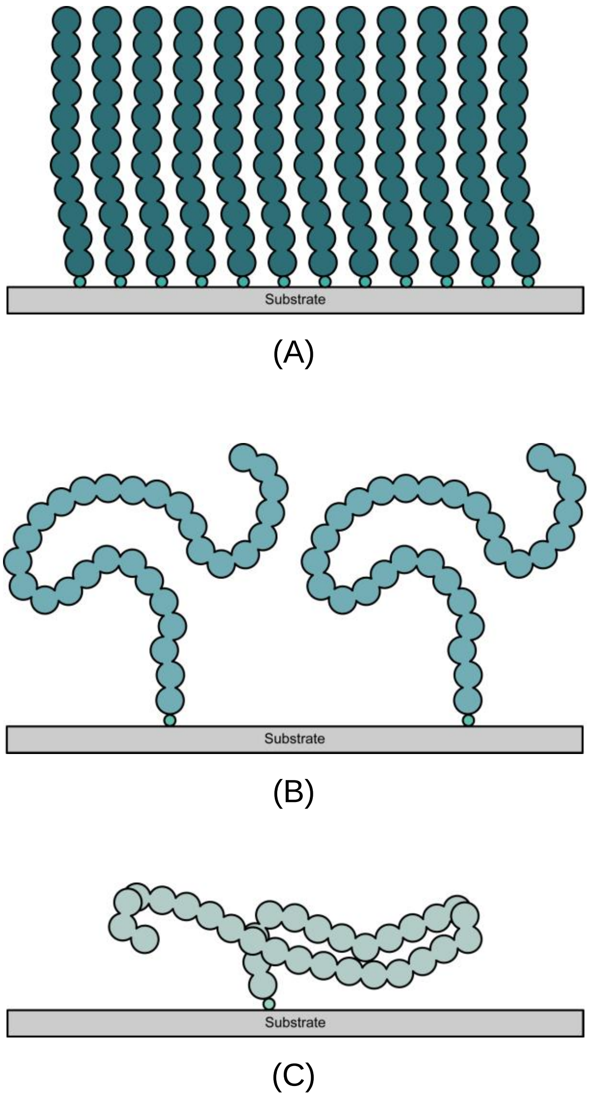

Figure 3.11 Different configurations of polymer brushes relating their grafting density. (A) Brush. (B) Mushroom. (C) Pancake.

Among different polymerization techniques, radical-based polymerization has dominated the synthesis of polymer brushes. The most utilized method is the surface-initiated atom transfer radical polymerization (SI-ATRP), which adopts the ‘grafting from’ synthesis technique which is mentioned below. SI-ATRP reaction was reported by Huang and Wirth. They synthesized poly(acrylamide) (PAM) brushes on silica (138). Ejaz et al. also used SI-ATRP to prepare poly(methylmethacrylate) (PMMA) brushes on silane SAM (139). Other than SI-ATRP, conventional free radical polymerization is also applicable in grafting polymer brushes in-situ (140-143). In 1998, Prucker and Rühe synthesized a smooth polystyrene film on a silicon wafer, with film thickness that could be adjusted over a wide range up to several hundred nm (140). In their approach, they first prepared the substrate surface with a layer of SAM of radical chain initiator. The polymer brushes were then fabricated on top by polymerizing monomers in-situ (Figure 3.12), which was the first concept of modifying the surface with SAM and subsequent free radical polymerization described in the literature.

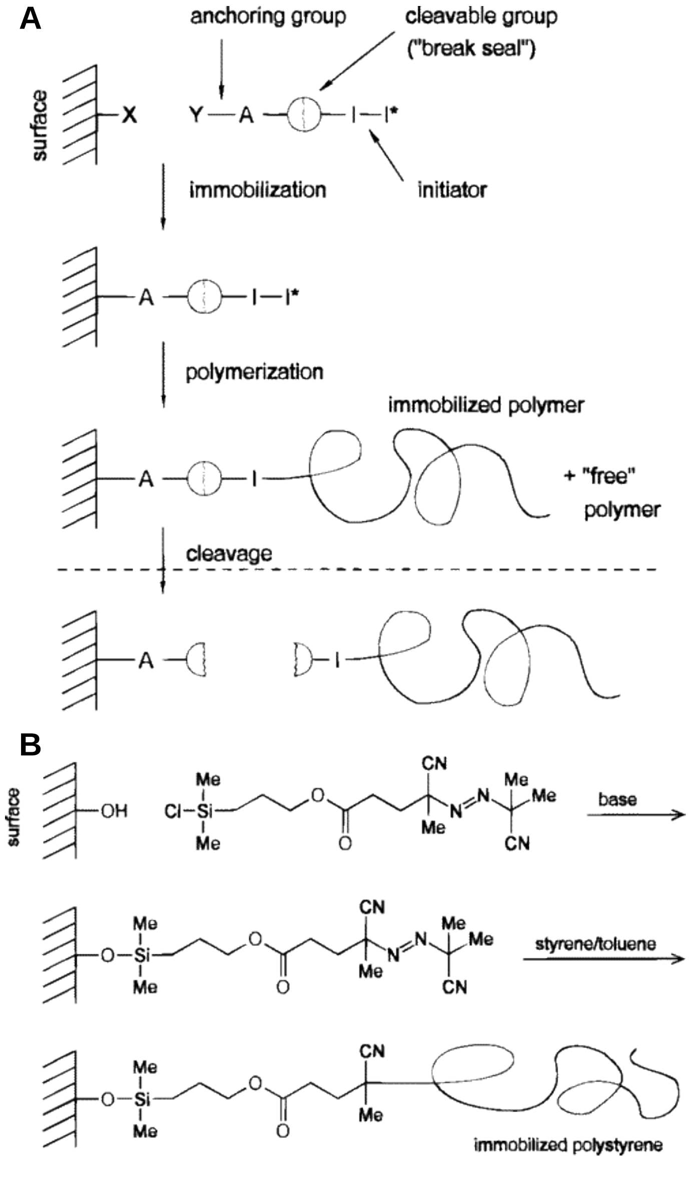

Figure 3.12 (A) Concept for the synthesis of covalently attached polymer monolayers via radical graft polymerization ("grafting from" technique) using immobilized initiators. (B) Synthesis of monolayers of polystyrene terminally

attached to SiO_x surfaces by using a self-assembled monolayer of AIBN like azo compound with a chlorosilane headgroup. (140)

3.3.2 Types of Polymer Brushes

Polymer brushes can be sub-categorized into three types, namely cationic polymer brushes, anionic polymer brushes and nonionic polymer brushes (55). Only cationic and anionic polymer brushes are described here briefly.

3.3.2.1 Cationic Polymer Brushes

Cationic polymer brushes are the positively-charged polyelectrolytes in aqueous condition, which are able to capture anionic moieties for further chemical reactions. Examples of cationic polymer brushes are the extensively reported poly[2-(methacryloyloxy)ethyl]trimethylammonium chloride (PMETAC) and poly[1,1'-bis(4-vinylbenzyl)-4,4'-bipyridinium dinitrate] (PVBVN). Chemical structures of PMETAC and PVBN are illustrated in Figure 3.13.

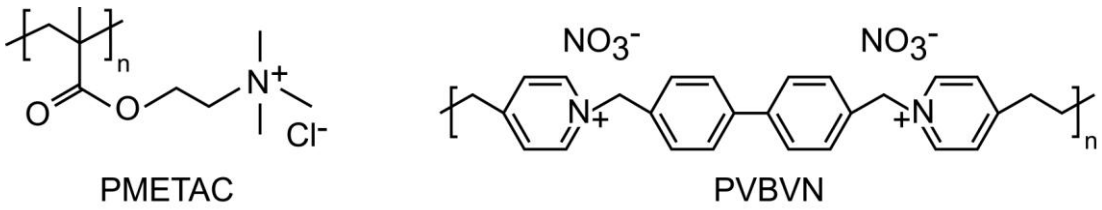

Figure 3.13 Chemical structures of PMETAC and PVBN.

Azzaroni et al. first demonstrated the utilization of a PMETAC brushes which were grafted selectively on substrate surface by SI-ATRP. PMETAC brushes could then capture anionic catalytic moieties $PdCl_4^{2-}$ for subsequent metal electroless deposition (ELD) where a robust metal layer was selectively deposited with outstanding adhesion properties (60). In 2010, Liu et al. reported a versatile approach to preparing highly durable conductive cotton yarns by growing PMETAC brushes on cotton fiber surfaces using surface-initiated atom transfer radical polymerization (SI-ATRP) (61), which was the first ever demonstration on grafting of PMETAC brushes on natural textile fibers. Subsequent metal ELD yielded conductive cotton yarns with high electrical stability that could withstand multiple bending, stretching, rubbing and even washing cycles (Figure 3.14).

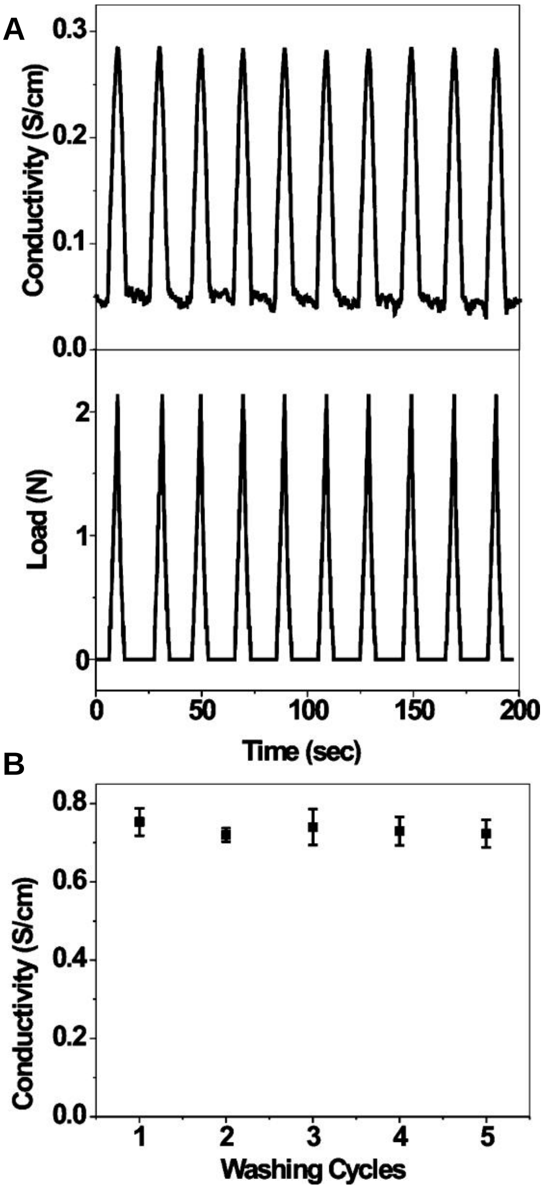

Figure 3.14 (A) Conductivity test of the conductive cotton yarn (30 min plating) under repeatable stretching and relaxing cycles. The upper part shows the conductivity readout, whereas the bottom part shows the loading readout. The conductivity of the conductive cotton yarn increases when the

applied load is increase. (B) Washability test of the conductive cotton yarns (60 min plating). The conductivity maintains constant after 5 washing cycles. (61)

Other than PMETAC, Cui et al. demonstrated the fabrication of silver-coated polyimide film via UV-induced surface graft copolymerization of 1,1'-bis(4-vinylbenzyl)-4,4'-bipyridinium dinitrate (VBVN) to yield PVBVN bonded to the PI film surface (144). The experimental procedures are illustrated in Figure 3.15. After grafting of PVBVN brushes, silver metal was deposited onto the polymer layer by electroless metal deposition (ELD).

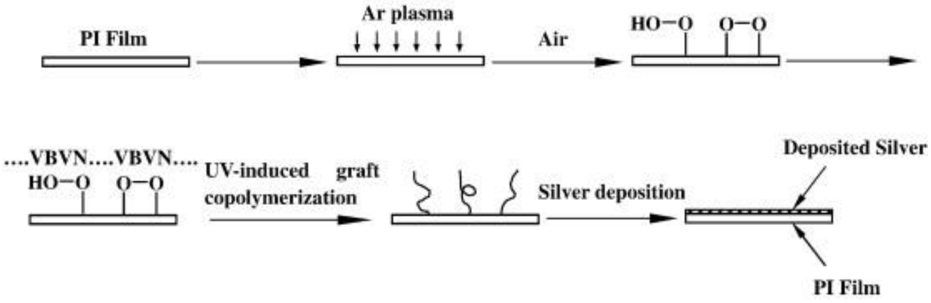

Figure 3.15 Schematic diagram illustrating the processes of Ar plasma pretreatment, graft copolymerization of VBVN with the PI, and electroless deposition of silver. (144)

3.3.2.2 Anionic Polymer Brushes

Anionic polymer brushes are the negatively-charged polyelectrolytes in aqueous solution, which are able to capture cationic moieties for subsequent chemical reactions. Examples of anioic polymers are poly(methacrylic acid sodium salt (PMANa), poly(acrylic acid sodium salt) (PAANa), poly(acrylic acid) (PAA) and polymethacryloyl ethyl phosphate (PMEP) (Figure 3.16). Grafting of PMEP was demonstrated by Liu et al. in 2009 (58). They fabricated two oppositely charges polymer brushes which were cationic PMETAC and anionic PEMP via SI-ATRP on a substrate. Respective immobilization of catalytic anionic moieties $PdCl_4^{2-}$ for PMETAC and cationic moieties $Pd(NH_3)_4^{2+}$ for PEMP were then carried out. Subsequent copper and nickel ELD yielded bimetallic patterns on the substrate (Figure 3.17). In 2010, Garcia et al. reported the electroless plating of copper on the acrylonitrile-butadiene-styrene-polycarbonate (ABS-PC) and polyamide (PA) polymers by grafting of poly(acrylic acid) (PAA) via a GraftFast process (145). They introduced such a process namely ligand induced electroless plating (LIEP). Later, they used LIEP to fabricate patterned localized copper tracks via photolithography and direct printing by laser printer (146).

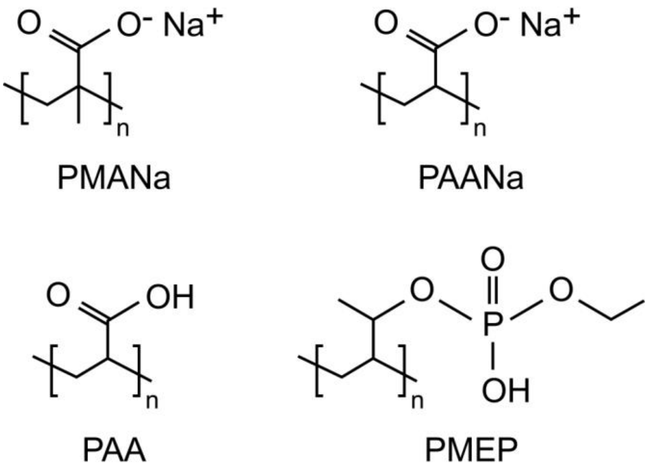

Figure 3.16 Chemical structures of PMANa, PAANa, PAA and PMEP.

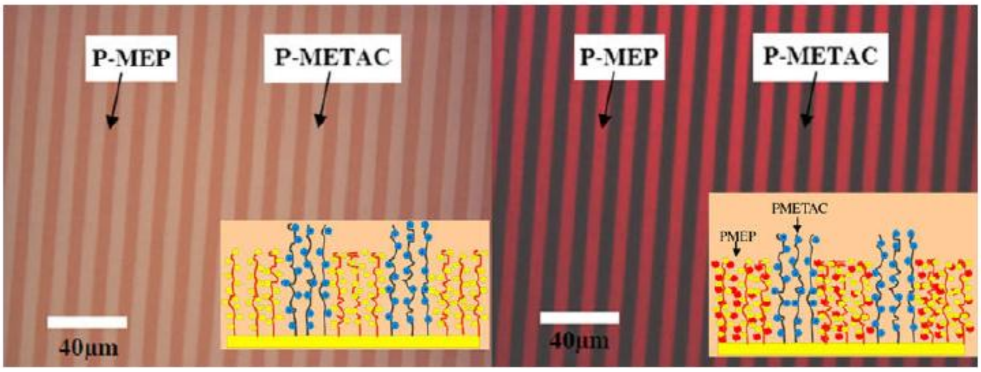

Figure 3.17 Binary PMEP/PMETAC brushes from patterned initiators and two-step surface-initiated polymerization and dye staining (acridine). (58)

3.3.3 Polymer Brush Synthesis

3.3.3.1 'Grafting To' Approach

'Grafting to' synthesis is the approach to chemically bind already-polymerized polymer chains to the complementary reactive groups on the substrate surface (Figure 3.18). Polymer brush layer synthesized by this approach usually results in a relatively limited brush thickness of ~1-5 nm (140). In the 'grafting to' process, already-polymerized polymer chains in the reaction solution compete with each other for the binding sites on the substrate, in which the rate of binding quickly levels off due to lesser binding sites available for reaction and steric hindrance from the polymer itself and also from the neighboring adsorbed chains. As a result, it is very difficult to achieve high grafting dentistry by this approach. In addition, once the substrate surface is soon occupied by competing polymer chains, the concentration of brush at the substrate surface is higher than that in the reaction solution. Additional polymer chains must diffuse against the concentration gradient to reach the substrate surface. Therefore the reaction soon becomes energetically unfavorable and self-limiting after certain reaction time (147).

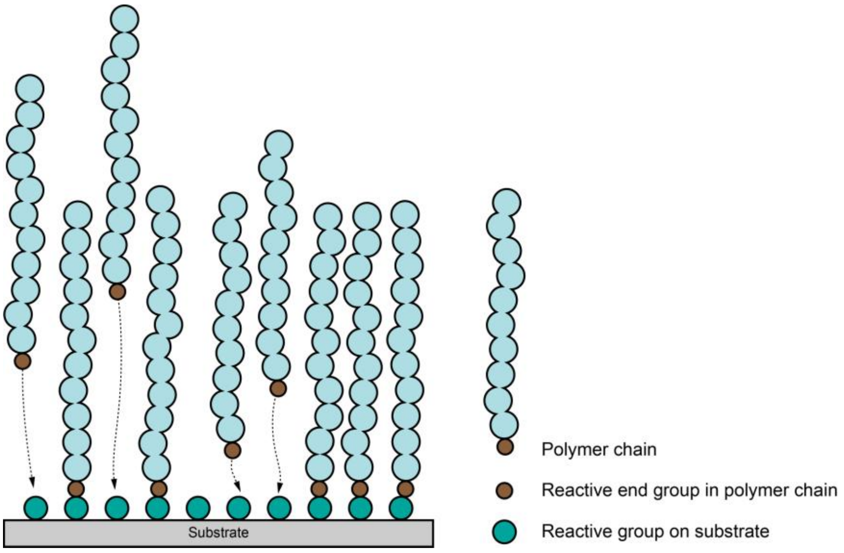

Figure 3.18 'Grafting to' synthesis of polymer brushes.

3.3.3.2 ‘Grafting From’ Approach

‘Grafting from’ synthesis is another approach for grafting polymer brushes on substrate surface. ‘Grafting from’ polymerization is also called ‘surface-initiated polymerization’ (148). Different from the ‘grafting to approach, already-polymerized chains are not present in the reaction solution but the monomer constituting the polymer chain to be polymerized. In a typical ‘grafting from’ process, a layer initiation site is first deposited onto the substrate surface. Introduction of monomer solution immediately induces the polymerization starting from the initiation site as illustrated in Figure 3.19.

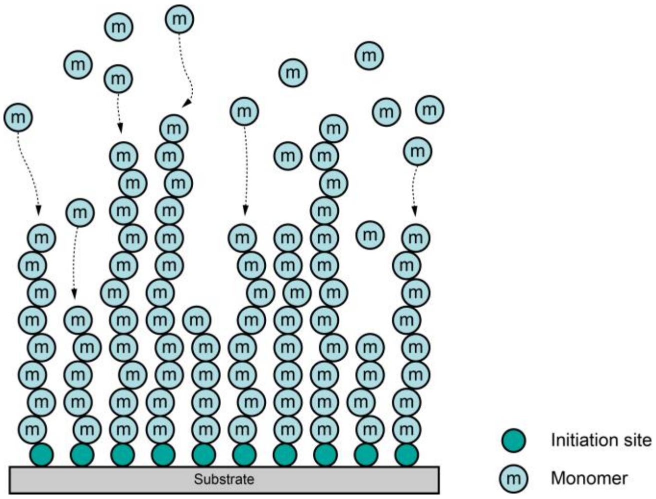

Figure 3.19 ‘Grafting from’ synthesis of polymer brushes.

Generally, ‘grafting from’ approach has many advantages over ‘grafting to’ approach. First, it allows the polymerization reaction to start from the initiation site, so polymer brush thickness can be tuned by adopting different polymerization strategies. Second, polymer brush density can be truly varied according to the density of the initiation sites on the substrate surface. Once the density of the brush is varied, the morphology, and therefore the properties and functionality of the polymer brush can be controlled.

3.3.4 Applications

Polymer brushes have long been used in fabrication of intelligent surface. Self-responsive polymer brushes, being able to respond to the surrounding environment such as solvent, temperature, pH and salt concentration, are always popular in fabricating smart devices. Sun et al. had successfully grafted a V-shaped polymer brushes with two arms of poly[2-(diisopropylamino)ethyl methacrylate] (PDPAEMA) and poly(methylacrylic acid) (PMAA), exhibiting a reversible and preciously controlled wetability and two-way responsive behavior as pH value varies (149). In 2003, Masuda et al. reported the self-oscillating polymer brushes on a glass substrate via SI-ATRP (150), in which a chemical wave that propagated in the polymer brush layer was observed (Figure 3.20). Such an autonomous functional surface can be potentially applied in nanoscale transport system.

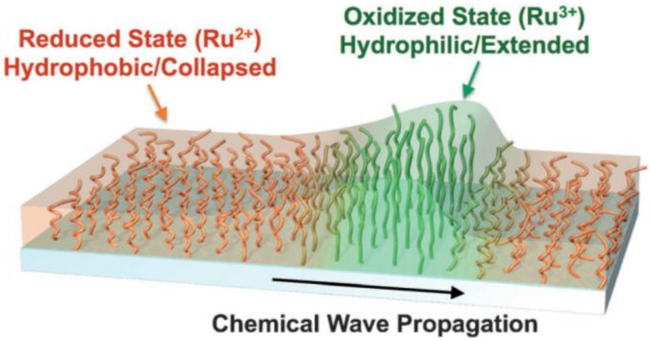

Figure 3.20 Illustration of the self-oscillating polymer brush in operation. (150)

Grafting of polymer brush on textile substrate surface had also been demonstrated in the literature. In 2002, Carlmark et al. first reported the SI-ATRP reaction on the cellulose fibers (151). They modified the cellulose fiber surface with a layer of 2-bromoisobutyryl-bromide as initiator for the subsequent SI-ATRP to graft poly(methyl acrylate) brush on the cellulose fiber surface (Figure 3.18). In 2015, Xue et al. reported the modification of poly(ethylene terephthalate) (PET) fabrics by SI-ATRP of fluorinated methacrylates to obtain a superhydrophobic surface (152). Remarkably, it was found that the superhydrophobic surface remained robust even after treated with 2500 cycles of abrasion, 100 launder cycles and long time exposure to UV radiation.

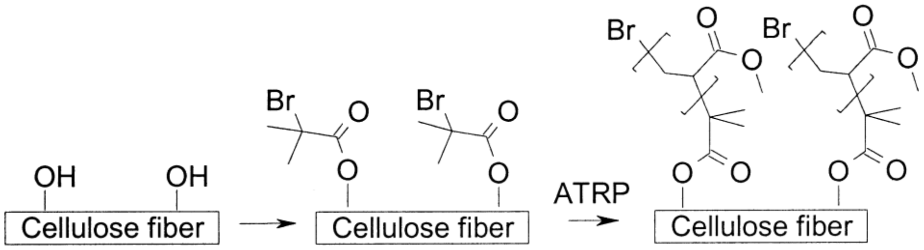

Figure 3.21 The synthetic pathway for the preparation of the PMA-grafted filter paper. (151)

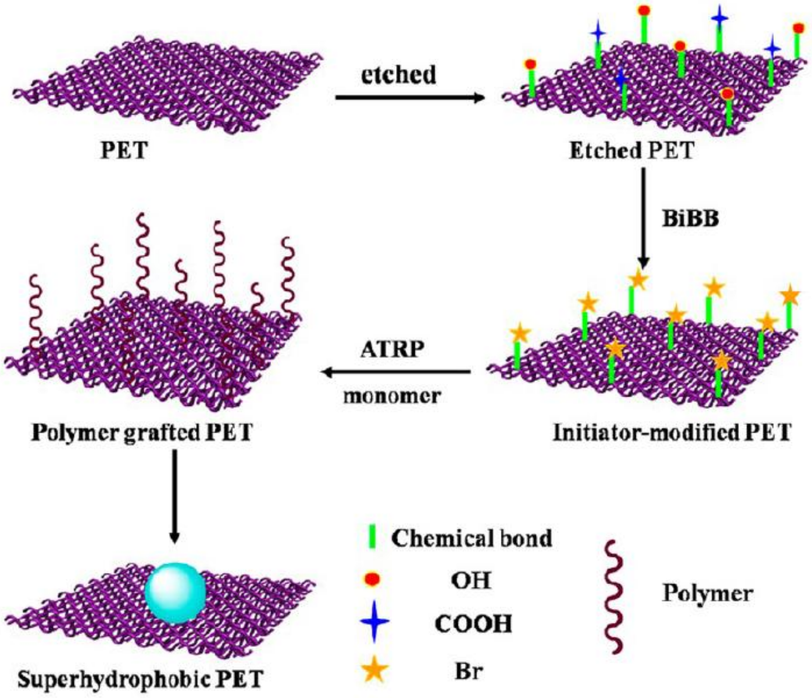

Figure 3.22 Schematic illustration of the fabrication of superhydrophobic fabrics. (152)

3.4 Chapter Conclusion

In this chapter, we review two major techniques to modify textile fiber surface, namely self-assembled mono- or multilayer (SAM) and polymer brush.

Surface modification by SAM involves the deposition of organosilane molecules on the substrate surface, which provides a direct, simple, and relatively-easy-to-control modification route for many industries to apply functionalities on the substrate surface. However, the surface modification by SAM is limited, as the modification is only restricted to a very thin layer of modified functional layer. Therefore, lesser amount of functional groups can be further utilized for high-rate chemical reactions. Alternatively, polymer brushes that grafted on the substrate surface can not only provide bio-sensing, smart switchable and responsive surface, they can also provide three-dimensional morphologies on the substrate surface which widen the flexibility and more functionalities imparted on a substrate.

CHAPTER 4: METHODOLOGY

4.1 Experimental Designs

In this section, the experimental designs are discussed. Surface pretreatment prior to any surface modifications on textiles and the strategy namely polymer-assisted metal deposition (PAMD) adopted in the experiment are introduced. Context will also be focused on the typical procedures in PAMD and its underlying mechanism to achieve robust metal layer on the substrate surface.

4.1.1 Pretreatment of the Textile Materials

Pretreatment of the as-received textile materials is necessary prior to the surface modification, mainly due to the unclean surface with sizing materials as well as machine lubricants imparted on the textile surface during yarn spinning and fabric weaving processes. Natural textile materials such as cotton are cleaned with 1:1 ratio of water and ethanol under ultrasonication, and then again put in DI water again in ultrasonication. Finally the textiles are bleached in the commercially available bleach solution and then rinsed thoroughly in DI water for several times. The natural textiles are then blown dry with compressed air.

The pretreatment of the synthetic textile follows a similar procedure as treating the natural textiles. Synthetic textiles such as polyester and nylon are cleaned with 1:1 ratio of water and ethanol under ultrasonication, and then again put in DI water again in ultrasonication. Finally the textiles are put into the 2 M sodium hydroxide solution for 2 hr at 80 ˚C, in order to render the surface hydroxyl functional groups. Synthetic textiles then neutralized in an acidic solution with few drops of acetic acid are rinsed thoroughly in DI water for several times. The synthetic textiles are then blown dry, and put in the oxygen plasma (Plasma Cleaner, Harrick Plasma PDC-32G) for 5 min to further render the surface hydrophilic.

4.1.2 Polymer-assisted Metal Deposition (PAMD)

After the pretreatment of the textile surface, staring from a pristine textile substrate, the surface of the textile fiber is modified through a series of procedures in which the whole fabrication is named as polymer-assisted metal deposition (PAMD). In a typical experiment, PAMD involves four steps as shown in Figure 4.1: 1) surface modification of substrate with a functional silane layer, 2) grafting of polymer brushes on the silane-modified substrate surface, 3) immobilization of catalytic moieties onto the polymer brushes, and 4) electroless metal deposition (ELD) of metal on the catalyzed areas.

In the first step, surface modification of substrate is carried out by depositing a layer of self-assembled organosilane. The usage of organosilane seems rather common, as the only requirement for silane deposition is the presence of hydroxyl groups on the textile substrate surface. Silane can therefore hydrolyze and condense on the substrate surface to from a well-constructed multilayers. It should be noted that modification of substrate surface with a functional silane layer is critical to the subsequent polymer grafting on the substrate surface, as most of the materials do not possess any functional groups for grafting of polymer brushes. In addition, the selection of silane to modify the substrate surface is of great importance because it determines the polymerization strategy to be adopted in the subsequent polymerization step. In this research, in order to explore the feasibility of grafting of polymer brushes using free radical polymerization strategy, typical silane selected in PAMD is vinyl-terminating, to allow the opening of C=C by free radicals in the subsequent grafting of polymer brushes via free radical polymerization.

After grafting of polymer brushes on the substrate surface, catalytic moieties are immobilized on the polymer brushes in an ion exchange process. The selection of catalytic moieties is highly specific and depends on the chemical properties of the polymer brushes that grafted in the previous step. For example, the most reported cationic polymer brush in PAMD: poly[2-(methacryloyloxy)ethyl]trimethylammonium chloride (PMETAC), is usually couples with anionic catalytic moieties such as $PdCl_4^{2-}$ due to their high affinity to quaternary ammonium group (QA^+) in the PMETAC.

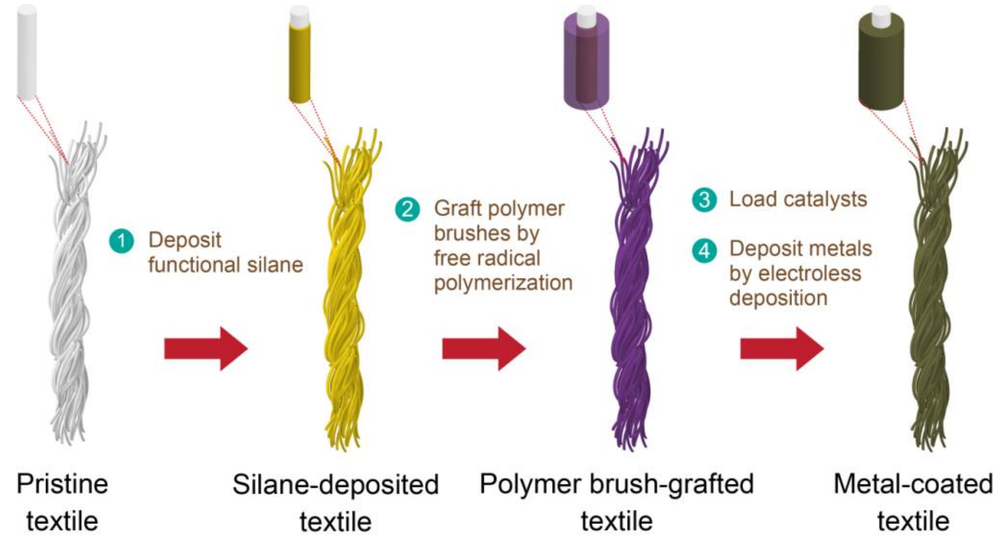

Figure 4.1 Schematic showing the typical process of preparing conductive textiles by grafting polymer brushes via free radical polymerization and subsequently depositing metals by electroless deposition. Such a process of modifying the substrate surface with the subsequent electroless metal deposition is denoted as polymer-assisted metal deposition (PAMD).

For the other polymer brushes such as anionic poly(methacrylic acid sodium salt) (PMANa) and poly(acrylic acid sodium salt) (PAANa), we adopt a slightly different strategy for the immobilization of catalytic moieties for the subsequent ELD. In order to incorporate the metal seeds as the nucleation sites for the growth of metal in ELD, sodium ions on PMANa and PAANa are ion-exchanged with the metal ions of the desired metal to be deposited, followed by the reduction in sodium borohydride solution. A very thin metal seeds for nucleation of metal in subsequent ELD process can be achieved.

In the final step of PAMD, the catalytic moieties loaded substrates are immersed in the ELD plating bath for metal deposition, where the areas immobilized with catalytic moieties act as effective catalytic sites or nucleation sites for ELD of metal. The metal ions in the ELD plating bath are reduced by a reducing agent (formaldehyde and dimethylamine borane for copper and nickel electroless plating, respectively). It should be noted that the loading amount of catalytic moieties plays an important role in the ELD process as scarce loading of the catalytic moieties can only result in thin metal deposited on the substrate.

4.1.3 Selection on Polymer Brush for PAMD

To help further understand the system, the selection on polymer brushes has been restricted in order to allow subsequent ELD to occur. The major criteria is that the polymer brush itself should be capable of being loaded with catalytic moieties or attachment of metal seeds (Cu, Ni, Ag and Au) for subsequent ELD. Some polymer brushes that can be selected for the interfacial layer in PAMD for subsequent ELD are shown in Figure 4.2.

The mostly reported cationic PMETAC brush can couple with anionic catalytic moieties ($PdCl_4^{2-}$) for the subsequent ELD, in which $PdCl_4^{2-}$ species are immobilized on the PMETAC brushes due to their strong affinity towards QA^+ in the brushes. However, another cationic PVBVN brushes assist ELD via a slightly different strategy. PVBVN is a kind of polymer brush that consists of viologen derivatives. Upon UV radiation, the viologen derivative carries out a redox reaction and the metal ions in the solution can be reduced directly on the surface of the viologen-grafted substrate to form a very thin layer of metal seeds. The metal-adsorbed substrate is then put into the ELD solution for the growth of metal. On the other hand, anionic brushes such as PAA, PMANa and PAANa assist ELD in a similar way like PVBVN. They also rely on the loading of a layer of metal seeds where metal can grow in the subsequent ELD process. However, after loading of metal ion on PAA, PMANa and PAANa brushes, an extra step of metal reduction is needed which is usually accomplished by a reducing agent (such as sodium borohydride). Reduction of metal ions can form a thin layer of metal seeds for the subsequent ELD to proceed. Another anionic polymer brush, PMEP, undergoes a very different strategy when comparing to the PAA, PMANa and PAANa brushes. PMEP brushes with phosphate groups have a strong affinity to the catalytic moieties of cationic $Pd(NH_3)_4^{2+}$, therefore grafting of PMEP brushes followed by an ion exchange process is readily for the ELD to grow metal layer on the substrate.

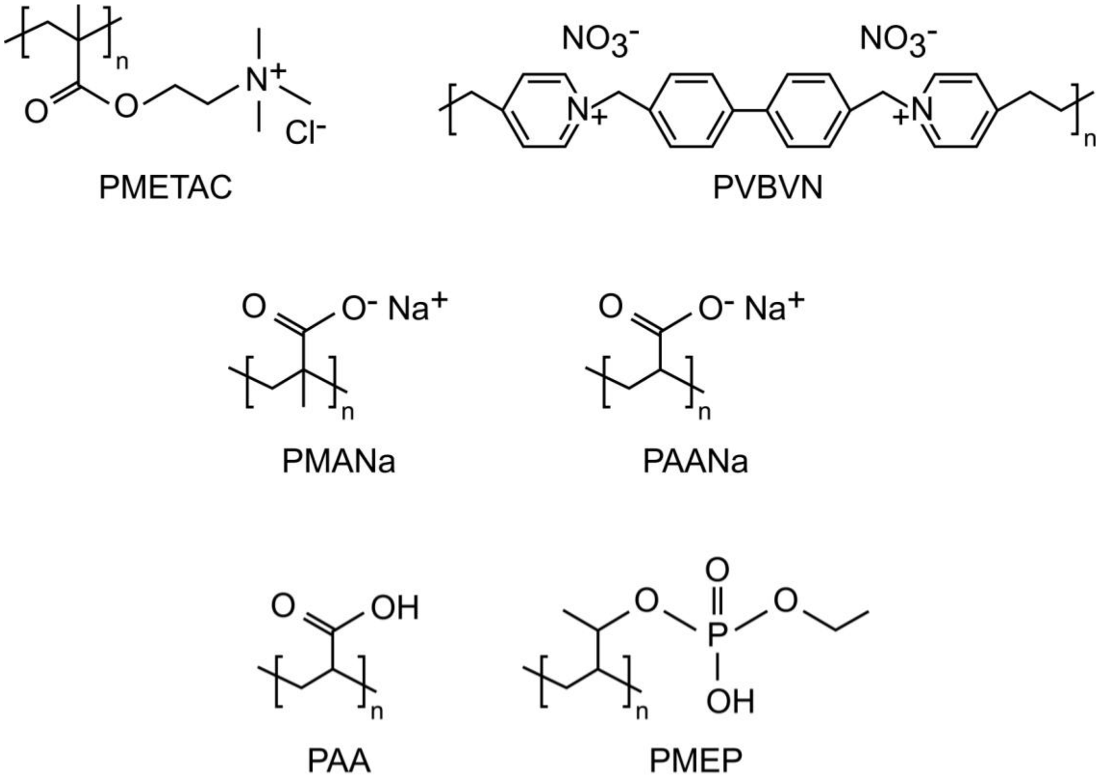

Figure 4.2. Polymer brushes that can be selected as the interfacial layer in PAMD assisting subsequent ELD.

In this research, grafting of cationic polymer brush such as PMETAC and also anionic polymer brushes such as PMANa and PAANa are only selected to graft on textile substrates such as cotton, nylon, polyester, nylon and silk.

4.2 Characterization Methods

To confirm successful surface chemistry of surface modifications on the textile surfaces, several characterization methods are applied, including Attenuated total reflectance-Fourier transform infrared spectroscopy (ATR-FTIR), scanning electron microscopy (SEM), energy dispersive X-ray spectroscopy (EDS) and X-ray photoelectron spectroscopy (XPS). All textile samples are conditioned under standard conditions (21˚C, 65% RH) for at least 24 hr before characterizations and evaluation.

4.2.1 Attenuated Total Reflectance-Fourier Transform Infrared Spectroscopy (ATR-FTIR)

Attenuated total reflectance-Fourier transform infrared spectroscopy (ATR-FTIR) is a kind of characterization method to detect the presence of particular molecular structures on the materials. By placing the sample materials on top of the ATR crystal and passing the infrared (IR) beam to the ATR crystal at an incident angle, total internal reflection of the infrared beam is allowed in the ATR crystal. The infrared beam bounces in the ATR crystal to form an evanescent wave that is in contact with the sample material. Owning to the fact that the vibration or rotation of a molecule is a result of the absorption of a discrete energy value, IR that illuminates on the sample material will be adsorb if that particular bonding is present on the sample materials. In our experiment, attenuated total reflectance-Fourier transform infrared spectrometer (Perkin Elmer Spectrum 100 FTIR Spectrometer) was used to confirm the presence of chemical bonding on the textile surface, to characterize the successful deposition of silane and grafting of polymer brushes.

4.2.2 Scanning Electron Microscopy (SEM)

Scanning electron microscopy (SEM) overcomes most of the optical limitations brought by optical microscopy. The electron beam as the sole ‘illumination source’ in SEM provides higher spatial resolution of the image captured with various magnifications. In a typical SEM, high energy electron beam strikes on the specimen surface, which causes the emission of secondary electrons, backscattered electrons, X-rays, Auger electrons and cathodoluminescence from the sample materials. Signals were collected by respective sensors. Apart from its high magnification performance, SEM can also provide surface topography and distribution of elemental compositions of the sample. In this research, SEM (JEOL JSM 6490) equipped with energy dispersive X-ray analyzer was used to obtain surface morphology of the as-treated textile materials.

4.2.3 Energy Dispersive X-ray Spectroscopy (EDS)

Energy dispersive X-ray spectroscopy (EDS) is to measure the energy of the X-ray emitted from the sample surface. By shining the sample materials with high energy incident electrons, an electron in the inner shell of an element is knocked out, therefore leaving a vacancy in the inner electron shell. Electrons in higher energy state will jump to fill the vacancy, where discrete energy as the characteristics of that specific element is emitted in the form of X-ray photons. As electron shells correspond to particular energy level for an element, the energy of the X-ray emitted is a representative of that specific element. However, as EDS involves the use of a beryllium (Be) window, only elements higher than Be can be detected. EDS is used to characterize the successful grafting of polymer brushes and also the metal deposited after the process of ELD.

4.2.4 X-ray Photoelectron Spectroscopy (XPS)

X-ray photoelectron spectroscopy follows a similar mechanism of the EDS, with the only difference is that the excitations of the inner shell electronics of an element is initiated by the illumination of X-ray photons instead of high energy electrons as in EDS. X-ray photoelectron spectrometer (XPS) (Sengyang SKL-12) was used to analyze the elements present in the sample. Confirmation of the specific elements on silicon wafer in the comparative experiment was confirmed by X-ray photo spectrometry (XPS).

4.2.5 Sheet Resistance

We then studied the electrical resistance of Cu-cotton samples. It should be noted that the conventional four-probe measurement used for Si wafer samples is not suitable for Cu cotton because the fabric surface is extremely rough and its resistance primarily comes from the fiber-to-fiber and yarn-to-yarn contact resistances. Therefore, we adopted a homemade four-probe method based on a recent report by Jur et al. (98). This modified method takes into account of the contact resistance of textile structures and is especially designed for measuring the resistance of fabrics The sheet resistance reported as ohms per square (ohm/sq) of the fabric sample was calculated by ratio of the potential difference to the current obtained in a four-probe setup (Figure 4.3) with Keithley 2400. As charges followed a path of the least resistance, the lower reading by direction was recorded. The electrical sheet resistance of fabric was calculated using Equation 4.1:

$$R_{Sheet} = \frac{V}{I}$$

Equation 4.1

where

R_{Sheet} = Sheet resistance in ohms per square (ohm/sq)

V = Potential difference measured by the voltmeter (V)

I = Current measured by the ammeter in amperes (A)

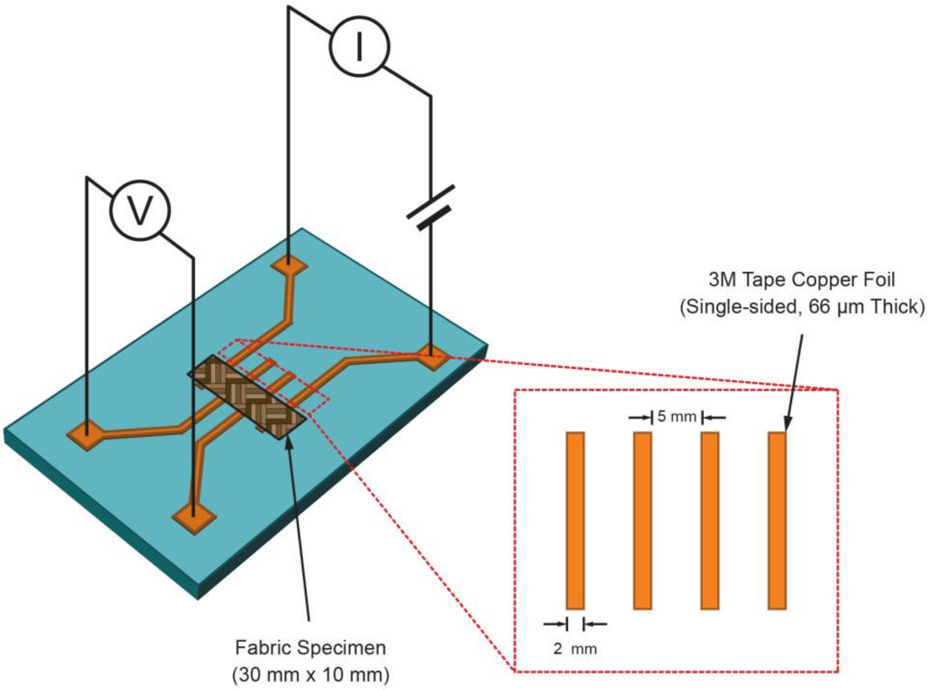

Figure 4.3 House-made four-probe setup for measuring sheet resistance of metal-coated textiles.

(Blank Page)

CHAPTER 5:

FABRICATION OF METALLIC TEXTILES ASSISTED WITH CATIONIC POLY{[2-(METHACRYLOYLOXY)ETHYL]TRIMETHYL-AMMONIUM CHLORIDE} (PMETAC) BRUSHES

5.1 Introduction

With the rapid development of wearable textile electronics that require high-performance flexible conductors for interconnects, contacts and electrodes, the demand for scale production of conductive textiles has been exponentially increasing. In particular, metal-coated textiles are very suitable candidates for wearable textile electronics mainly due to their relatively low-cost fabrication and also high conductivity that metals can achieve when comparing to other conductive materials such as carbon nanotubes (CNTs) and intrinsically conducting polymers (ICPs). To fabricate robust metallic textiles, in 2010, Liu et al. utilized the PAMD approach to fabricating highly durable metallic cotton yarns by growing cationic poly{[2-(methacryloyloxy)ethyl]trimethyl-ammonium chloride} (PMETAC) brushes on cotton fiber surfaces using surface-initiated atom transfer radical polymerization (SI-ATRP) (61), which was the first ever demonstration on grafting of PMETAC brushes on natural textile fibers. Subsequent metal ELD on the PMETAC-grafted cotton yielded metal-coated cotton yarns with high performance and stability that could withstand multiple bending, stretching, rubbing and even washing cycles. However, concerning the feasibility of scale production, demonstration of their work is definitely inappropriate because SI-ATRP suffers two major drawbacks. First, SI-ATRP cannot be carried out under ambient conditions but requires nitrogen protection. Second, SI-ATRP reaction takes up a long period of time that is undesirable and cost ineffective if the process is brought to industrial scale (62, 63). Thus, there is a need to further modify the synthesizing routes to replace SI-ATRP in the fabrication process.

Other than the limitations of SI-ATRP that impede mass production of durable and high-performance metallic textiles, to date, there is still no practical, and user-friendly technology transfer, to allow textile manufacturing sector to utilize current textile manufacturing technology to produce high-performance and durable conductive textiles in bulk. Although surface coating techniques such as physical vapor deposition (PVD) and chemical vapor deposition (CVD) discussed in the literatures are available technologies to give conformal metal coatings on textiles, they often involve great investment in advanced instrumentation, specialized workforce and precise control on parameters. A recent advance on using jig-dye machine, a commonly used textile dyeing machinery, has shown great potential to fabricate conductive cotton fabrics. However, the conductivity achieved is far from satisfactory. Hence, a reliable yet scalable process using textile finishing technologies to voluminously produce high-performance, durable and washable conductive textile still remains a significant challenge.

To address the aforementioned challenges, the versatile approach from Liu et al. is adopted. However it is proposed that conventional free radical polymerization can be carried out to replace SI-ATRP to graft polymer brushes in-situ so as to eliminate the undesirable condition required during SI-ATRP. Conventional free radical polymerization is a rather simpler chemical reaction to grow polymer chains (64-66) and can be carried out under ambient conditions, which is highly advantageous over other means of polymerizations. To fully solve the industrial compatibility problem, we report here the grafting of PMETAC brushes via a first free radical polymerization on the cotton surface, aided by two compatible technologies available in the textile finishing industry for preparing copper-coated cotton fabrics and yarns. The first technology is called pad-dry-cure and the second one is called hank dyeing, respectively suitable for making copper-coated cotton fabrics and yarns. Both pad-dry-cure and hank dyeing assist the PAMD process, in which pad-dry-cure can aid the even monomer uptake of the textile material and the whole polymerization process of PMETAC on textile surface, resulting in the uniform growth of PMETAC brushes for the subsequent ELD to yield high-performance copper-coated cotton fabrics. On the other hand, hank dyeing is a traditional dyeing method to dye hanks of yarn in batches. Remarkably, hank dyeing machine can assist ELD process in PAMD by providing an even distribution and constant flow of ELD solution so as to facilitate the metal deposition process. In this chapter, experimental section will explain the procedures in details, and followed by sample characterizations using ATR-FTIR, EDS, SEM and water contact angle measurement. The sheet resistance and the washing durability according to AATCC 61-2A will also be reported.

5.2 Experimental

5.2.1 Materials

Chemicals used in the experiment were used upon received without further purification unless specified. Commercially purchased 100 % plain weave cotton fabric and cotton yarns (40 s) were pre-treated by singeing, desizing, scouring, bleaching and mercerizing. Vinyltrimethoxysilane (VTMS) (98 %), [2-(methacryloyloxy)ethyl]trimethylammonium chloride (METAC) solution (80 wt. % in H_2O) and ammonium tetrachloropalladate(II) (97 %) were purchased from Sigma-Aldrich®. Potassium persulphate powder and copper(II) sulphate pentahydrate were procured from Acros Organics. Acetic acid, potassium sodium tartrate tetrahydrate and sodium hydroxide were obtained from VWR BDH Prolabo®. Formaldehyde solution (36.5 to 38.0 %) was purchased from Thermo Fisher Scientific Inc.. Deionized (DI) water was used throughout the whole experiment.

5.2.2 Procedures

Silanization. Cotton fabric (15 cm × 10 cm) and 900 m cotton yarns in reel form was cleaned with 1:1 ratio of water and ethanol under ultrasonication for 30 min. Further rinsing of cotton fabric and yarns were carried out by immersing the fabric into DI water for three times, to remove dirt residue physisorbed on the fabric surface. Cleaned cotton fabric and yarns were then dipped into a 5-10 % (v/v) vinyltrimethoxysilane (VTMS) solution (pH = 3.5 adjusted by acetic acid) for 15-30 min. Cotton fabric and yarns were then slightly rinsed by using DI water and subsequently put into a 110 ˚C oven for 15-30 min to yield VTMS-deposited cotton fabric and yarns (VTMS-cotton).

Grafting of cationic PMETAC brushes by in-situ free radical polymerization. The polymerization solution was prepared by mixing 20 % (v/v) of [2-(methacryloyloxy)ethyl]trimethylammonium chloride (METAC) solution (80 wt. % in H_2O), with potassium persulphate powder as initiator (3 mg added per 1 mL of METAC added). Cotton fabric was first immersed into the polymerization solution and rolled through a horizontal padding machine (Rapid Labortex Co., Ltd., PA-0 413). The rolled cotton fabric was then put into the reaction mixture in an oven (Shanghai Jinghong Laboratory Instrument Co., Ltd., DHG-9076A) at 80 ˚C for 1 hr. Cotton yarns were directly put into solution mixture in an oven (Shanghai Jinghong Laboratory Instrument Co., Ltd., DHG-9076A) at 80 ˚C for 1 hr. After polymerization of PMETAC, cotton fabric and yarns were rinsed with DI water for three times. The PMETAC-graft cotton fabric and yarns (PMETAC-cotton) was then hanged dry.

Ion Exchange. The PMETAC-cotton was immersed in freshly prepared 5 mM ammonium tetrachloropalladate(II) solution for 30 min, where $PdCl_4^{2-}$ moieties were immobilized onto the polymer brushes by ion exchange due to their high affinity to QA^+. Rinsing of cotton fabric and yarns were carried out with DI water.

Electroless deposition of copper metal. Cotton fabric was then cut into six small swatches (5 cm × 3 cm). Electroless deposition was performed in each fabric sample for 15, 30, 45, 60, 75 and 90 min, respectively, in a ELD bath containing 1:1 mixture of freshly prepared solution A and B. Solution A contained 13 g/L copper(II) sulphate pentahydrate, 29 g/L sodium potassium tartrate tetrahydrate and 12 g/L sodium hydroxide. Solution B contained 9.5 mL/L formaldehyde solution (36.5 to 38.0 %). Constant stirring of the solution mixture was necessary to provide agitation to the ELD solution throughout the whole ELD process. Cotton yarns were then hanged ontot eh house-made hank dyeing machine filled with 40 L ELD solution. As-deposited copper-coated cotton fabrics and yarns (Cu-cotton) were rinsed thoroughly in DI water for three times and hanged dry under standard conditions (21±1 ˚C, 65±2 % relative humidity) for 24 hr.

Comparative experiment on silicon wafer. Silicon (Si) wafer was used as substrate to confirm the grafting of polymer brush via free radical polymerization. Prior to silanization and grafting of polymer brushes, cleaned Si wafer was exposed to an oxygen plasma in a plasma cleaner (Harrick Plasma Cleaner, PDC-32G-2, USA) for 3 min to render the surface hydrophilic. Free radical polymerization of PMETAC was carried out in beaker for 15, 30 and 60 min under 60 ˚C, 70 ˚C and 80 ˚C. Ion exchange process was carried out by immersed the Si wafer in freshly prepared 5 mM ammonium tetrachloropalladate(II) solution for 30 min, where $PdCl_4^{2-}$ moieties were immobilized onto the polymer brushes by ion exchange due to their high affinity to QA^+. Rinsing of Si wafer was carried out with DI water.

5.3 Results and Discussion

5.3.1 Grafting of PMETAC Brushes on Silicon Wafer

Successful grafting of PMETAC brush by free radical polymerization should first be verified. It is worthy of note that detailed study of the *in-situ* free radical polymerization process directly on textiles is difficult because of their high surface roughness as well as the existence of other physisorbed chemicals. Therefore, we carried out comparative experiments where we grafted PMETAC brushes on flat silicon (Si) wafers following the same procedures and conditions as stated in the experimental section. Prior to any chemical modifications, Si wafers were exposed to an oxygen plasma to render the surface hydrophilic. Oxygen plasma-exposed Si wafers were then allowed to carry out VTMS deposition, free radical polymerization of PMETAC and ion exchange.

Attenuated total reflectance-Fourier transform infrared spectroscopy (ATR-FTIR) was used to confirm the successful deposition of VTMS. As shown in Figure 5.1, ATR-FTIR spectrum of the VTMS-modified silicon wafer (VTMS-Si) shows several distinctive peaks at 1004 cm^{-1} and 1026 cm^{-1} which are attributed by the Si-O-Si stretching vibrations of VTMS, suggesting successful deposition and cross-linking of VTMS on the Si wafer. Distinctive peaks contributed by the stretching vibrations of C=C in VTMS are also observed at 1408 cm^{-1} and 1599 cm^{-1}.

Subsequently, in-situ free-radical polymerization on VTMS-Si was carried out by immersing the VTMS-Si in an aqueous monomer solution under air for 15-60 min at 60-80 °C. ATR-FTIR spectrum of the PMETAC-grafted silicon wafer (PMETAC-Si) shows a relatively weak band between 1700 cm^{-1} to 1800 cm^{-1}, which belongs to the C=O stretching vibration of the PMETAC brushes.

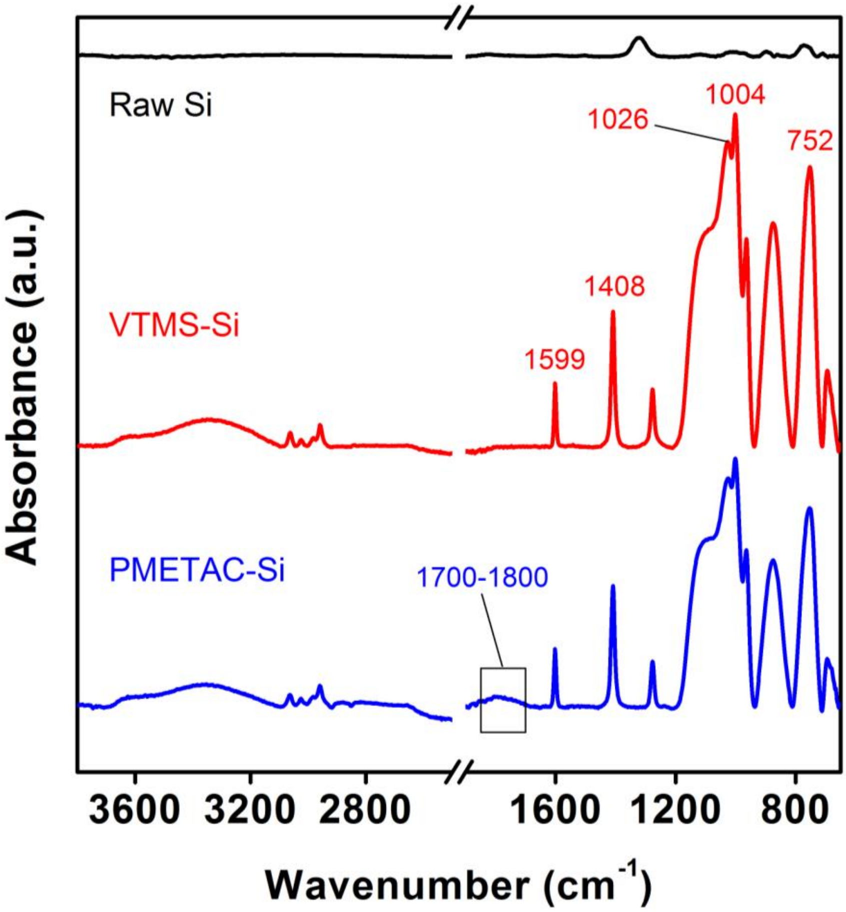

Figure 5.1 ATR-FTIR spectra of the modified Si wafer samples.

Sample	**Distinctive Peaks at Wavenumber (cm^{-1})**	**Corresponding Functional Group**
VTMS-Si	752	Si-C
	1004	Si-O-Si
	1026	Si-O-Si
	1408	C=C
	1599	C=C
PMETAC-Si	1700-1800	C=O

Table 5.1 Summary of the ATR-FTIR data of the modified Si wafer samples.

Successful grafting of PMETAC brushes on Si wafer was also confirmed by X-ray photoelectron spectroscopy (XPS). As indicated in the XPS spectrum shown in Figure 5.2, raw Si wafer mainly possesses silicon and oxygen. After grafting of PMETAC to yield PMETAC-Si, distinctive peaks situates at binding energy value of 404.1 (N 1s) and 200.5 eV (Cl 2p) are attributed by the photoelectrons generated from the nitrogen and chlorine in the PMETAC brushes, respectively (Figure 5.3).

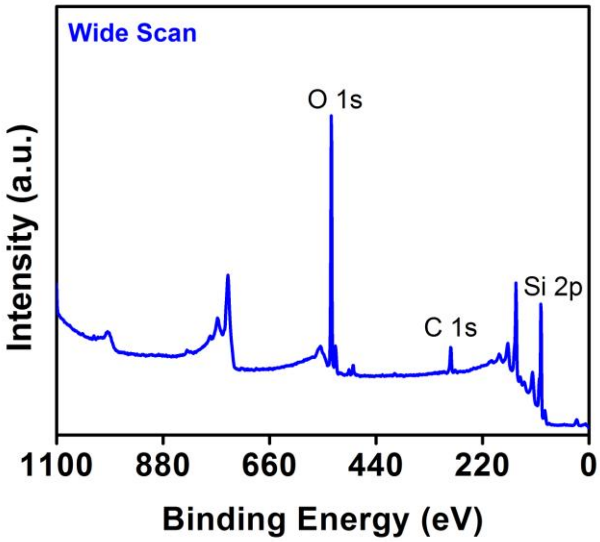

Figure 5.2 XPS of raw Si wafer.

To further evidence the surface modification on Si wafer, water contact angle of the modified Si wafer was measured by a static sessile drop method (EasyDrop, KRUSS GmbH Germany). As depicted in Figure 5.4, the changes of water contact angle after each consecutive treatment are observed. Raw Si wafer is hydrophobic in nature. After exposing to an oxygen plasma, water contact angle of the raw Si decreases from 50.8 ° to 2.5 °. As the hydrophilic hydroxyl groups are rendered on the Si wafer surface, VTMS molecules condense on the Si wafer and finally the water contact angle increases to 89.9 ° after VTMS deposition. Finally, the water contact angle decreases to 34.3 ° after grafting of PMETAC brush. The decrease in water contact angle in PMETAC-Si is due to the hydrophilic nature of the cationic PMETAC brushes.

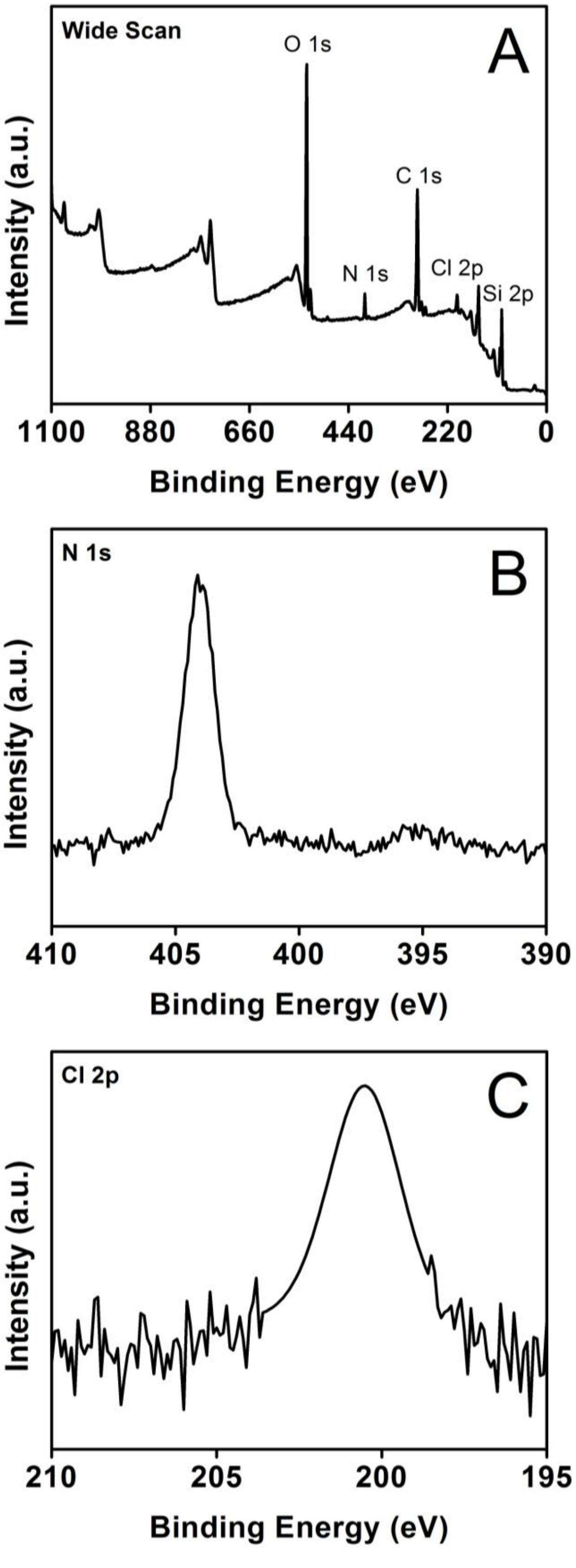

Figure 5.3 XPS of PMETAC-Si. (A) Wide scan spectrum. (B) N 1s spectrum. (C) Cl 2p spectrum.

Sample	Binding Energy (eV)	Corresponding Element	Figure
PMETAC-Si	404.1 (1s)	Nitrogen	5.3B
	200.5 (2p)	Chlorine	5.3C

Table 5.2 Summary of the XPS data on PMETAC-Si.

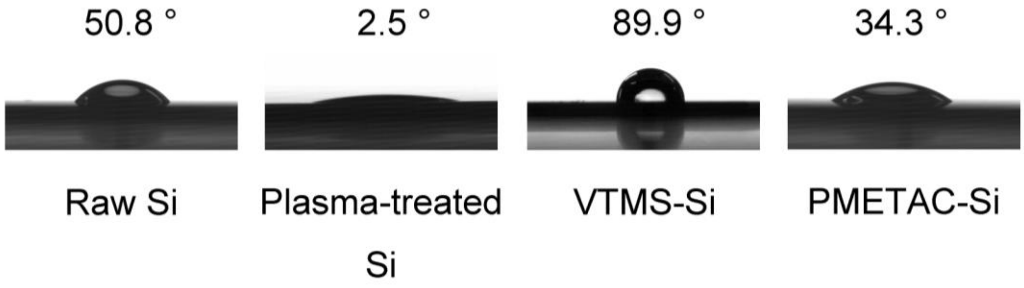

Figure 5.4 Water contact angle measurement on the treated Si samples.

The thickness of the PMETAC brush layer under different monomer concentrations and polymerization temperatures was investigated by a subtraction approach, in which PMETAC brush thickness was estimated by subtracting the VTMS thickness of the VTMS-Si from the PMETAC thickness of the PMETAC-Si. The thickness of the VTMS layer was estimated in a range from 30 nm to 200 nm (surface profiler, TENCOR P-10), depending on the concentration of the VTMS used. The height of the PMETAC brushes was found to range from 2 nm to 23 nm (Figure 5.5), depending on the polymerization conditions. It reveals that longer the polymerization time and higher the polymerization temperature, thicker is the polymer brush layer. Apparently, it is reasonable to have thicker polymer brush when the reaction is subject to longer period of polymerization reaction as well as higher polymerization temperature as both of them affect the polymerization kinetics. However, it is found that when the reaction time prolongs to 60 min at 60 ˚C, the PMETAC brush thickness decreases to around 10 nm. Thus, it is proposed that prolonged polymerization time for PMETAC at 60 ˚C is undesirable and breakage of the polymer chains may occur.

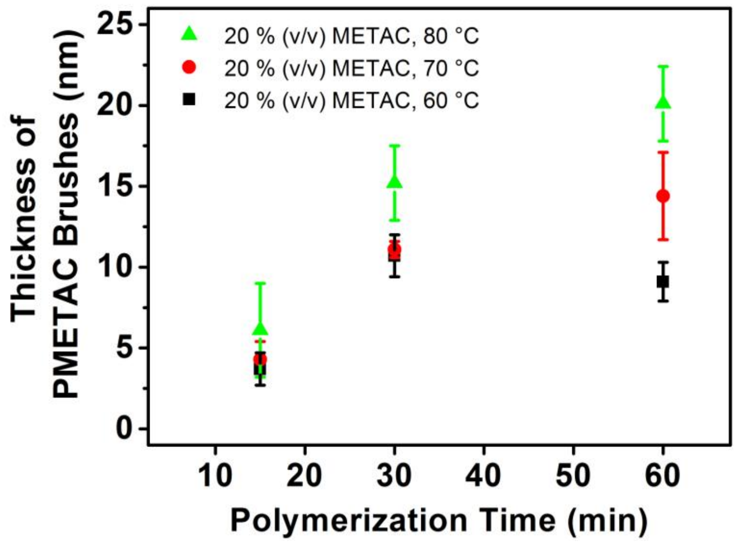

Figure 5.5 Thickness of PMETAC brushes as a function of polymerization time on Si wafers.

PMETAC-Si was further preceded with ion exchange with the catalytic moieties $PdCl_4^{2-}$. XPS in Figure 5.6 reveals that prominent peaks situates at binding energy value of 532.4 (Pd $3p_{3/2}$), 343.3 (Pd $3d_{3/2}$), and 337.8 eV (Pd $3d_{5/2}$), which evidences the successful immobilization of $PdCl_4^{2-}$ moieties on PMETAC during the ion exchange process.

Sample	Binding Energy (eV)	Corresponding Element	Figure
PMETAC-Si after ion exchange	532.4 ($3p_{3/2}$)	Palladium	5.6B
	343.3 ($3d_{3/2}$)	Palladium	5.6C
	337.8 ($3d_{5/2}$)	Palladium	5.6C

Table 5.3 Summary of the XPS data on treated Si samples.

ELD of copper was finally carried out by immersing the $PdCl_4^{2-}$-loaded PMETAC-Si into a copper ELD bath for 5-30 min, where the $PdCl_4^{2-}$ moieties act as effective catalytic sites for the growth of copper in the ELD process. After 30-min ELD, the sheet resistance of the copper-coated Si wafer (Cu-Si) measured by four probe method is ~0.45 ohm/sq.

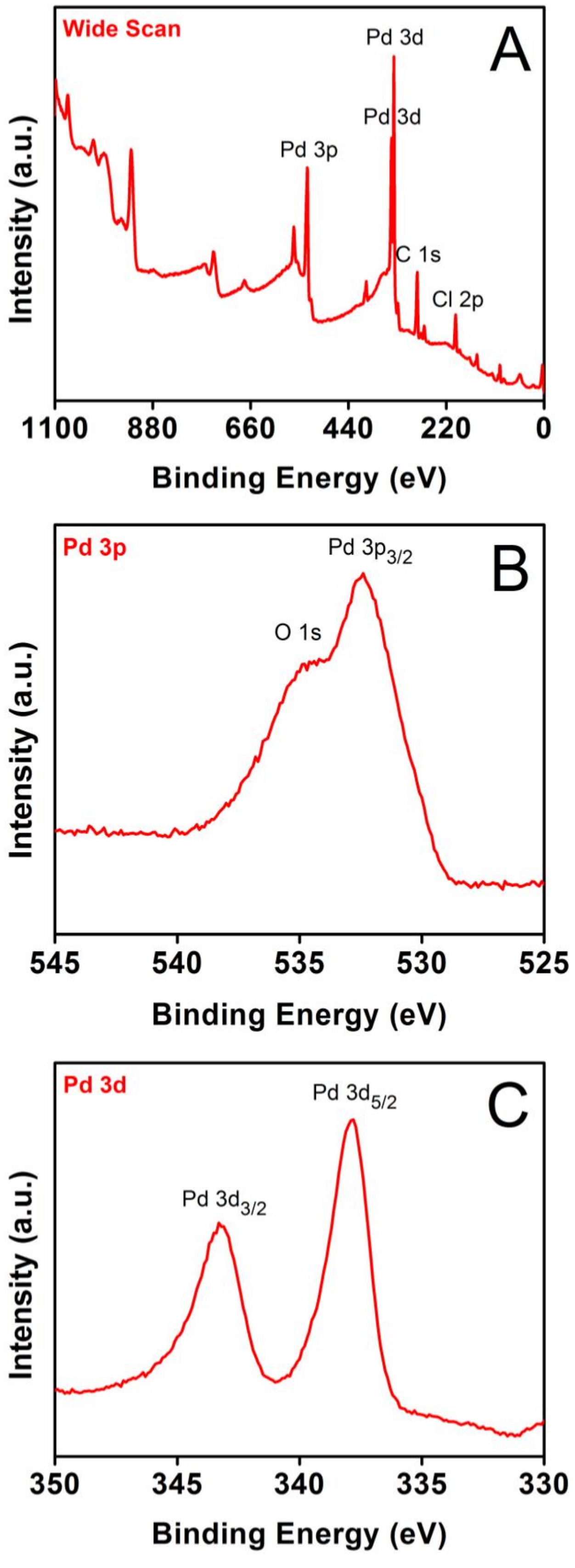

Figure 5.6 XPS of PMETAC-Si after ion exchange. (A) Wide scan. (B) Pd 3p spectrum. (C) Pd 3d spectrum.

The thickness of the PMETAC brushes is important in determining the sheet resistance of the Cu-Si. When using thinner brushes (e.g. 5 nm), the resistance increased to ~80 ohm/sq under the same ELD conditions after 30 min (Figure 5.7). Increasing the thickness of PMETAC brushes to ~20 nm results in sheet resistance of 0.6 ohm/sq. The increase in resistance can be explained by the fact that thinner PMETAC brushes immobilize lesser catalytic $PdCl_4^{2-}$ moieties, therefore leading to a slower rate of ELD as well as thinner copper film.

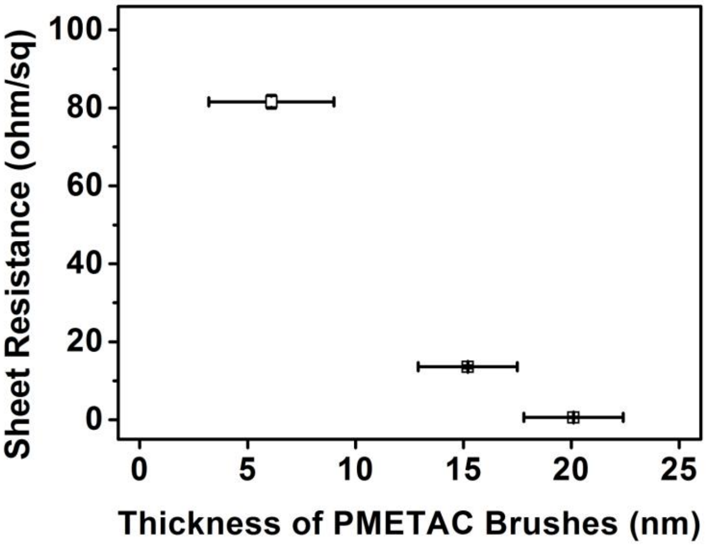

Figure 5.7 Sheet resistance of the Cu-Si at different PMETAC brush thickness.

5.3.2 Fabrication of Metallic Cotton Fabrics by Pad-Dry-Cure Technology

Cotton fabric was used as the substrate to fabricate metallic textiles by pad-dry-cure technology. Successful silanization of VTMS on cotton was confirmed by ATR-FTIR (Figure 5.8). Additional peaks situated at wavenumber 1410 cm^{-1} and 1602 cm^{-1} from the stretching vibration of C=C confirmed the successful surface deposition of VTMS. After VTMS deposition, VTMS-cotton was immersed into the METAC solution and brought to the pad-dry-cure process. The pad-dry-cure process is the most critical step involved in the impregnation of METAC monomer. In a typical pad-dry-cure process, fabrics are first dipped into chemical solution to be applied on, followed by a series of squeezing action through a pair of padding mangles under certain pressure. During padding, the shape of the padding cylinder in the contact point generates a nip area, where the pressure reaches the highest value. In this experiment, VTMS-cotton with METAC monomers absorbed was fed into the nip area of a horizontal padding machine at a constant speed. Heavy pad mangles squeezed out the excess METAC monomer at a constant pressure. The padded cotton fabric was then put into the reaction mixture in an oven at 80 ˚C for 1 hr. Successful grafting of PMETAC brushes on VTMS-cotton was confirmed in the ATR-FTIR spectrum. A distinctive peak at wavenumber 1716 cm^{-1} which contributed by the stretching vibration of C=O that originated from the PMETAC brushes is observed in Figure 5.8.

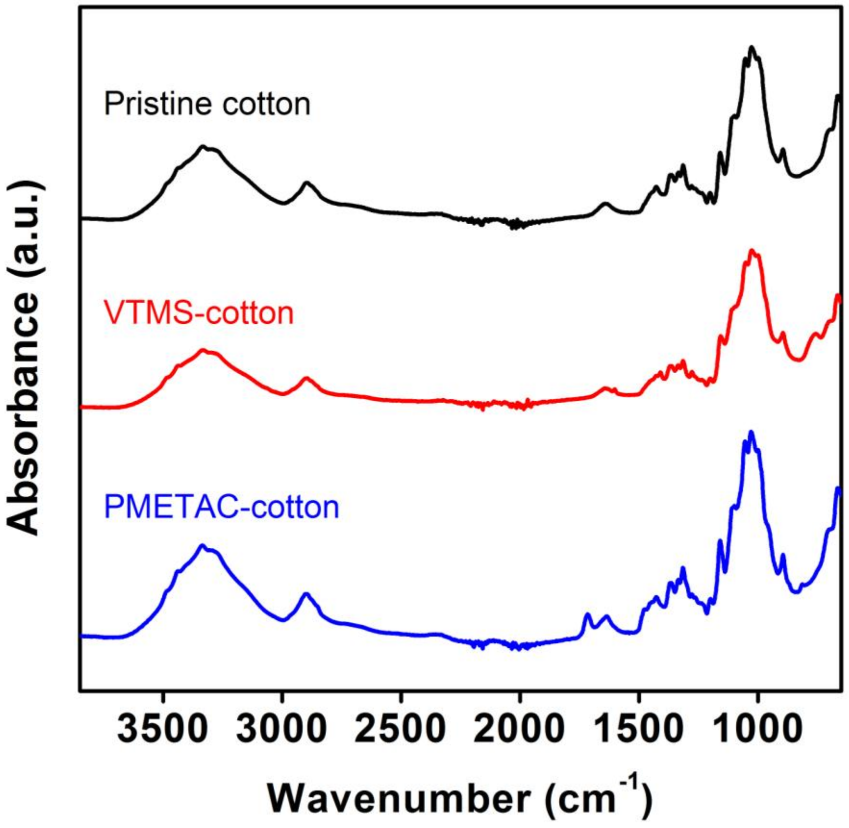

Figure 5.8 ATR-FTIR spectra of the modified cotton samples.

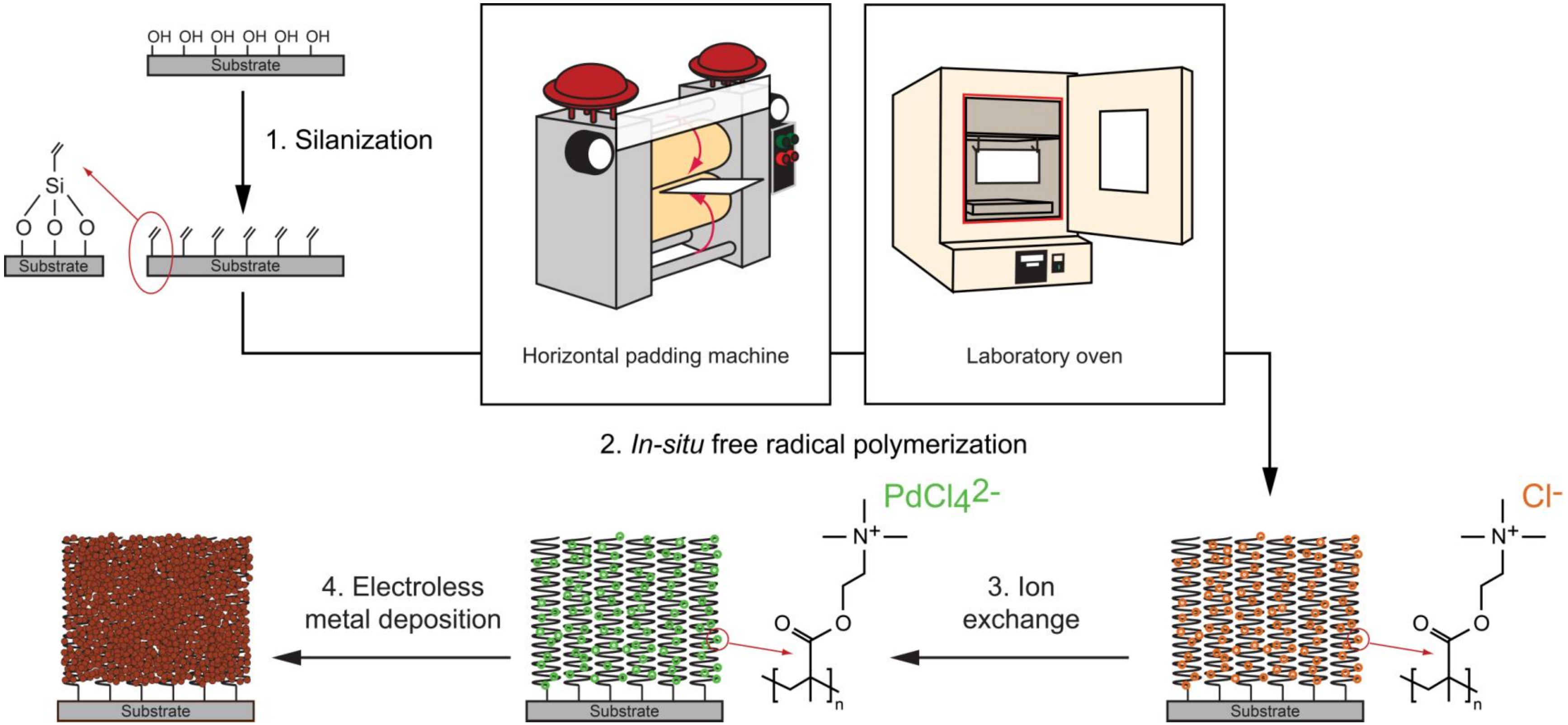

Figure 5.9 Schematic illustrations of the experimental procedures for the fabrication of metallic cotton fabrics by pad-dry-cure compatible technology.

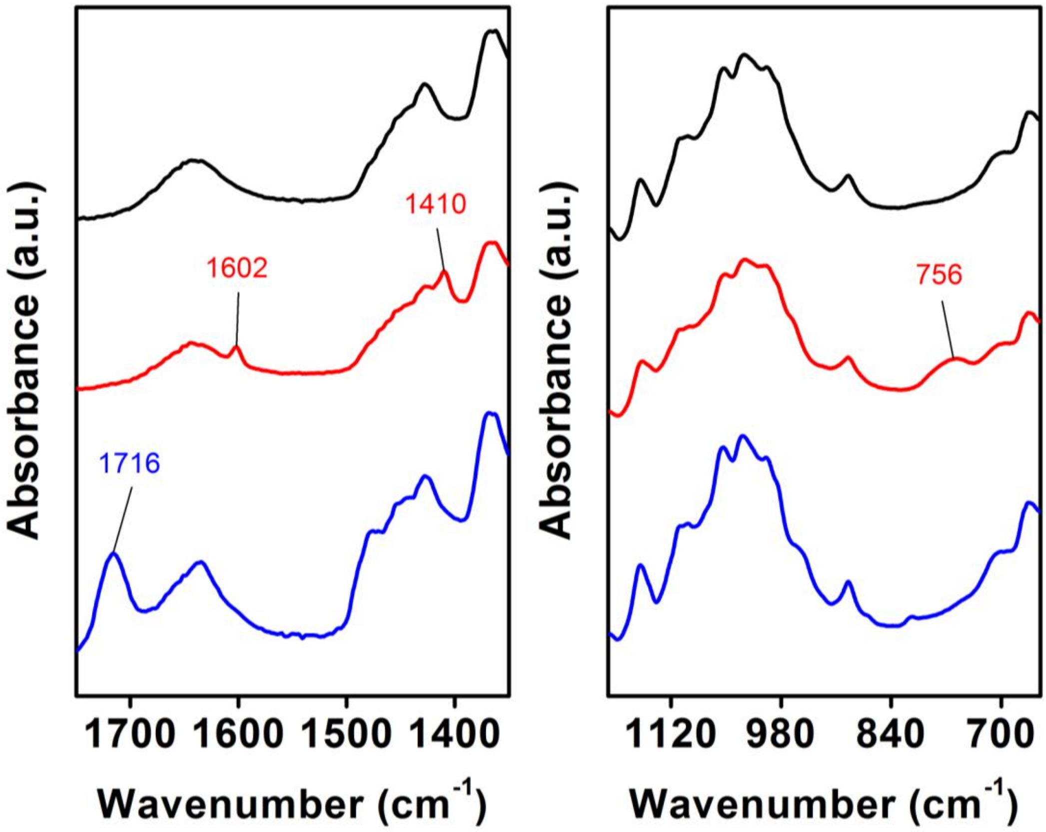

Figure 5.8 ATR-FTIR spectra of the modified cotton samples. (Cont')

Sample	**Distinctive Peaks at Wavenumber (cm^{-1})**	**Corresponding Functional Group**
VTMS-cotton	756	Si-C
	1410	C=C
	1602	C=C
PMETAC-cotton	1716	C=O

Table 5.4 Summary of the ATR-FTIR data of the modified cotton samples.

5.3.2.1 Surface Morphology

The digital image of the as-synthesized Cu-cotton is showed in Figure 5.10, which clearly showed that white cotton fabric turned into copper brown color after grafting of polymer brush with subsequent copper ELD process. Confirmation of copper composition on Cu-cotton was conducted by EDS. In the EDS spectrum as shown in Figure 5.11, the emission of characteristic X-rays with specific energy values as stated in two distinctive peaks labeled at 8.0 and 8.9 keV corresponded to the Kα and Kβ transition of copper, respectively; while that at 0.9 keV corresponded to the L transition of copper. Trance amount of gold was also detected due to the gold sputtering on the cotton fabric surface prior to the SEM imaging.

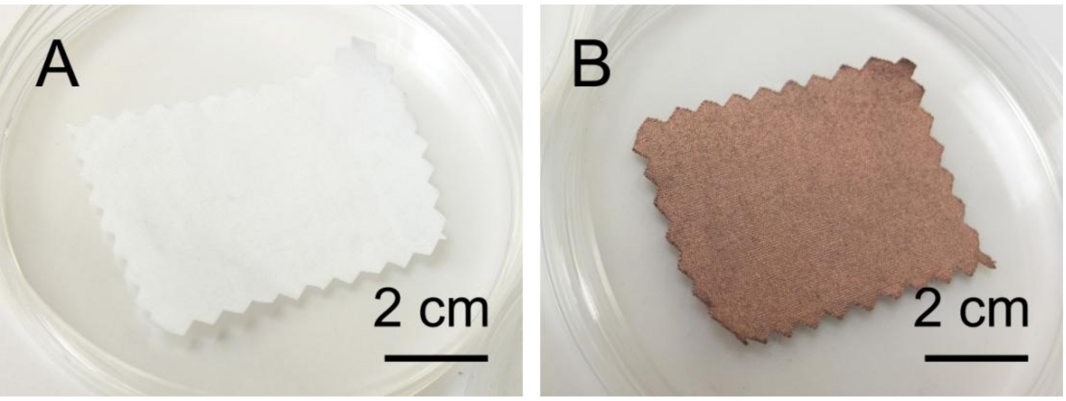

Figure 5.10 Digital images of (A) unmodified cotton fabric and (B) copper-coated cotton fabric after 30-min ELD.

The influence on the surface appearance with varied ELD time was investigated. Cotton fabric samples treated under various time in ELD bath were showed in Figure 5.12. It could be observed that the surface color changed significantly as the ELD time prolonged to 90 min. At 0 min, the dull color of the cotton fabric was due to the ion exchange treatment in the $PdCl_4^{2-}$ solution. Even copper distribution was observed starting from 60 min ELD. Therefore, it is suggested that the optimum ELD time for cotton fabrics time should at less 60 min.

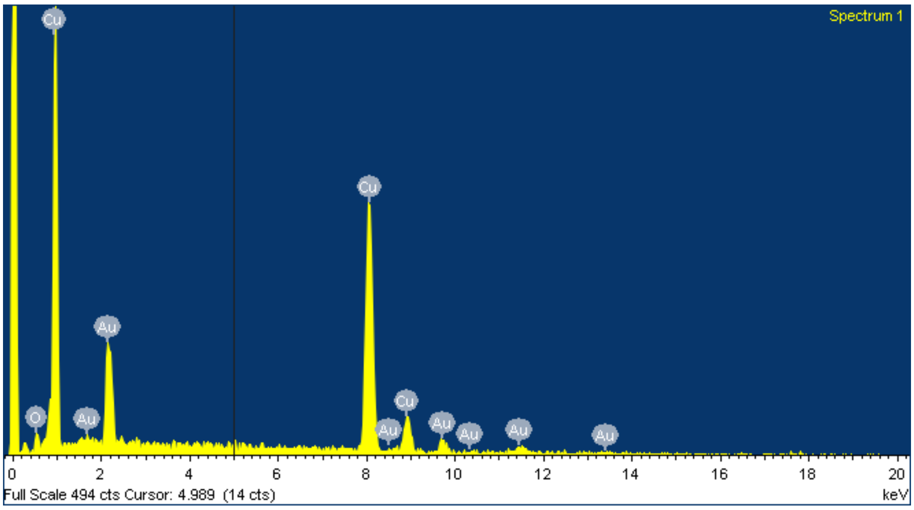

Figure 5.11 EDS spectrum of the Cu-cotton fabric.

Surface morphology of the modified cotton was characterized by SEM (Figure 5.13). Pristine cotton showed that there were many cellulose microfibrils present on the cotton fiber surface. After the VTMS deposition on the cotton fibers, cotton fiber surface became slightly smooth, so as the cotton fabric samples after PMETAC grafting. Final ELD of the PMETAC-cotton yielded Cu-cotton. The copper coating on Cu-cotton is compact, without any signs of crack.

We also carried out water contact angle measurement on the VTMS-cotton and PMETAC-cotton. As shown in Figure 5.13 insets, when a water droplet was dropped on the raw cotton fabric surface, it was quickly absorbed by the fabric. However, the water contact angle changed drastically to 138.2 ° after deposition of VTMS. As compared to the results obtained from VTMS-Si wafer (Figure 5.6), VTMS-Si only exhibited a water contact angle of 89.9 °. Though hydrophobicity was observed in the VTMS-cotton, it became hydrophilic again after grafting of PMETAC brushes on the cotton fabric surface. Final deposition of copper rendered the cotton fabric a hydrophobic surface, which was a typical property of metal.

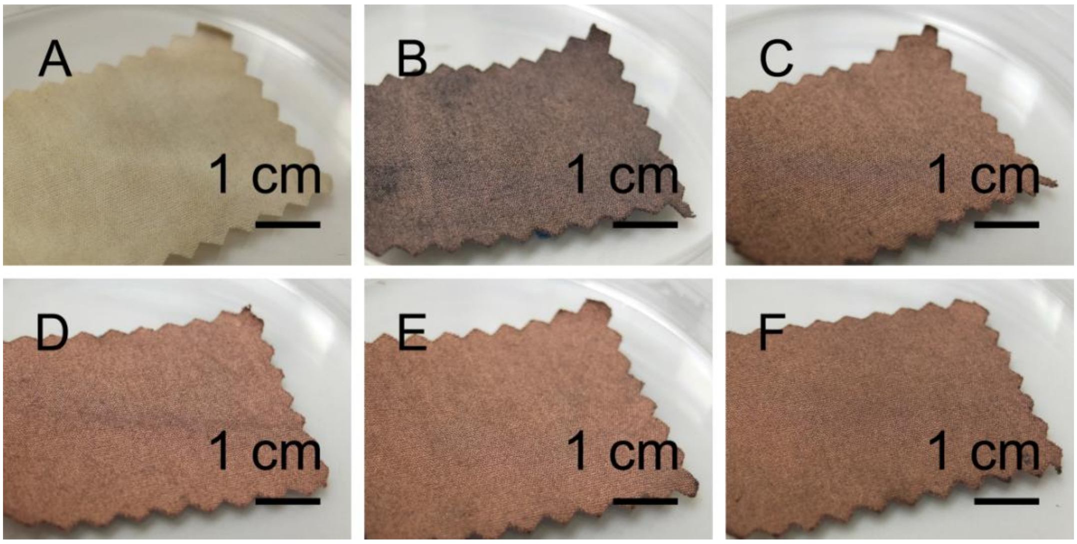

Figure 5.12 Cotton fabric samples under different ELD time. (A) 0 min. (B) 15 min. (C) 30 min. (D) 60 min. (E) 75 min. (F) 90 min.

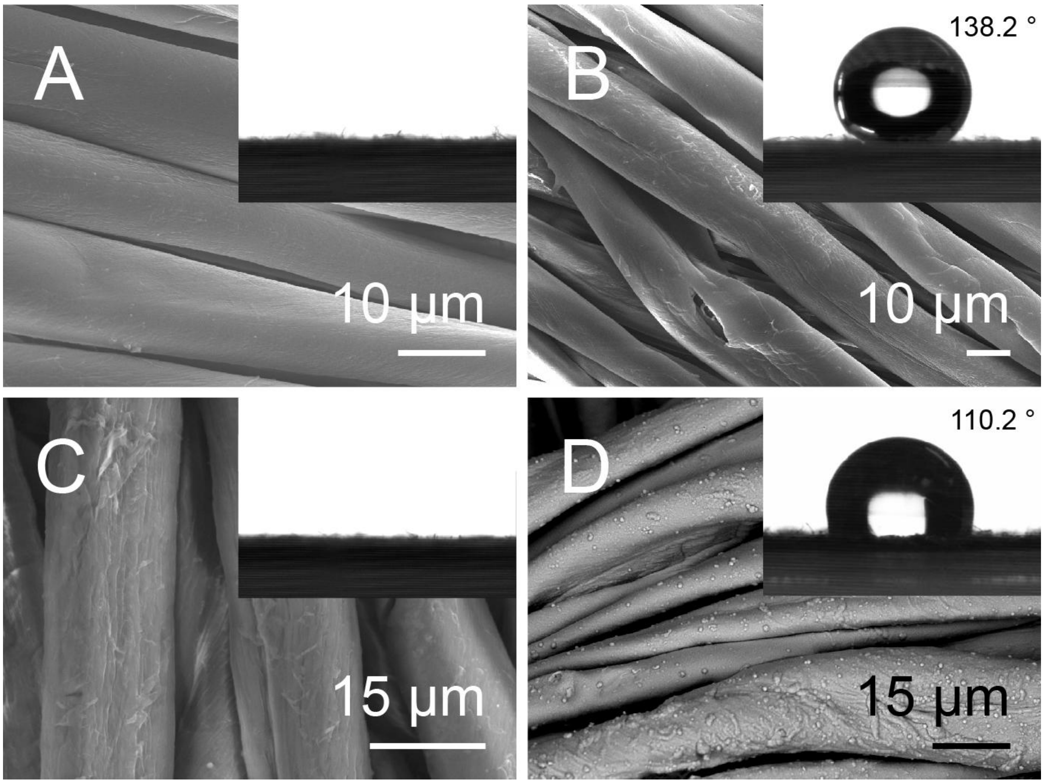

Figure 5.13 SEM images of (A) unmodified cotton fabric, (B) VTMS-cotton, (C) PMETAC-cotton obtained at 40 min polymerization, and (D) Cu-cotton obtained at 30 min ELD. Insets are the corresponding images of water contact angle measurements.

5.3.2.2 Sheet Resistance

We also demonstrated the effect on sheet resistance when ELD time varied from 15 min, 30 min, 45 min, 60 min, 75 min and 90 min. The average sheet resistance was calculated by averaging the measurement obtained from both sides of the as-made Cu-cotton. It was found that all of the samples demonstrated more or less the same sheet resistance on both sides, indicating even distribution of the as-deposited copper metal. The average sheet resistance of sample was plotted against ELD time (Figure 5.14). 30-min ELD sample reached an average sheet resistance as 1.22 ohm/sq, showing very good surface conductance. Prolonging the ELD time could result in a lower sheet resistance of the Cu-cotton. The average sheet resistance of the 90-min ELD sample reached as low as 0.24 ohm/sq.

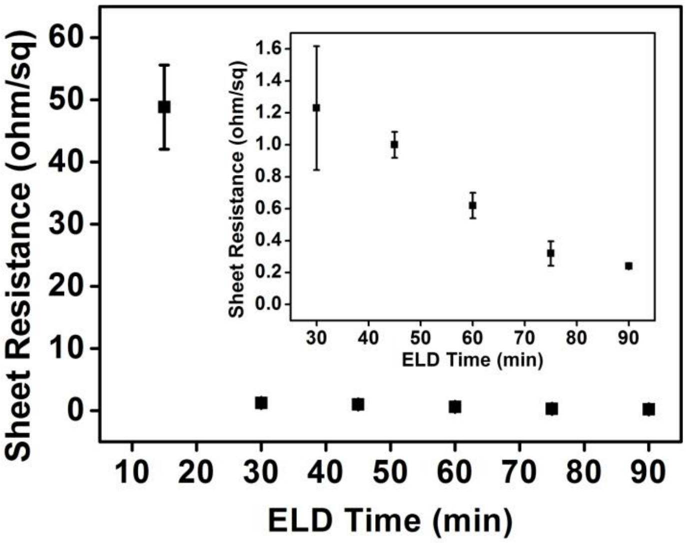

Figure 5.14 Average sheet resistance of Cu-cotton at different (B) ELD plating times.

We tested the electrical resistance change of Cu-cotton upon bending. First of all, the sample was bent at different radius of curvature from 30 mm down to 0.5 mm. Surprisingly, the electrical resistance decreases with decreasing bending angles (Figure 5.15A). This can be explained by the fact that when Cu-cotton is bent to a small radius, higher tensile strain is applied on the sample. In this case, the cotton fibers and yarns of the fabric are actually stretched to form a more compact contact between each other, leading to a lower contact resistance of the whole fabric. We further bent and unbent this sample at r=5 mm for 1000 times as illustrated in the inset of Figure 5.15B. It is found that the resistance increased to 3.5 folds after the cyclic tests. We believe that this is due to the continuous abrasion among the cotton fibers and yarns of the fabric. As we discussed above, when the fabric is repeatedly stretched and relaxed during the bending tests, fibers and yarns are continuously switching between compact and loose forms from each other. At such, friction among them occurs, which may lead to partial removal of the surface copper.

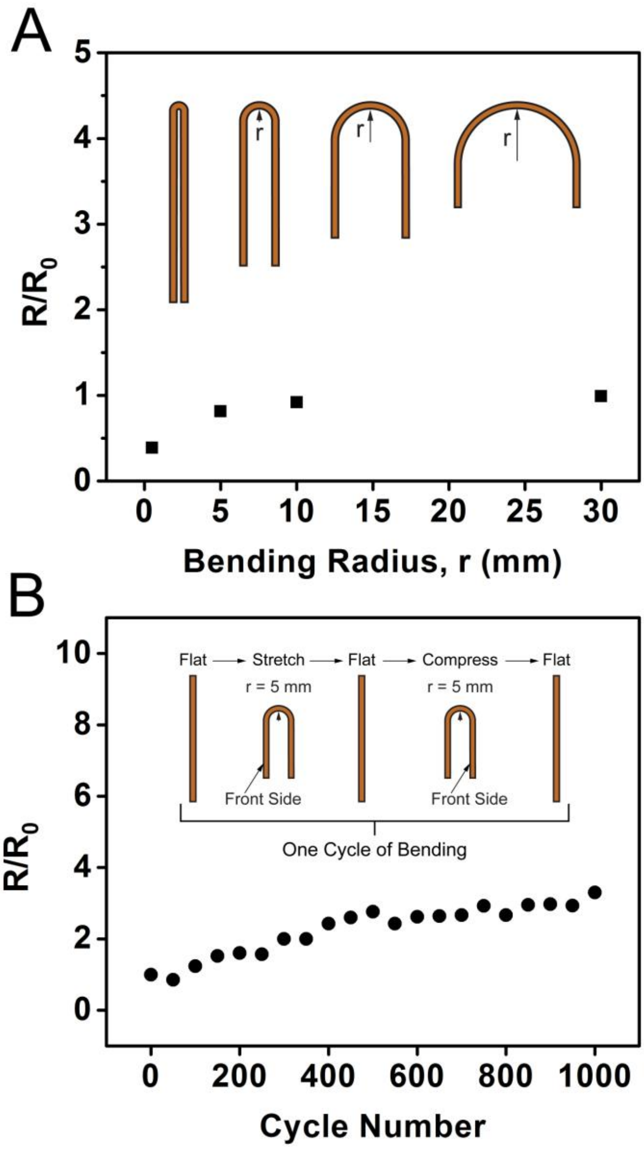

Figure 5.15 (A) Electrical resistance change of Cu-cotton at different bending radii. (B) Cyclic tests of electrical resistance of Cu-cotton with bending radius=5 mm.

5.3.2.3 Washing Durability

With the aim of fabricating high performance washable conductive textiles, the washing ability of the as-made 45-min ELD Cu-cotton was challenged under hand wash with vigorous rubbing, bending and squeezing with palms for 1 min. Fabric samples were then hanged dry for 24 hr under standard conditions. Same four-probe method was conducted as mentioned. As showed in Figure 5.16, after 5 hand washing cycles, less than 5 ohm/sq of the average sheet resistance could still be achieved, which indicated that the adhesion was good between copper and the fabric substrate.

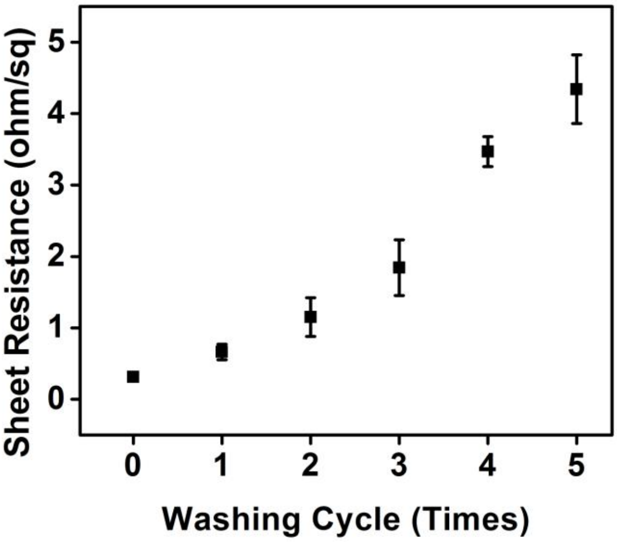

Figure 5.16 Average sheet resistance of a 45-min ELD fabric sample (measured in weft direction) with five hand washing cycles.

5.3.2.4 Incorporation in Electronic Circuit

Due to the low sheet resistance of the Cu-cotton, we further demonstrated that Cu-cotton could act as conductive intern connects in a circuit. A very simple parallel circuit was constructed by using Cu-cotton with eight LEDs depicted in Figure 5.17. When the two poles of a 9 V battery were put on the fabrics, LEDs were immediately lighted up. For clearer understanding of this system, a schematic presentation was illustrated in Figure 5.17(D). ir clearly shows that the two poles of the LEDs were mounted tightly on the two separated Cu-cotton, where a top fabric printed with pattern served as protection and decoration purpose. The ON and OFF action of LEDs could be repeated by connecting and disconnecting for more than 20 times.

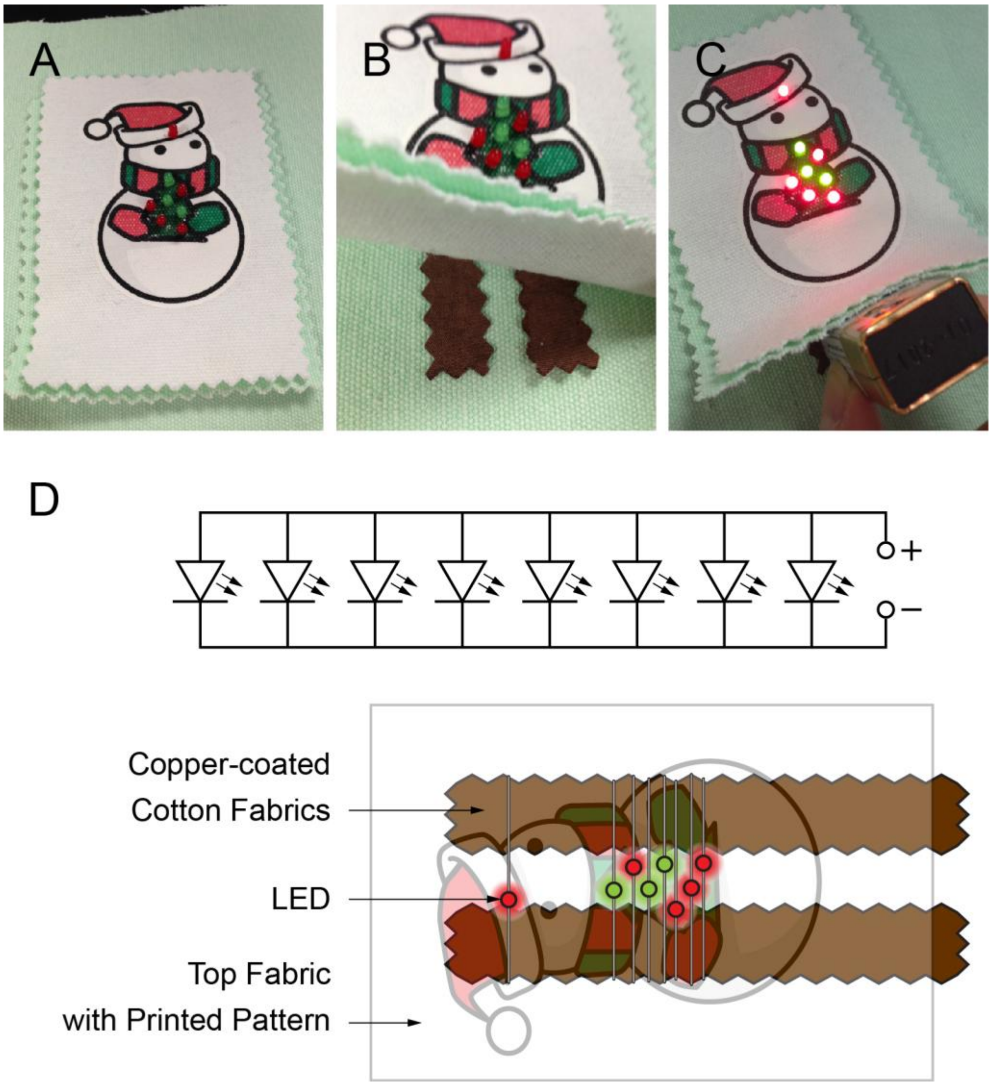

Figure 5.17 Demonstration of the copper-coated cotton fabric acting as a conductive component in a circuit. (A-C) Two copper-coated cotton fabrics served as electrodes and connected to eight LEDs in parallel. (D) Schematic illustration of the circuit construction.

5.3.3 Fabrication of Metallic Cotton Yarns by Miniaturized Hank Dyeing Machine

Hank dyeing machine is a kind of widely used dyeing machine which is used to dye yarns in batches of hank. Usually, yarns are reeled into what the industry called as ‘hank’ and placed on the hanging bar inside the machine. Dye stuff is then injected into the dyeing chamber, with stirrer at the bottom that provides constant movement of the dyeing solution to facilitate dyeing. In the fabrication of metallic cotton yarns, hank dyeing machine had been incorporated into the fabrication process, to demonstrate the compatibility of this technology with the current textile manufacturing industry. For this purpose, a miniature hank dyeing machine was designed and fabricated as shown in Figure 5.18. The miniature hank dyeing machine consisted of 40-liter main container, two perforated plates and a cover.

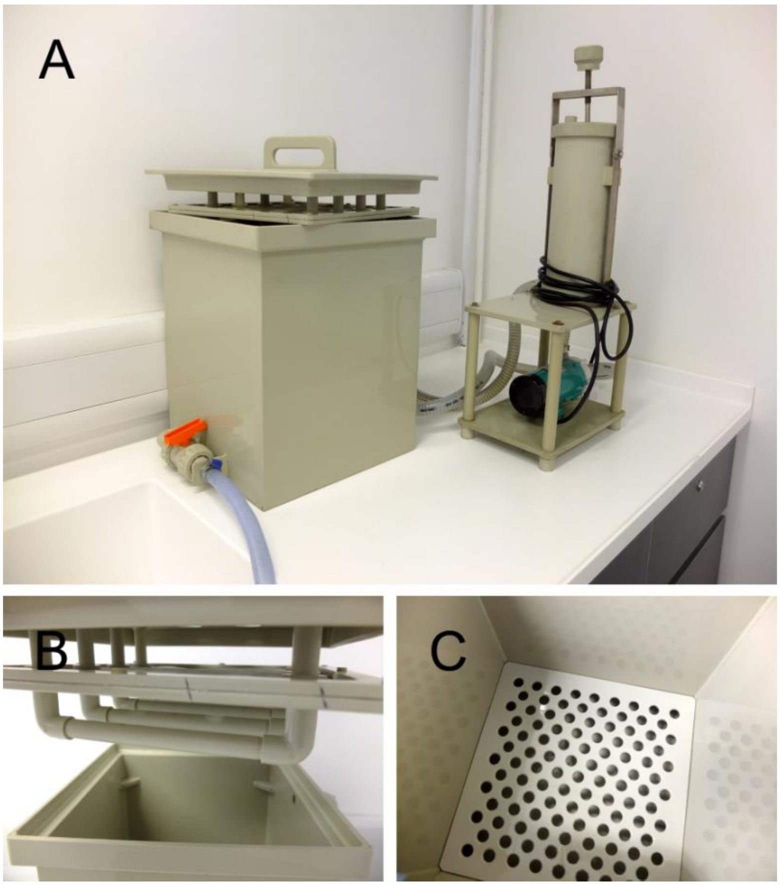

Figure 5.18 Digital images of (A) house-made miniaturized hank dyeing machine equipped with a pump, (B) cover of the hank dyeing machine, with hanging bars for hanging of the reeled yarns, and (C) perforated plate inside the container for the control of liquid movement.

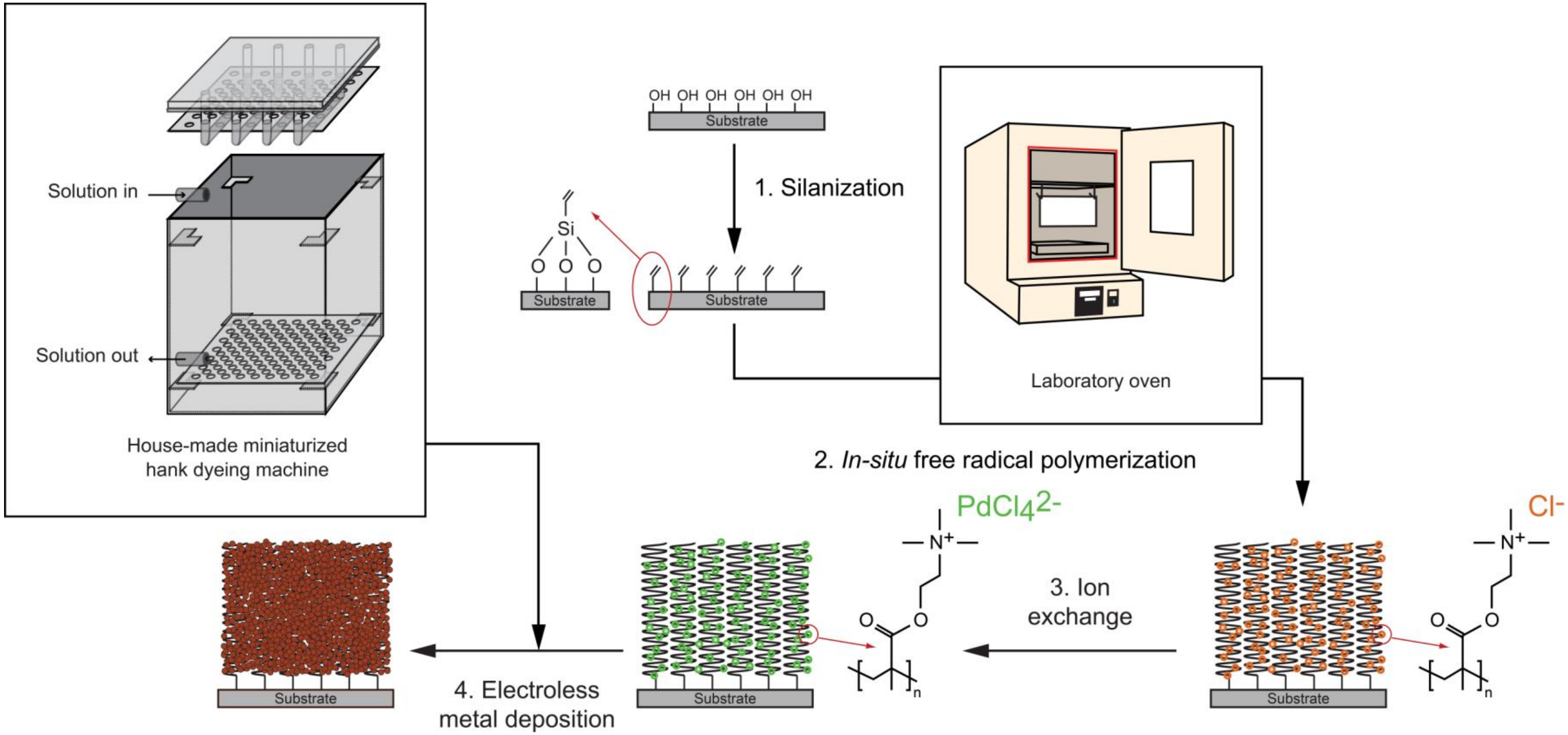

Figure 5.19 Schematic illustrations of the experimental procedures for the fabrication of metallic cotton yarns by hank dyeing technology.

5.3.3.1 Sample Appearance

Same experiment procedures were conducted for the cotton yarns. Figure 5.20 shows the modified cotton yarns at different stages, from raw cotton yarn, VTMS-cotton, PMETAC-cotton and the final Cu-cotton. The cotton yarns at (A-C) fabrication stages exhibited similar surface appearance. After ELD of copper metal, significant difference could be seen where shiny copper color was observed.

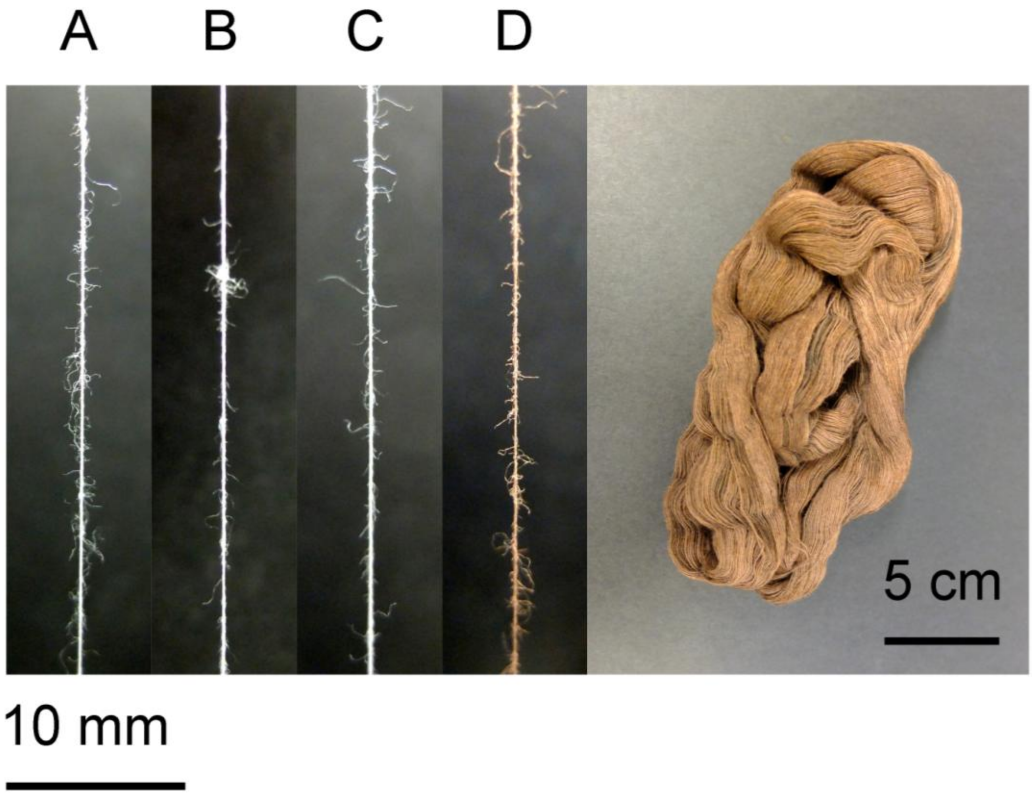

Figure 5.20 Digital images of the cotton yarn samples. (A) Pristine cotton yarn. (B) VTMS-cotton. (C) PMETAC-cotton. (D) Cu-cotton.

5.3.3.2 Linear Resistance

Linear resistance of the as-made Cu-cotton yarns was measured using two-probe method. Both ends of a Cu-cotton yarn were secured by conductive copper adhesive tapes (3M). The resulting linear resistance was estimated as 1.40 ohm/cm (Figure 5.21), which was highly satisfactory comparing to the currently market available metal-coated polyester yarns (< 5 ohm/cm).

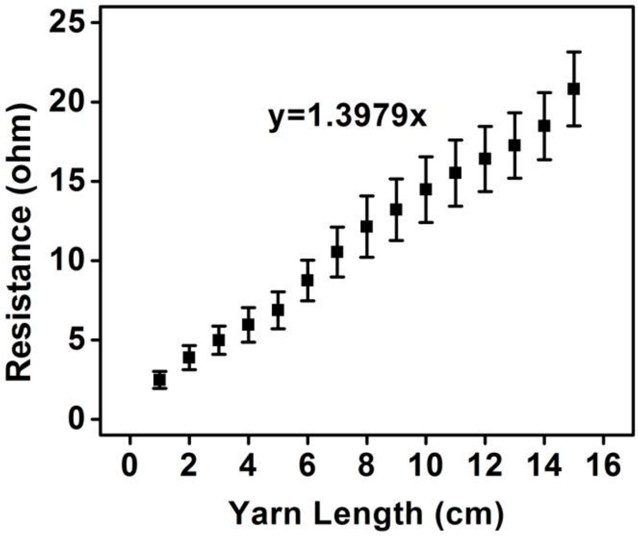

Figure 5.21 Average linear resistance of the copper-coated cotton yarn.

5.3.3.3 Tensile Properties

For the tensile properties of the a-made copper-coated cotton yarns, the maximum load the yarn could withstand increased by 30% after the deposition of copper comparing to the pristine cotton. For the tensile extension at maximum load, the values among all the samples showed a more or less the same result, indicating that the chemical treatment would not impose a decrease in tensile properties, especially the copper coating could remarkably strengthen the tensile properties of the cotton yarns.

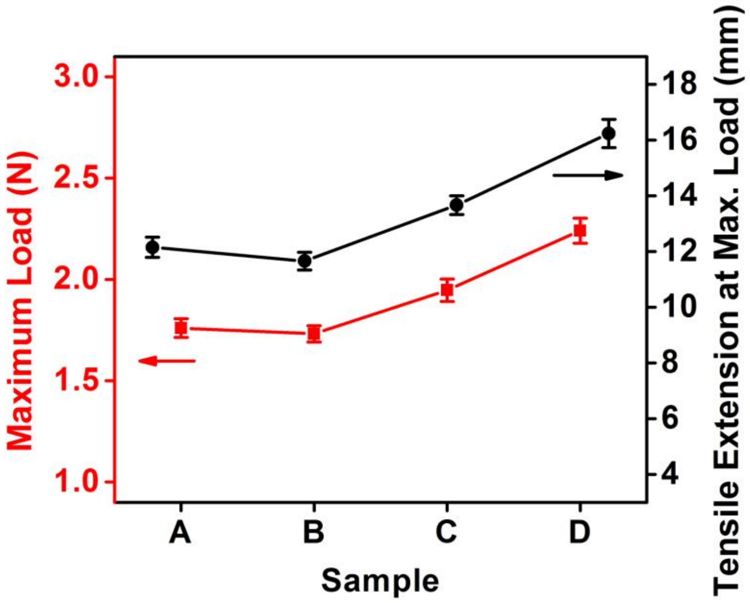

Figure 5.22 Tensile properties of the cotton yarn samples. (A) Pristine cotton yarn. (B) VTMS-deposited cotton yarn. (C) PMETAC-grafted cotton yarn. (D) Copper-coated cotton yarn.

5.3.3.4 Washing Durability

To evaluate the washing durability of the copper-coated cotton yarns, as-synthesized Cu-cotton yarns were first wound on a cone (Figure 5.22B) using an industrial cone winder. The cone was then transferred to the CCI weaving machine (Figure 5.22C) to carry out weaving process. In the weaving setting, the Cu-cotton yarns were the wefts while the warps were the pristine cotton yarns (Figure 5.22D, right inset). After weaving, the fabric was cut into pieces of 5 cm × 15 cm and overlocked at the four edges (Figure 5.22D), and subsequently undergone a series of washing cycles according to the testing standard AATCC Test Method 61 – Test No. 2A: Colorfastness to Laundering, Home and Commercial: Accelerated (Machine Wash) in the Launder-Ometer® (Figure 5.22E) at specific washing conditions as shown in Table 5.5.

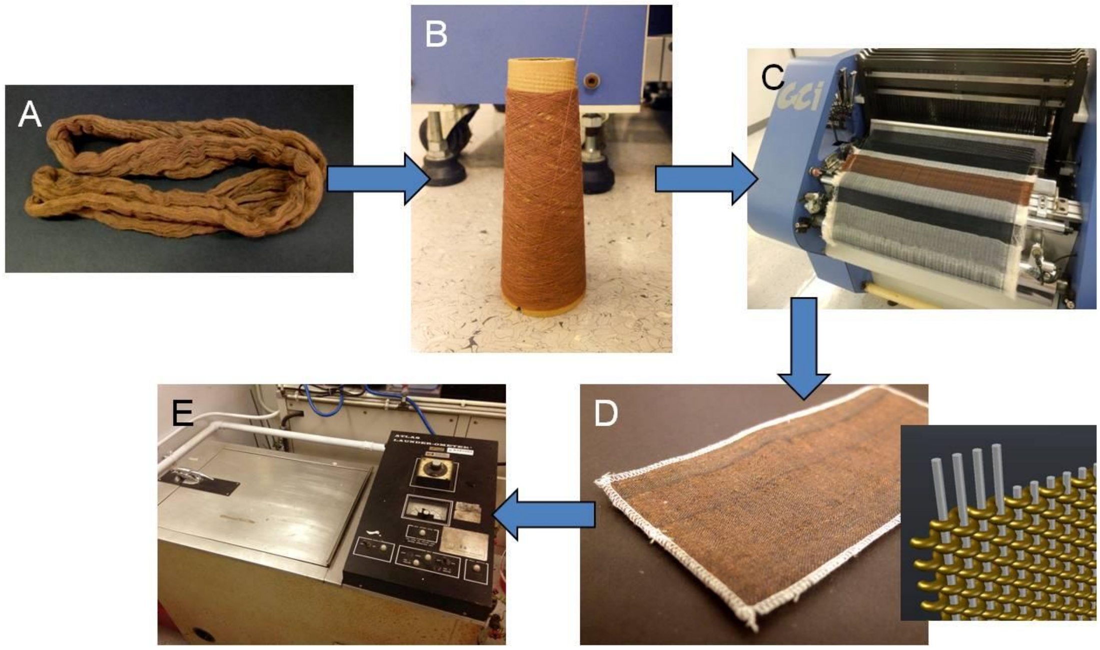

Figure 5.23 Process showing the fabrication of the woven fabric using as-prepared copper-coated cotton yarns. (A) Copper-coated cotton yarns. (B) Cone of copper-coated cotton yarns. (C) Copper-coated cotton yarns woven into fabric (D). (E) The Launder-Ometer® used in standard washing.

Washing temperature	49±2 ˚C
Volume of DI water	150 mL
No. of steel balls added	50 pcs
Time of washing	45 min

Table 5.5 Washing conditions in the standard washing.

We further evaluated the changes in the sheet resistance of the washed fabrics. Using four-probe method, the sheet resistances of the fabrics were measured to be 0.9 ± 0.2 ohm/sq (unwashed) while 73.8 ± 13.4 ohm/sq after the 20th wash (Figure 5.23). To evaluate the surface morphology of the washed Cu-cotton, washed yarns were unraveled from the fabric, and were examined under SEM. It was found that the copper metal particles were remained on the surface of the cotton fibers as shown in Figure 5.25. The reason for the increase in sheet resistance is mainly because of the loosen structure of the cotton fibers upon repeated cycles of washing. It is worthy of note that in the standard washing cycle, 50 pieces of steel balls are added into the washing canisters to resemble a vigorous washing action in the laundering machine. The abrasion of the steel balls on the fabrics can seriously make impact on the fiber and fabric structure. As the fibers of the Cu-cotton are no longer stayed in a tightened manner, they lose contact with each other, making lesser conductive pathways for the movement of the electrons. Therefore, the sheet resistance increases upon repeated washing cycles. This issue was found to be the only limitation while using staple fiber as the substrate.

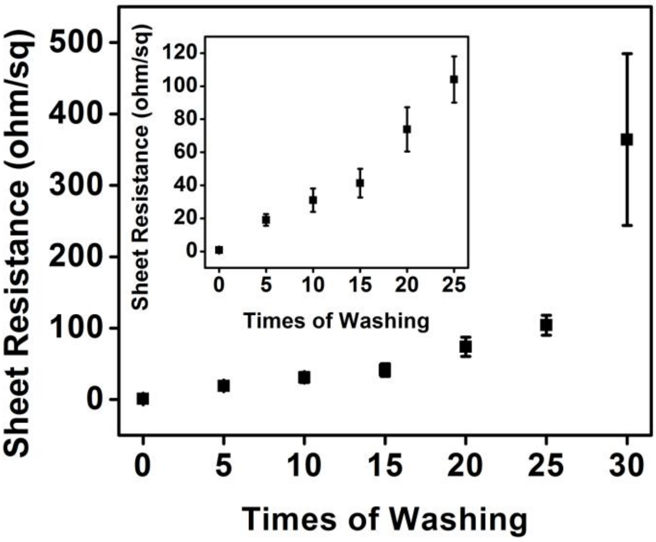

Figure 5.24 Sheet resistances of the fabrics woven by Cu-cotton yarns after washing up to 30 cycles.

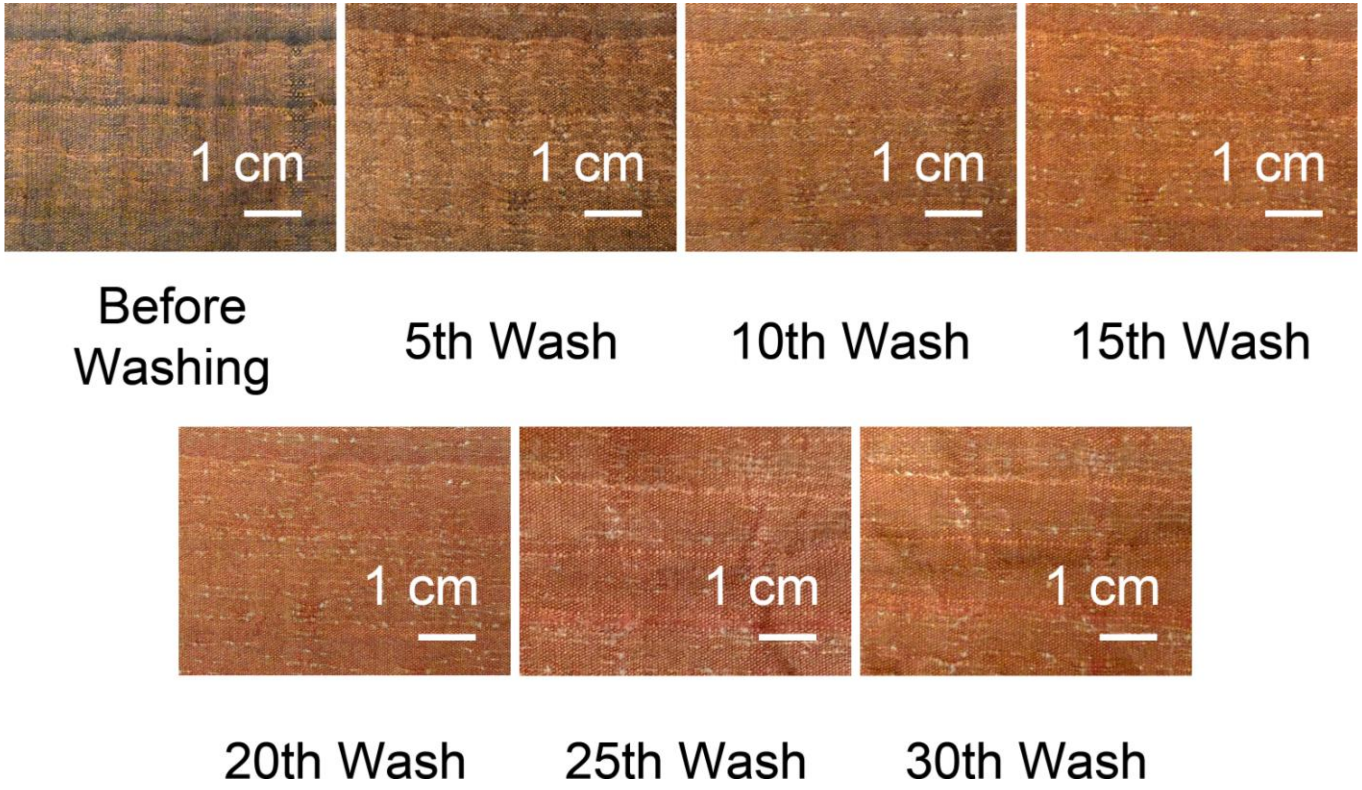

Figure 5.25 Appearances of the fabrics washed up to 30 cycles.

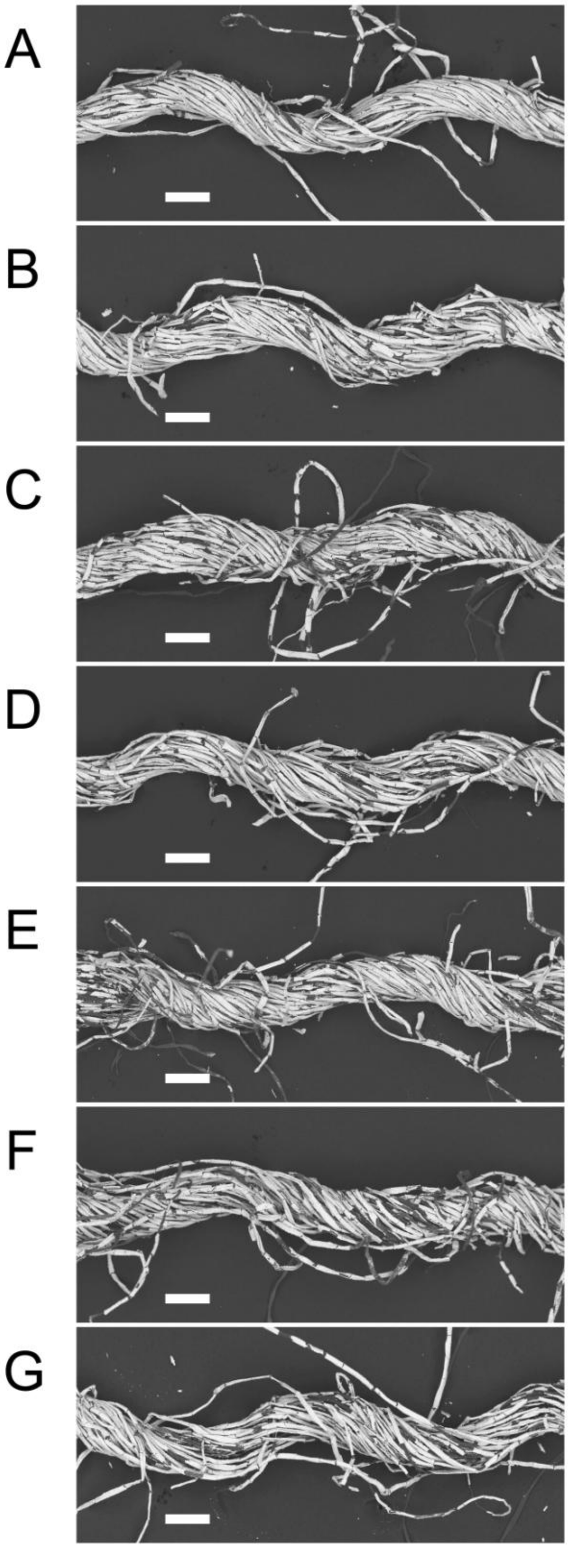

Figure 5.26 SEM images of yarns unraveled from the washed fabrics woven by Cu-yarns after different times of washing: (A) unwashed, (B) 5 times, (C) 10 times, (D) 15 times, (E) 20 time, (F) 25 times and (G) 30 times. Scale bar is 200 μm.

5.3.3.5 Optimization for ELD Process

ELD process in the miniaturized hank dyeing machine was further optimized. A rough estimation on the change of concentration of Cu^{2+} ions was conducted by UV-Vis spectrometry. It was found that the absorbance of the spectrum of ELD solution at 30 min was almost one-third the absorbance of that of the original ELD solution at around 660 nm.

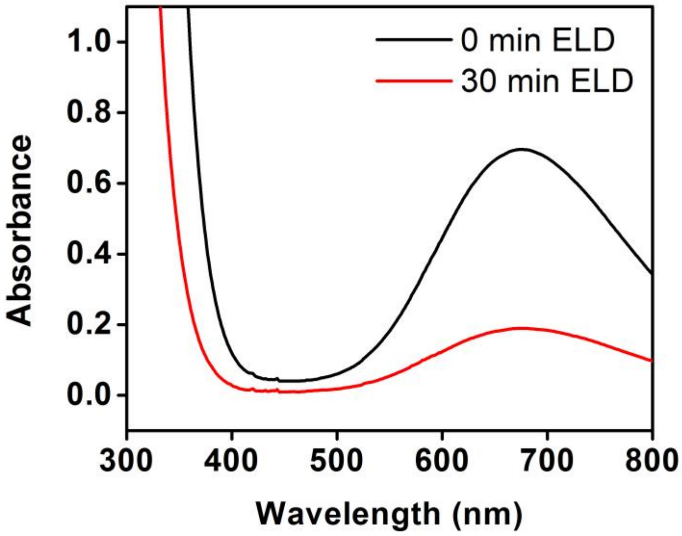

Figure 5.27 Absorption spectra of the ELD solutions at 0 min and 30 min.

5.3.3.6 Incorporation in Electronic Circuit

The Cu-cotton yarn was incorporated into an electric circuit to demonstrate its capability in the wearable electronics. The Cu-cotton yarn was connected to the jumping wires, which were in turn connected to an Arduino UNO board (Figure 5.28). A potential output powered by the Arduino UNO board was 3.3 V. The green LED lighted up immediately when the jumping wire was connected to the Cu-cotton yarn. This repeating OFF and ON cycle can be repeated for more than 100 times.

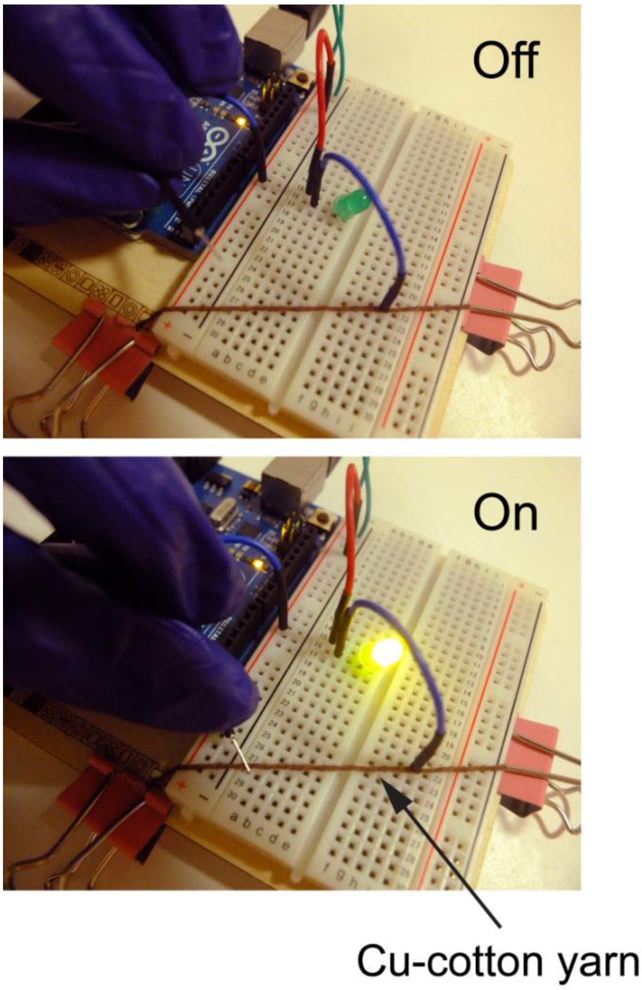

Figure 5.28 ON and OFF action of green LED when Cu-cotton yarn was connected to the circuit.

5.3.4 Versatility in Other Textile Substrates

Though cotton is one of the most abundant natural textiles used in the garment industry, its hydrophilic property may not be ideal for making conductive textiles as water molecules absorbed and adsorbed on the cotton fiber surface may hinder the electrical performance. Investigation on other synthetic textile substrate such as polyester, nylon and silk were also carried out. The as-synthesized metal-coated textiles are shown in Figure 5.29. Not only restricted to cotton textile substrate, the fabrication described herein is a universal metal deposition strategy for both copper and nickel, and can be readily extended to various textile substrates including both natural and other synthetic fibers.

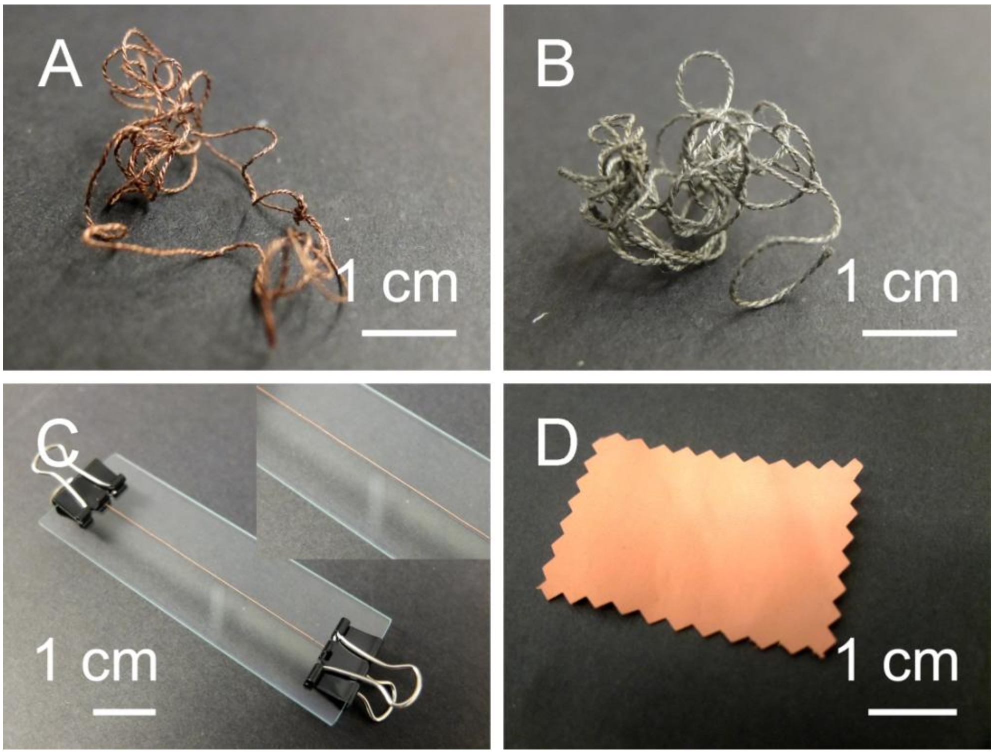

Figure 5.29 Digital images of the as-prepared metal-coated textiles of different substrates. (A) Cu- and (B) Ni-silk yarn. (C) Cu-nylon monofilament yarn and (D) polyester fabric.

5.4 Chapter Conclusion

Electrically conductive cotton fabrics and yarns are successfully prepared by first free radical polymerization of PMETAC brushes on cotton fiber surface, followed by subsequent ELD of copper thin layers on cotton fiber surfaces. For the Cu-cotton fabric, it exhibits a sheet resistance of 10^3 to 10^{-1} ohm/sq, depending on the ELD conditions. Pad-dry-cure takes a major role in the even uptake and penetration of the monomer METAC solution throughout the cotton fabrics, making subsequent ELD plating of copper metal uniform. Moreover, the padding process fully demonstrates a low-wastage approach, as pad-dry-cure only involves simple and repeated immersion of cotton fabrics into solutions, plus drying and curing in simple equipment, which is highly applicable in industrial scale textile wet processing. Other than pad-dry-cure, hank dyeing machine can also be used to incorporate into the whole fabrication procedures. For the Cu-cotton yarns, the linear resistance is found to be 1.4 ohm/cm. The copper layer on the as-synthesized Cu-cotton yarns exhibits an excellent robustness, which can withstand up to 30 repeated cycles of machine laundering. To demonstrate that as-synthesized copper-coated textile can act as active components in electronics, the copper-coated cotton textiles are successfully incorporated into electronic circuits as interconnects to light up a series of LEDs.

(Blank Page)

CHAPTER 6:

FABRICATION OF METALLIC TEXTILES ASSISTED WITH ANIONIC POLY(METHACRYLIC ACID SODIUM SALT) (PMANA) OR POLY(ACRYLIC ACID SODIUM SALT) (PAANA) BRUSHES

6.1 Introduction

In the previous chapter, the grafting of a positively-charged poly[2-(methacryloyloxy)ethyl]trimethylammonium chloride (PMETAC) brushes on textile surface is demonstrated. With the loading of anion catalytic moieties tetrachloropalladate(II) ($PdCl_4^{2-}$) for the subsequent metal electroless deposition (ELD), a robust metal layer is deposited on the textile surface with outstanding adhesion and washing durability. As the selection of catalytic moieties highly depends on the properties and nature of polyelectrolyte brush that grafted on the textile surface, cationic PMETAC is restricted to only couple with anionic $PdCl_4^{2-}$ for subsequent electroless metal deposition. Therefore, this approach suffers one serious drawback in which the fabrication is associated with high cost as $PdCl_4^{2-}$ is expensive (USD 80 per gram for 97% ammonium tetrachloropalladate(II) from Aldrich). Even though the $PdCl_4^{2-}$ can be re-collected and reused, it is still not economical if it is used in the mass production. As a result, to eliminate the use of $PdCl_4^{2-}$, a strategy to graft another kind of polyelectrolyte brush on the textile surface for subsequent ELD is highly desirable.

In this chapter, we report the results of grafting negatively-charged polymer brushes, such as poly(methacrylic acid sodium salt) (PMANa) and poly(acrylic acid sodium salt) (PAANa), from monomers methacrylic acid sodium salt (MANa) and acrylic acid sodium salt (AANa), respectively. The chemical structures of MANa and AANa monomers are illustrated in Figure 6.1. In fact, these two monomers are very similar in their chemical structures, in which the MANa monomer only has one extra methyl group comparing to the AANa monomer. Theoretically, MANa should be more reactive than AANa in the radical polymerization as methyl group is an electron releasing group that is more likely to be attacked by free radicals during free radical polymerization.

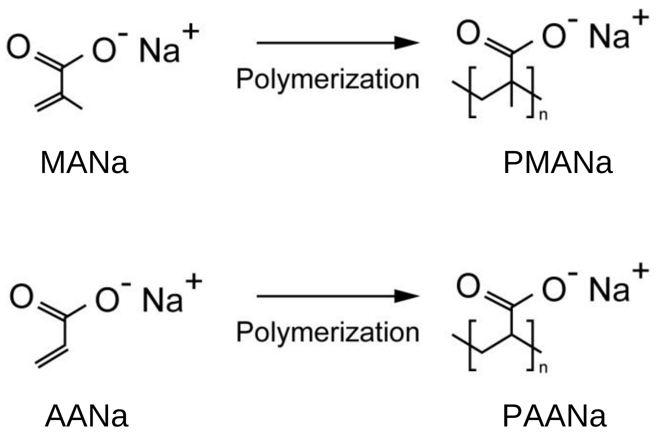

Figure 6.1 Polymerization of MANa and AANa monomers to PMANa and PAANa.

As PMANa and PAANa are anionic polymer brushes, after grafting PMANa or PAANa brushes on the textile surfaces, without using the costly palladium-bearing catalyst but simply by loading cationic copper ion and also reducing adhered copper ions to copper metal, electroless copper deposition can be carried out simultaneously to yield a layer of robust copper metal on the textile surfaces. Experimental section will explain the procedures in details followed by sample characterizations using ATR-FTIR, EDS, SEM and water contact angle measurement. The sheet resistance and the washing durability according to AATCC 61-2A will also be reported.

6.2 Experimental

6.2.1 Materials

Chemicals used in the experiment were used upon received without further purification unless specified. Commercially purchased 100 % plain weave cotton fabric was pre-treated by singeing, desizing, scouring, bleaching and mercerizing. Vinyltrimethoxysilane (VTMS) (98 %), Monomers including MANa (99 %) and AANa (97 %) were obtained from Sigma-Aldrich®. Potassium persulphate powder and copper(II) sulphate pentahydrate were procured from Acros Organics. Acetic acid, potassium sodium tartrate tetrahydrate and sodium hydroxide were obtained from VWR BDH Prolabo®. Formaldehyde solution (36.5 to 38.0 %) was purchased from Thermo Fisher Scientific Inc.. Deionized (DI) water was used throughout the whole experiment.

6.2.2 Procedures

As a proof-of-concept, surface modification on cotton was firstly carried out using VTMS. Then, an all-solution process based on in-situ free radical polymerization method was carried out to prepare PMANa-coated cotton (PMANa-cotton). Subsequent ion exchange, ion reduction and electroless deposition of metal particles onto the PMANa-cotton yielded electrically conductive fabrics. In particular, we carried out electroless copper deposition on the cotton surface to yield copper-cooated cotton fabrics (Cu-cotton). The procedure for preparing PMANa polyelectrolytes is schematically illustrated in Figure 6.2 (top). The preparation of PAANa polyelectrolytes on textile substrate is similar to the PMANa one, which is shown in Figure 6.2 (bottom).

Silanization. In a typical experiment, textiles were first immersed in a solution of 5-20 % (v/v) vinyltrimethoxysilane (VTMS) under a pH condition of around 4.5 for 30 min, allowing the hydroxyl groups of cellulose to react with the VTMS molecules. Then the cottons yarns were rinsed thoroughly with fresh DI water to remove any excess physical adsorbed VTMS and other by-product molecules. The rinsed cotton yarns were put into an oven at 110 ˚C for 15-30 min to complete the condensation reaction. VTMS-deposited cotton (VTMS-cotton) is fabricated.

Grafting of PMANa or PAANa brushes by in-situ free radical polymerization. Subsequently, VTMS-cotton was immersed into 50 mL aqueous solution comprising of 3.5 g of MANa (MANa for PMANa; AANa for PAANa) powder and 37.5 mg of potassium persulphate. The whole solution mixture with textiles was heated at 80 ˚C in an oven for 1 h to carry out the free radical polymerization. In the free radical polymerization process, the double bond of VTMS can be opened by the free radical resulting in the growth of PMANa (or PAANa) polyelectrolyte onto the cotton fiber surface to yield PMANa-grafted cotton (PMANa-cotton) or PAANa-grafted cotton (PAANa-cotton).

Ion exchange and reduction. The PMANa-cotton (or PAANa-cotton) was immersed into a 39 g/L copper(II) sulphate pentahydrate solution for 0.5-1 h, where the Cu^{2+} ions were immobilized onto the polymer by ion exchange. The fabric was then rinsed with DI water for two times. Reduction of copper ions was carried out by immersing the fabric into 0.1 M sodium borohydride solution. Copper ions immobilized on the polymer brush will be reduced to copper seed particles which acted as nucleation sites for the growth of copper in the subsequent electroless deposition.

Electroless copper deposition. After reduction in 0.1 M sodium borohydride solution, the cotton was rinsed thoroughly with DI water and immersed in a copper electroless plating bath consisting of 12 g/L sodium hydroxide, 13 g/L copper(II) sulphate pentahydrate, 29 g/L potassium sodium tartrate, and 9.5 mL/L formaldehyde in water for 180 min. The as-synthesized copper-coated cotton (Cu-cotton) were rinsed thoroughly with DI water and blown dry.

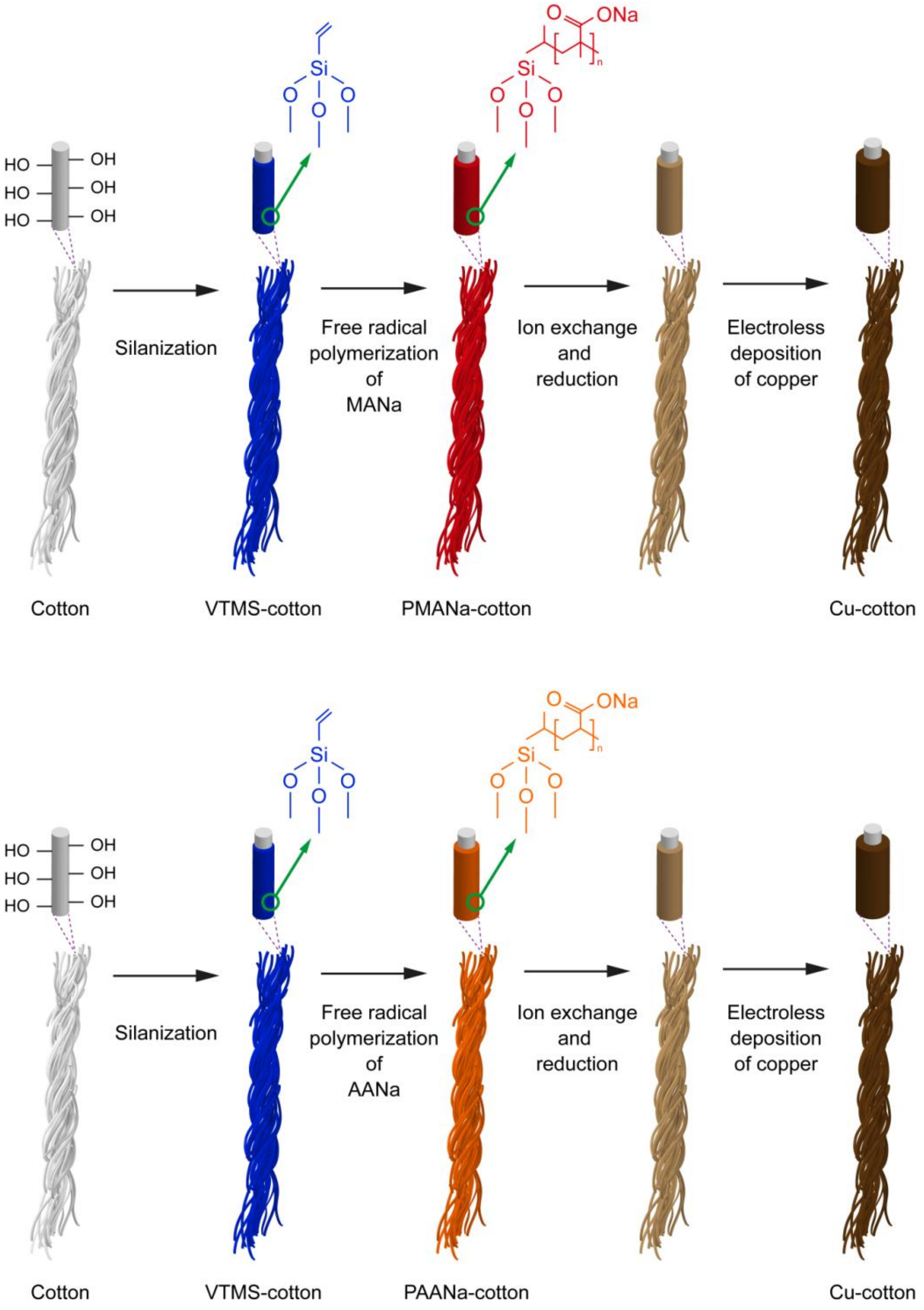

Figure 6.2 Schematic illustrations of the fabrication procedures of Cu-cotton by grafting anionic PMANa brushes on the cotton surface, with subsequent ion exchange and reduction followed by electroless deposition of copper.

The grafting of anionic PAANa brush follows the same procedures as shown in the bottom scheme.

6.3 Results and Discussion

6.3.1 Fabrication of Copper-coated Cotton Fabrics

6.3.1.1 Sample Characterizations

The VTMS-cotton, PMANa-cotton and PAANa-cotton were characterized by attenuated total reflection Fourier transform infrared spectroscopy (ATR-FTIR). As shown in Figure 6.3, a distinctive peak located at 769 cm^{-1} was attributed to Si-O-Si symmetric stretching, indicating the VTMS molecules were successfully cross-linked with each other on the cotton fiber surface. For the PMANa-cotton sample, new peak located at 1548 cm^{-1} standing for carboxylate salt asymmetrical stretching vibrations confirmed the successful PMANa grafting. Other peaks located at 1454 cm^{-1} and 1411 cm^{-1} were both attributed to carboxylate salt symmetrical stretching vibrations of the carboxylate group in PMANa. For the PAANa-cotton, the ATR-FTIR spectrum follows a similar pattern as that of the PMANa. Distinctive peaks located at 1550 cm^{-1} was attributed to the carboxylate salt asymmetrical stretching vibrations. Other peaks such as 1453 cm^{-1} and 1410 cm^{-1} indicated the presence of carboxylate salt symmetrical stretching vibrations of the carbonxylate group in PAANa.

The presence of the anionic polymer brushes in PMANa-cotton and PAANa-cotton were also characterized by energy-dispersive X-ray spectroscopy (EDS). It showed that after polymerization of MANa, the cotton fabric contained sodium element, indicating the presence of PMANa (Figure 6.4). The PAANa-cotton was also detected with sodium element (Figure 6.5), indicating successful grafting of PAANa on the cotton fiber surface.

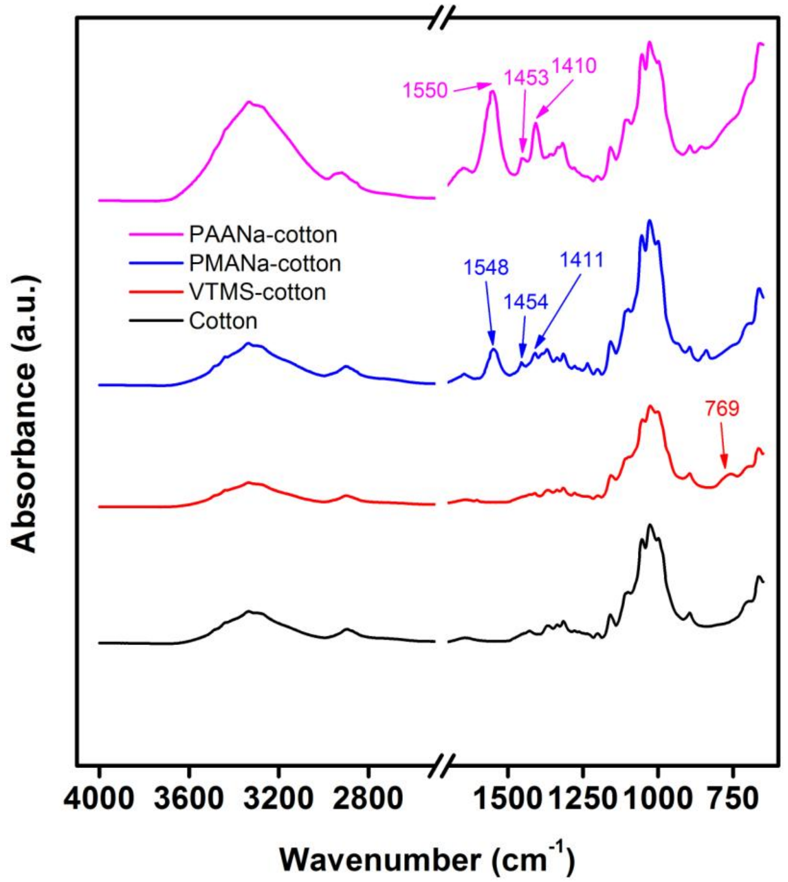

Figure 6.3 ATR-FTIR spectra of the modified cotton fabrics.

Sample	Distinctive Peaks at Wavenumber (cm^{-1})	Corresponding Functional Group
VTMS-cotton	769	Si-O-Si
PMANa-cotton	1548	$RCOO^-$
	1454	$RCOO^-$
	1411	$RCOO^-$
PAANa-cotton	1550	$RCOO^-$
	1453	$RCOO^-$
	1410	$RCOO^-$

Table 6.1 Summary of the ATR-FTIR data of the VTMS-cotton, PMANa-cotton and PAANa-cotton samples.

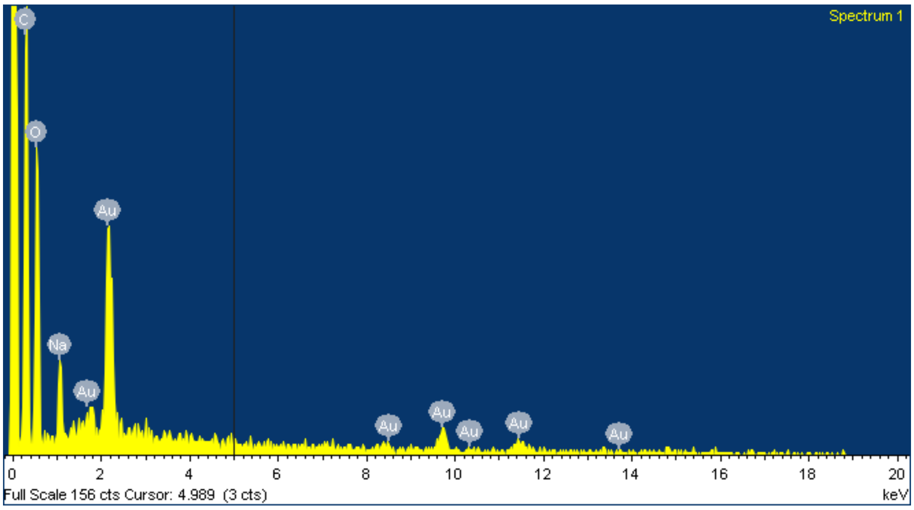

Figure 6.4 EDS spectrum of PMANa-cotton.

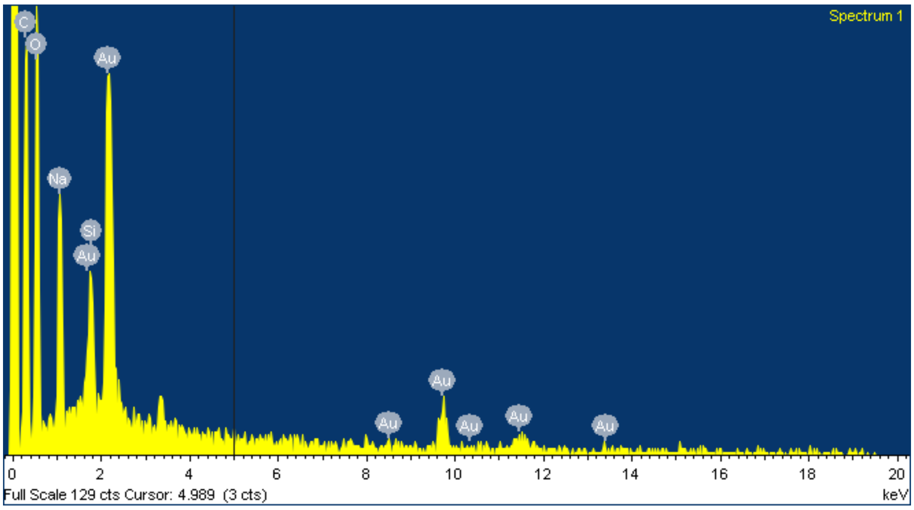

Figure 6.5 EDS spectrum of PAANa-cotton.

The surface morphology of the cotton samples was characterized by scanning electron microscopy (SEM). As shown in Figure 6.6, SEM images showed no obvious difference between the surface morphology of the VTMS-cotton and the pristine cottons. However, after polymerization of PMANa or PAANa on the VTMS-cotton fiber surface, it was significant that a layer of coating was wrapped on the cotton fiber surface. Figure 6.6 (E and F) showed that the copper metal particles were deposited very evenly on both of the surfaces of PMANa- and PAANa-cotton, without any signs of cracks.

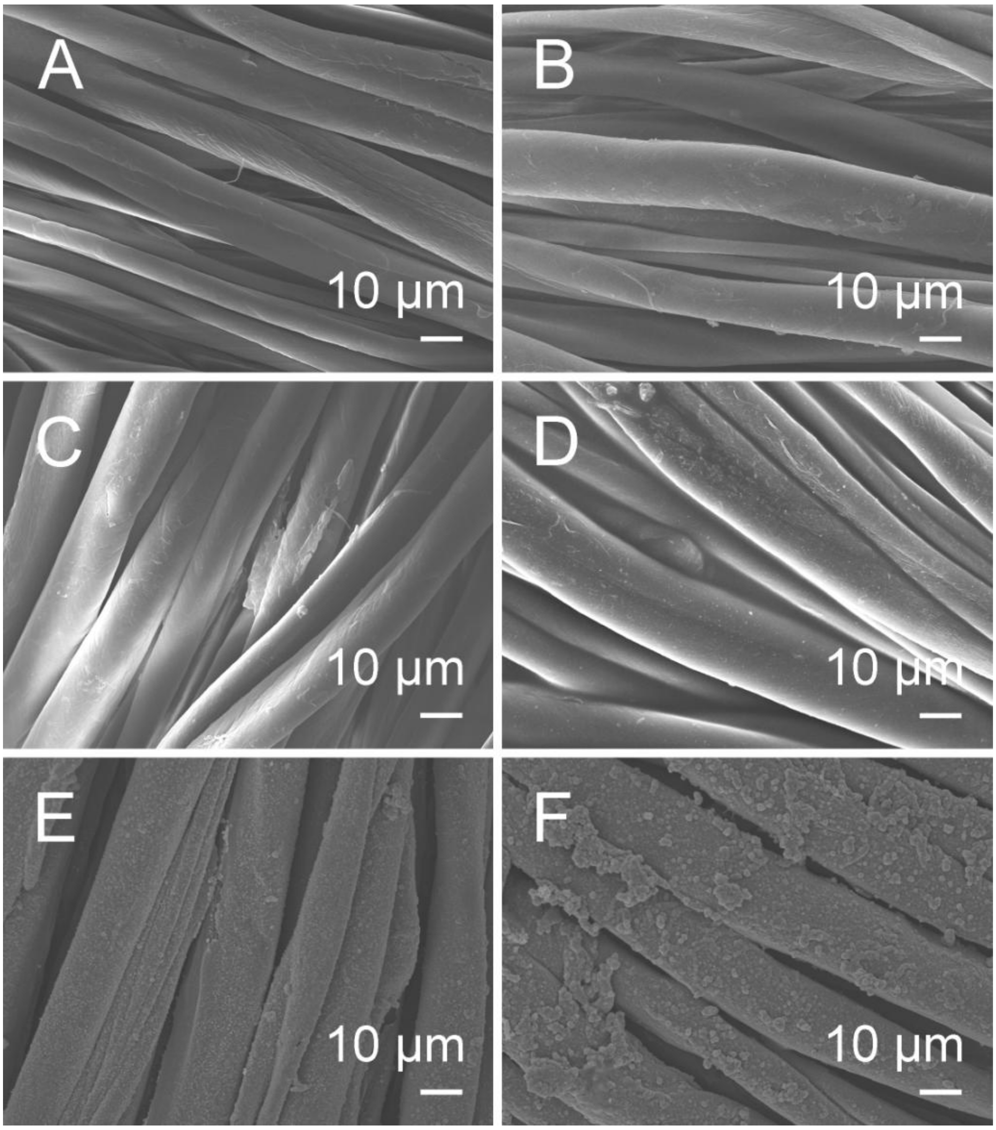

Figure 6.6 SEM images of (A) cotton; (B) VTMS-cotton; (C) PMANa-cotton; (D) PAANa-cotton; (E) PMANa-assisted Cu-cotton and (F) PAANa-assisted Cu-cotton.

To further confirm the surface modification, comparative experiment was conducted and silicon wafer (Si) was used to be the substrate. The surface modification by grafting PMANa or PAANa brushes on Si wafer was characterized by water contact angle measurement. Prior to the modifications, the Si wafer was treated with an oxygen plasma to render the surface hydrophilic, in which the water contact angle dropped from 50.8 ° to 2.5°. After depositing a multilayer of VTMS, the water contact angle on the

VTMS-Si increased to 87.5 °. Grafting of PMANa and PAANa rendered a drop in water contact angle again with 45.7 ° and 48.6 °, respectively.

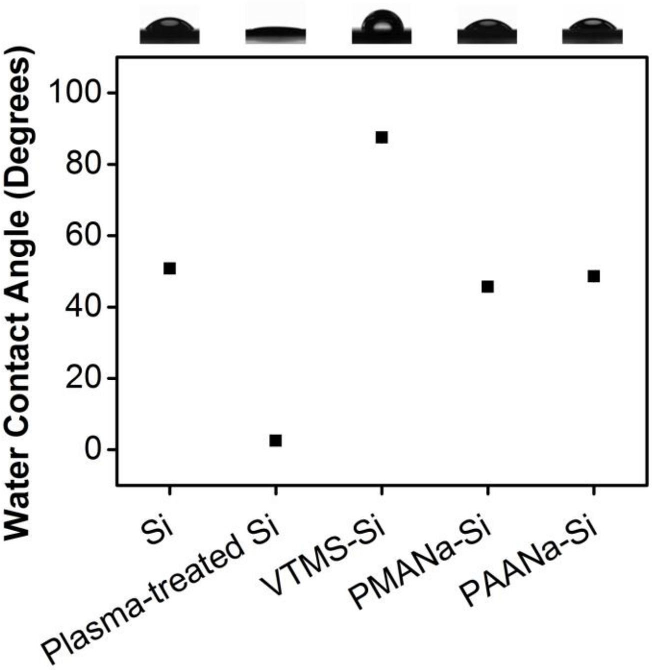

Figure 6.7 Water contact angle measurement of silicon wafer under different treatments.

For the cotton fabric sample, as expected, after VTMS deposition, the water contact angle increased to 135.9 °. However, after grafting PMANa or PAANa, the hydrophilicity resumed back and can be reflected in the high water absorbance of the fabric.

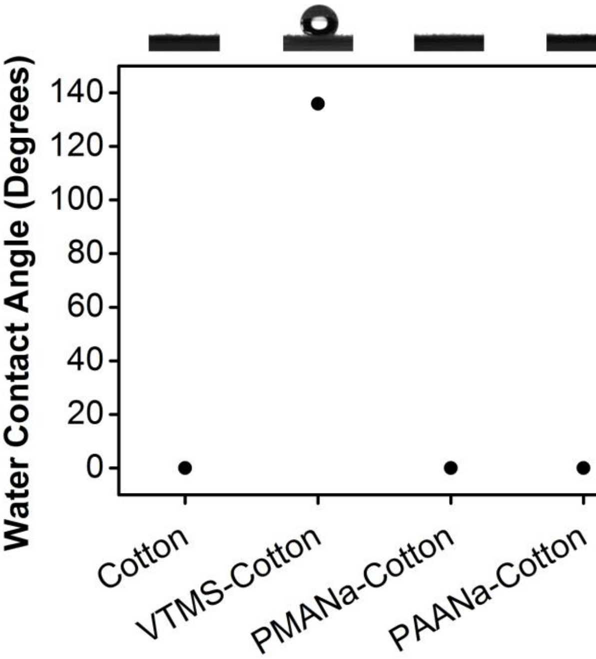

Figure 6.8 Water contact angle measurement of cotton fabric under different treatments.

6.3.1.2 Sheet Resistance and Washing Durability

It was found that the fabric color after copper ion exchange was not very prominent and only a slight shade of grey color could be obtained after copper ion reduction by sodium borohydride solution. Such results may attribute to comparatively short polymer brushes grown on the fabric surface. With prolonged ELD time to 180 min, the final copper-coated cotton fabric had an even coating of copper, with sheet resistance measured as ~0.5 ohm/sq. The as-made copper-coated fabric was challenged by repeated laundering test according to AATCC 61-2A, Colorfastness to Laundering: Accelerated. The laundering ability of the Cu-cotton (Figure 6.9) is very satisfactory. It is worthy of note that one wash in the test resembles five machine launderings. The average sheet resistances of these fabrics after 15 machine washes are reported in Table 6.2. The surface appearance of the fabric after washing up to 3rd time, copper coating remains good without partially falling off. It is thus deduced that thicker copper coating under prolonged ELD time is more desirable for fabric samples to withstand machine washing.

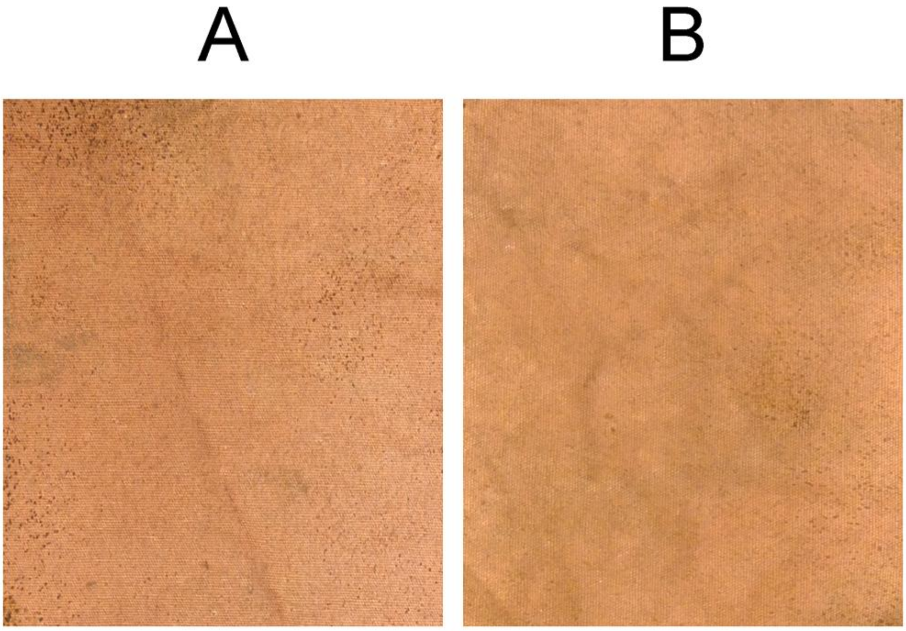

Figure 6.9 Appearances of (A) PMANa- and (B) PAANa-assisted Cu-cotton fabrics after 15 cycles of machine laundering.

Times of washing	**0**	**5**	**10**	**15**
Average sheet resistance of PMANa-assisted Cu-cotton fabric (ohm/sq)	0.6	0.7	0.7	1.2
Average sheet resistance of PAANa-assisted Cu-cotton fabric (ohm/sq)	0.5	0.6	0.9	0.9

Table 6.2 The average resistance of the PMANa- and PAANa-assisted Cu-cotton under different times of standard washing.

6.3.2 Fabrication of Copper-coated Polyester Yarns and Nylon Mesh

Other than cotton substrate, a trial on fabricating copper-coated polyester yarn (Cu-PET) and copper-coated nylon (Cu-nylon) mesh had been carried out. Prior to any surface modifications, pristine nylon was immersed into 2 M sodium hydroxide solution at 80 ˚C for 2 hr and followed by 5-min oxygen plasma to render the surface hydrophilic, following the same procedures of grafting PMANa brushes on the nylon surface with subsequent ELD of copper.

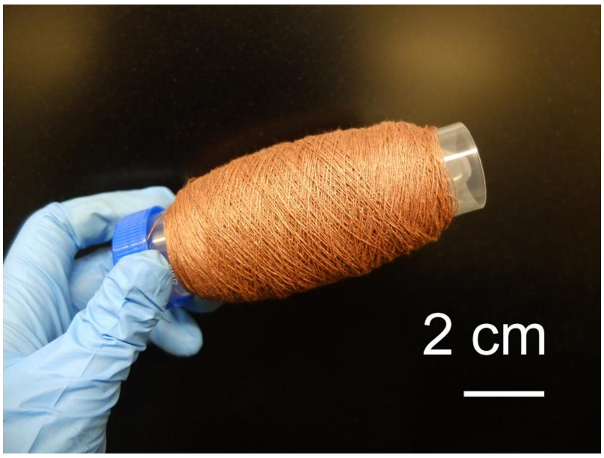

Figure 6.10 Cu-PET yarns assisted by grafting of PMANa.

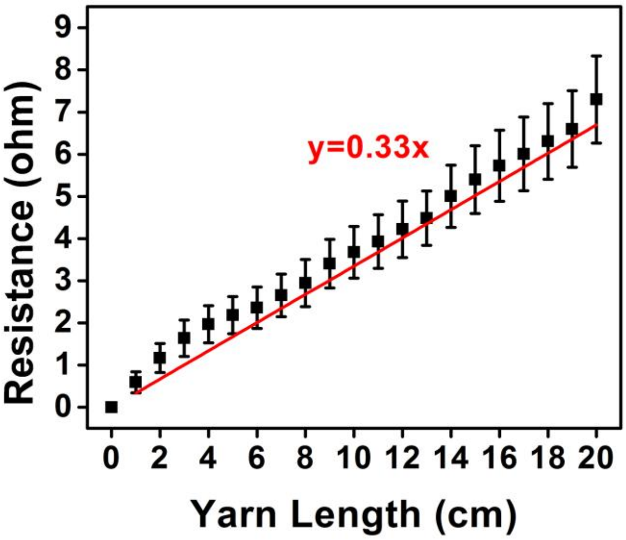

Figure 6.11 Linear resistance of single strand Cu-PET yarn.

Grafting PMANa to yield Cu-nylon mesh was also carried out. As-made Cu-nylon mesh exhibited a sheet resistance of ~4 ohm/sq (Figure 6.12). Copper remained adhered on the nylon mesh even after several bending. It was also found that when the thickness of the copper layer deposited was too thick, there might be a possibility that copper fall off as individual flakes. Thus, the time for metal electroless deposition should be well controlled. To further investigate the versatility of nickel deposition using this polymer grafting on textile substrate, same experimental procedures were followed but the source of nickel was from nickel(II) sulphate solution in the ion exchange procedure. As shown in Figure 6.13, the Ni-cotton fabric has a high evenness of nickel metal, with bulk resistance measured as ~3.2 ohm.

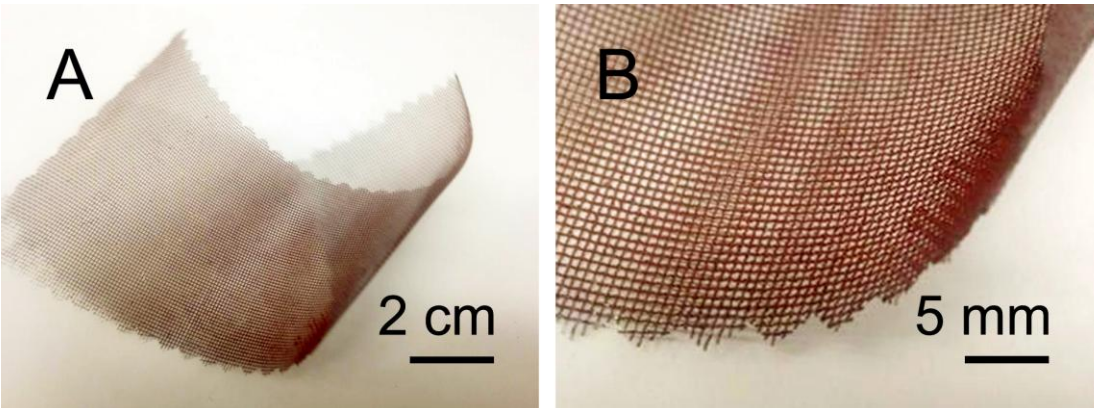

Figure 6.12 Cu-nylon mesh assisted by grafting of PMANa.

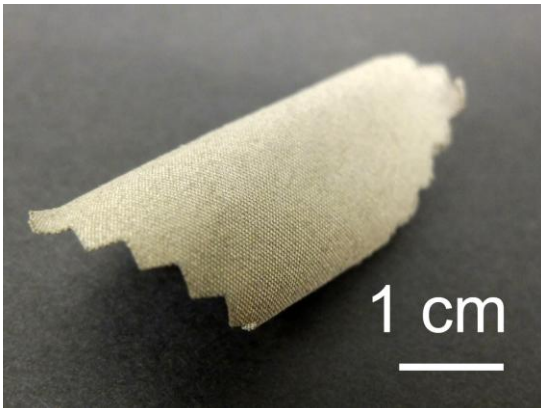

Figure 6.13 Ni-cotton fabric assisted by grafting of PAANa.

6.3.3 Incorporation in Electronic Circuit

The as-synthesized Cu-PET yarns were incorporated into electronic circuits to light up several LEDs in series to demonstrate the potential applications in wearable electronics.

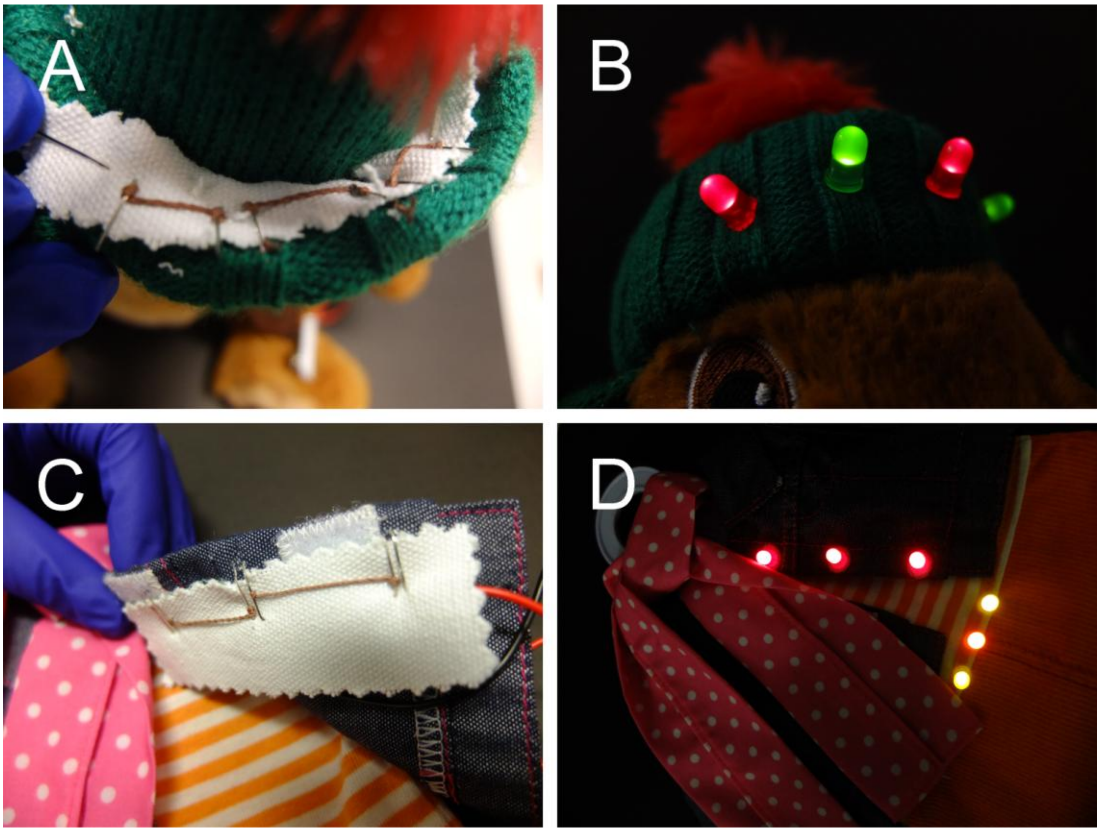

Figure 6.14 Cu-PET yarns were stitched onto (A, B) a knitted hat and (C, D) clothes on dolls, with several LEDs connected in series.

6.4 Chapter Conclusion

In this chapter, metallic textiles are successfully fabricated by grafting anionic polymer brushes such as PMANa and PAANa on the textile surface. With subsequent copper ion loading and reduction, copper seed particles are successfully deposited on the textile surface, and act as nucleation sites for electroless copper deposition. Comparing to the cationic polymer PMETAC which is reported in the previous chapter, grafting of anionic polymers such as PMANa or PAANa can eliminate the use of expensive palladium-bearing catalyst, but in fact requires an extra reduction step to reduce the already-loaded metal ions. The detailed experimental flow is shown in Figure 6.15.

Without using the costly palladium-bearing catalyst in ELD, the cost of the experiment can be reduced by ~30 % (Appendix 4 and 5). This versatile approach provides a great potential in fabricating low-cost but high-performance conductive textiles. As-synthesized Cu-cotton exhibits outstanding conductivity as well as washing durability. As demonstrated, the Cu-cotton can withstand 15 standard washing cycles with only slight increase in sheet resistance. As this approach is also aqueous and air-compatible, and does not require any high-end facilities for the fabrication, it is expected that it is more suitable for the mass scale production of metallic textiles in the textile industry.

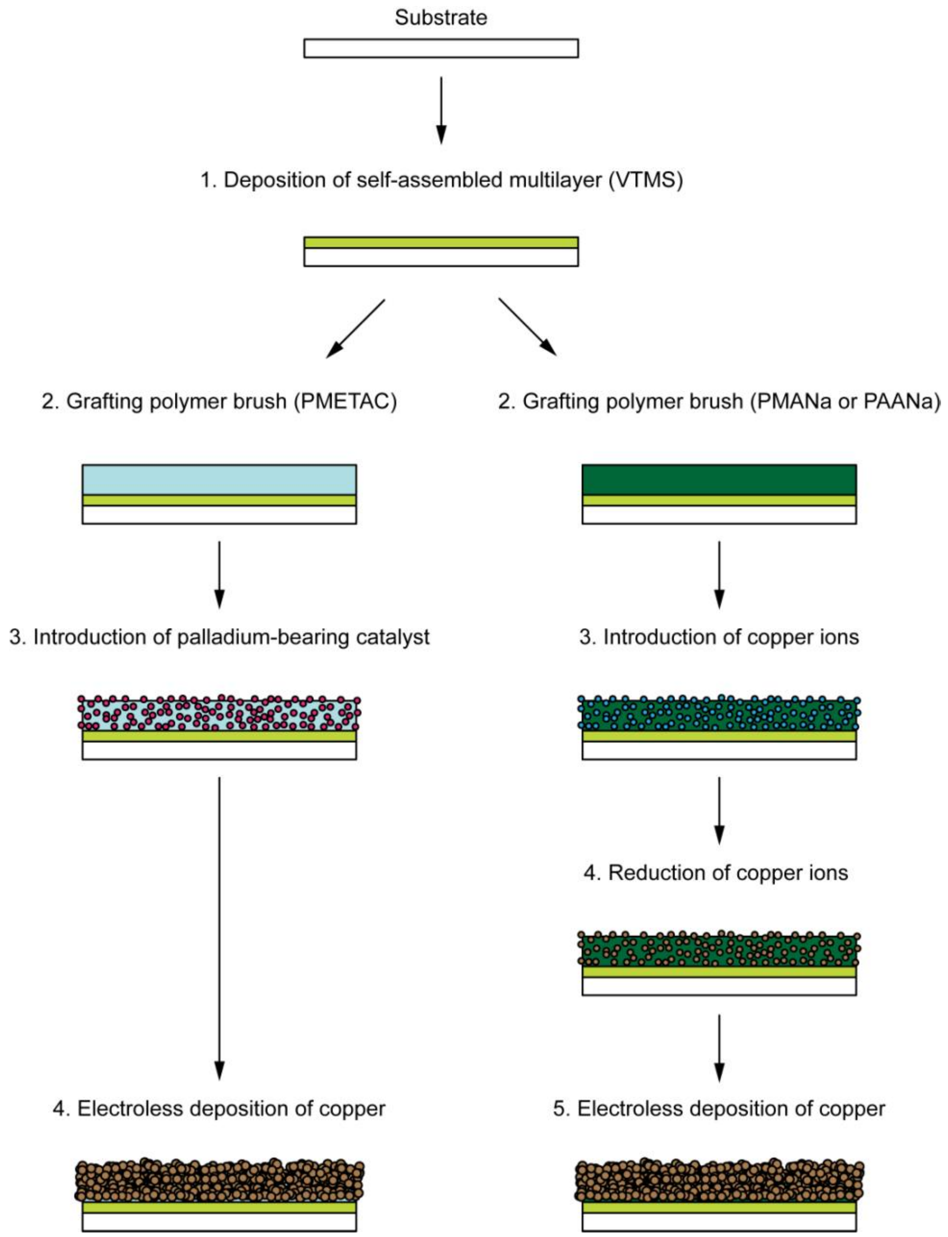

Figure 6.15 Comparison of the experimental steps involving grafting of cationic PMETAC and anionic PMANa or PAANa brushes to yield Cu-cotton.

(Blank Page)

CHAPTER 7: PRELIMINARY RESULTS OF THE FABRICATION OF TEXTILE TRIBOELECTRIC GENERATORS WITH METALLIC TEXTILES SYNTHESIZED BY POLYMER-ASSISTED METAL DEPOSITION (PAMD)

7.1 Introduction

Now we come to the era of wearable electronics, in which power supply is one of the inevitable components in powering all the wearable devices. To realize wearable power source especially for wearable electronics, thinner, lighter, and cheaper solution is a must to go for. Recently, Li-ion batteries and supercapacitors in lightweight, durable, flexible and stretchable form are invited as fiber- or textile-based. However, these energy devices are non-sustainable, which cannot be used continuously but require external energy sources to charge up the devices. Once the energy stored is used up, they need to be replaced or re-charged again, which is very inconvenient and troublesome especially for those continuous signal monitoring devices in healthcare and smart displays.

Harvesting ambient mechanical energy to power up wearable devices may be the alternative approach. Particularly, harvesting ambient energy by triboelectricity attracts much attention in recent years due to their simple fabrications. In 2012, the first triboelectric nanogenerator was invented by Fan et al., in which the triboelectric generator utilized charge transfer during electrification of the two selected materials when rubbed against each other, to generate a triboelectric potential (119). Upon contact and release action of the two materials' surfaces with potential developed therein, current was generated when connected to an external load. Such a triboelectric generator could generate an open circuit voltage of ~3 V and short circuit current of ~3 μA. Later, tremendous designs of triboelectric generators emerged and the triboelectric generator was considered as a hot topic (119, 120, 153-166). However, all those designs reported suffer high difficulty in scale production as most of the designs involve the application of nanoparticles to increase the surface area so as the surface roughness for better output performance. Moreover, as triboelectric generators harvest the mechanical ambient energy mostly from the repeated bending, stretching and releasing actions from human body motions, the conductive electrodes in the device should be robust enough to withstand such a high number of repeated bending and relaxing cycles. However, those reports from the literature mostly failed in fabricating durable electrodes. Addressing these challenges, we report here the preliminary results of fabricating triboelectric generator using the metallic textiles that were developed previously using polymer-assisted metal deposition (PAMD). As demonstrated in the previous sections, the metallic textiles synthesized by PAMD exhibit a remarkable durability in repeated bending and even washing cycles, which is highly desirable in making the robust electrodes in the triboelectric devices.

In particular, we synthesize the textile triboelectric generators using polyimide/nylon coupling and polyimide/copper coupling. Copper-coated textiles (Cu-textiles) synthesized by polymer-assisted metal deposition (PAMD) and reported in the previous sections are used as the electrodes. The textile triboelectric generators are fabricated by either stacked fabrics or twisted yarns to form fabric-based and yarn-based triboelectric generators, respectively; while the third type namely woven-based triboelectric generator is fabricated by textile weaving technique (Figure 7.1). Each fabrication is further discussed in details in the following sections.

7.2 Experimental

7.2.1 Materials

Chemicals used in the experiment were used upon received without further purification unless specified. Commercially purchased 100 % plain weave cotton fabric and yarns (40 s) were pre-treated by singeing, desizing, scouring, bleaching and mercerizing. Commercially purchased 100 % plain weave polyester fabric and yarns (298 dtex) were pre-treated with 2 M sodium hydroxide and also 5-min oxygen plasma to render the surface hydrophilic. 100 % plain weave nylon fabric used as the triboelectric coupling layer was purchased from the market. Polyimide precursor polyamic acid (PAA) was obtained from Shanghai Jiao Tong University. The viscosity of the precursor was 5600 cP.

7.2.2 Procedures

The materials used in the triboelectric coupling were selected according to the triboelectric series as shown in Figure 7.1 (154, 167). According to the sequence shown in the triboelectric series, which is a list showing the tendency of a material to gain or lose electrons upon friction. The higher position the material is listed in the series, the higher the tendency to lose electron to become positively-charged. Vice versa applies to those materials which are located at the lower position of the series.

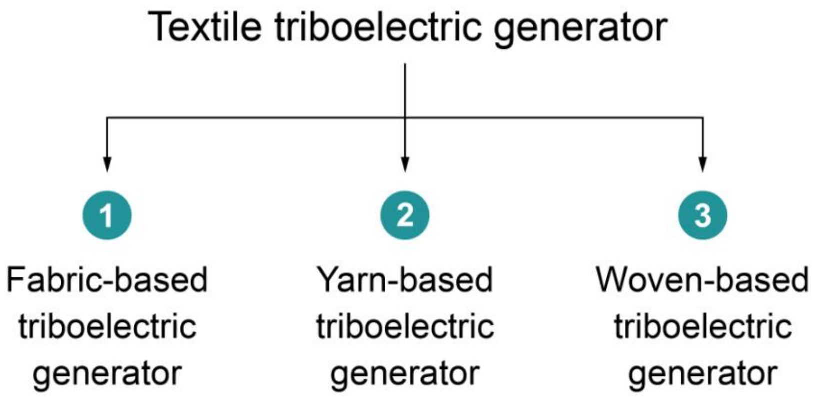

Figure 7.1 Three types of textile triboelectric generator fabricated in this research.

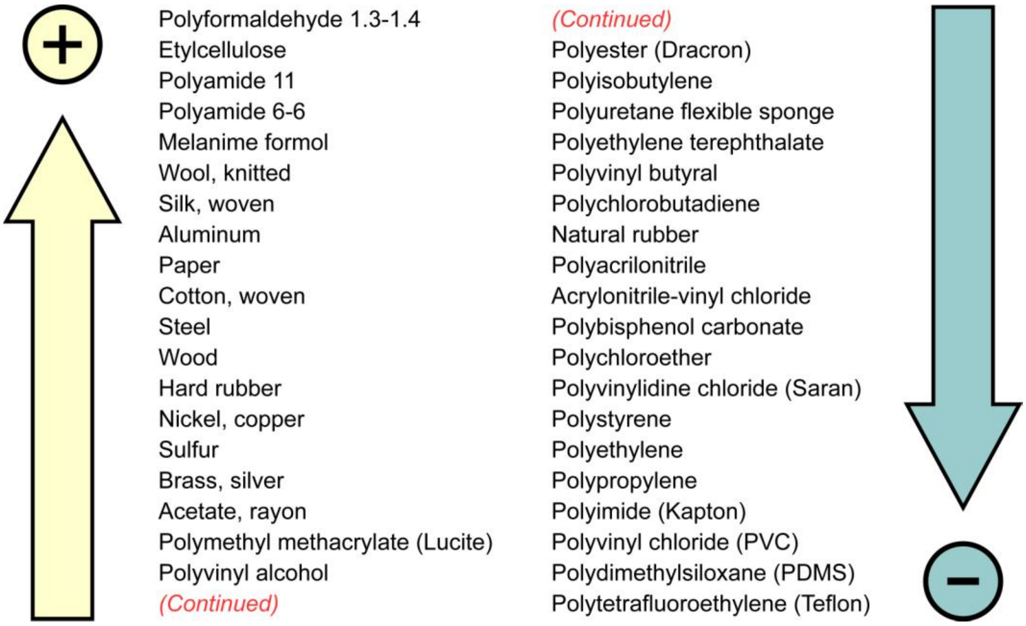

Figure 7.2 The triboelectric series.

Evaluation on the performance of textile triboelectric device was performed by an electrometer (Keithley 6517A) linked with a connector block (National Instruments BNC-2120). The bending action of the triboelectric generator was performed by a linear motorized actuator, in which the triboelectric generator was clamped and secured at one side of the triboelectric generator while the other side was left free to allow a mild collision by the linear motorized actuator.

7.3 Results and Discussion

7.3.1 Optimization for Polyimide Coating

Polyimide (PI), with a registered trademark as Kapton, was developed by DuPont in late 1960s. It shows excellent thermal stability as well as electrical insulation properties. Therefore it is widely used in the electronic sector. Formation of PI originated from two monomers, which are pyromellitic dianhydride and 4,4’-diaminodiphenyl ether. By reacting these two monomers in solvents like N,N-dimethylacetamide (DMAc) or N-methylpyrrolidinone (NMP), an intermediate polymer known as polyamic acid (PAA) is formed. Condensation reaction of PAA under sufficient drying and curing condition yields PI. The synthesis of PI is illustrated in Figure 7.3.

In order to get the conformal PI coating on the textile surface, optimization of PI on the cotton fabric was first investigated. PI-coated cotton (PI-cotton) was fabricated by immersing cotton fabric into PAA for 15 min and then transferred to the vacuum oven at various temperatures. To study the imidization process of PI, we conducted repeated experiments by varying the temperatures at 80 ˚C, 150 ˚C, 180 ˚C and 200 ˚C at a fixed time period of 2 hr. It is worthy of note that most of the textile materials cannot withstand a high temperature as high as 300 ˚C, where full imidization of PI occurs. Therefore, we opt for a restricted curing temperature below 200 ˚C. PI-cotton fabrics prepared under different temperatures were examined by ATR-FTIR. As depicted in Figure 7.4, the intensities of the characteristic peaks of PAA, situated at 1652 cm^{-1} and 1539 cm^{-1} respectively corresponding to the C=O and C-NH of the amide in PAA, gradually decreased when the oven temperature increased from 80 ˚C to 200 ˚C, indicating that the amount of PAA decreased when the curing temperature increased. At the same time, the intensities of the characteristic peaks for PI located at 1775 cm^{-1} (C=O asymmetric stretching), 1718 cm^{-1} (C=O symmetric stretching), 1373 cm^{-1} (C-N stretching) and 724 cm^{-1} (C=O bending) increased respectively, showing the gradual formation of PI from PAA upon increasing temperatures. Apparently, complete disappearance of the distinctive peaks of PAA was observed at 180 ˚C. Therefore, 180 ˚C was selected for further optimization for the curing time of PI.

Optimization of the curing time of PI was investigated by curing the precursor-coated fabric sample in different time period of 1 hr, 2 hr, 4 hr and 6 hr at a fixed temperature of 180 ˚C under vacuum. As shown in Figure 7.5, complete disappearance of the characteristic peaks of PAA at 1652 cm^{-1} and 1539 cm^{-1} corresponding to C=O and C-NH in amide is observed in each spectrum. Even though the ATR-FTIR spectra in each curing condition are more or less the same, the spectrum of 6 hr curing time gives more intensive peaks of PI at 1775 cm^{-1} (C=O asymmetric stretching), 1722 cm^{-1} (C=O symmetric stretching) and 724 cm^{-1} (C=O bending). Therefore, the optimized curing temperature and time for PI are selected as 180 ˚C and 6 hr, respectively.

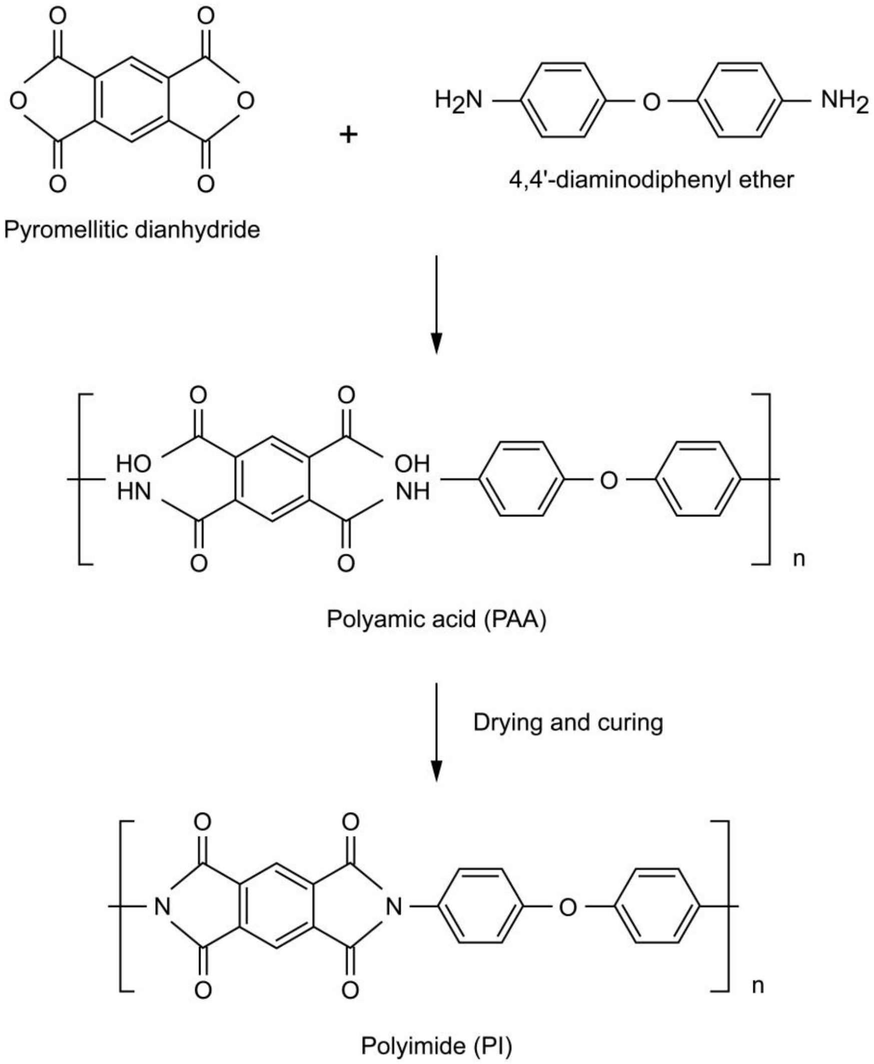

Figure 7.3 Synthesis of polyimide (PI) from precursor polyamic acid (PAA).

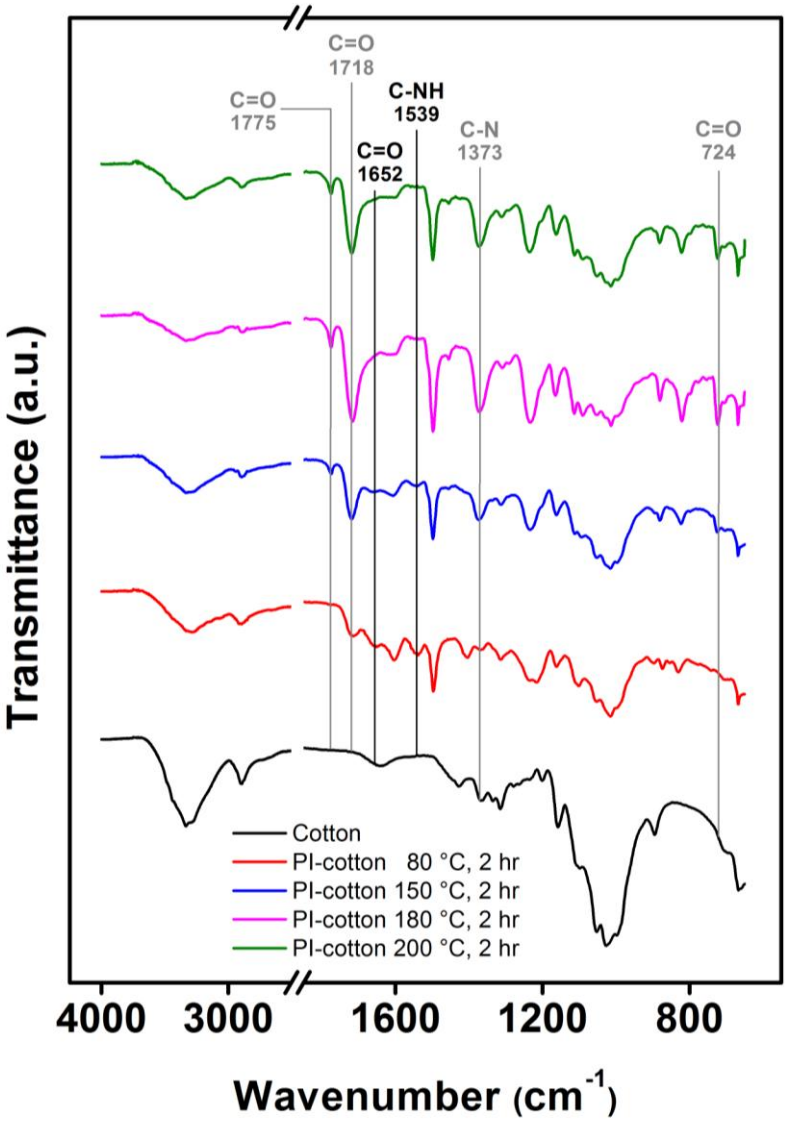

Figure 7.4 ATR-FTIR spectra of the PI-coated cotton fabrics under varying curing temperatures at a fixed curing period of 2 hr.

Sample	Distinctive Peaks at Wavenumber (cm^{-1})	Corresponding Functional Group
Polyamic acid (PAA)	1652	C=O
	1539	C-NH
Polyimide (PI)	1775	C=O
	1718	C=O
	1373	C-N
	724	C=O

Table 7.1 Summary of the ATR-FTIR data of the PAA and PI in Figure 7.4.

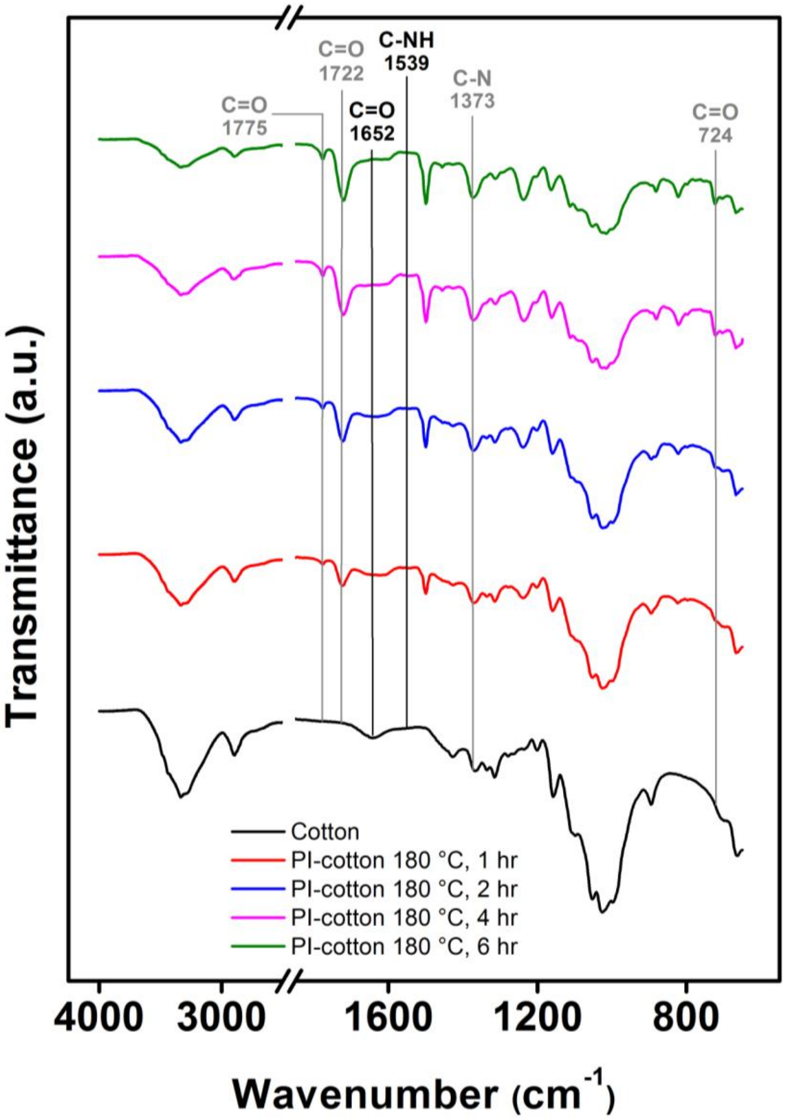

Figure 7.5 ATR-FTIR spectra of the PI-coated cotton fabrics under varying curing period at a fixed curing temperature of 180 ˚C.

Sample	Distinctive Peaks at Wavenumber (cm^{-1})	Corresponding Functional Group
Polyamic acid (PAA)	1652	C=O
	1539	C-NH
Polyimide (PI)	1775	C=O
	1722	C=O
	1373	C-N
	724	C=O

Table 7.2 Summary of the ATR-FTIR data of the PAA and PI in Figure 7.5

As-synthesized PI-cotton fabricated using the optimized recipe of coating PI is shown in Figure 7.6C. Comparing to the pristine cotton (Figure 7.6A), PI-cotton is in yellow color and more rigid in handfeel. SEM image shown in Figure 7.6D reveals that the surface of the cotton fabric is fully covered with a layer of PI, which is a plain and smooth layer of non-conductive coating. Comparing to the pristine cotton (Figure 7.6B), however, a typical woven structure is shown.

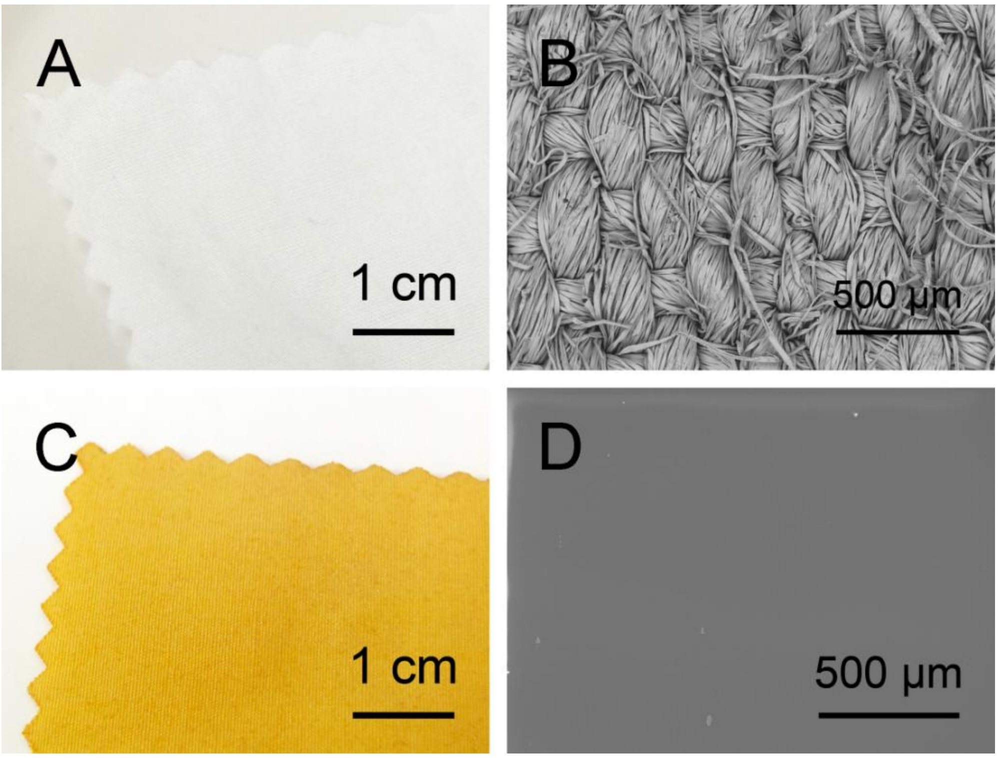

Figure 7.6 (A) Digital image and (B) SEM image of pristine cotton. (C) Digital image and (D) SEM image of PI-cotton.

7.3.2 Fabrication and Performance Evaluation of Fabric-based Triboelectric Generator

In the fabrication of fabric-based triboelectric generator, according to the triboelectric series in Figure 7.1, PI/nylon is one of the suitable couplings to generate triboelectric potential as PI tends to gain electrons to become negative while the nylon tends to lose electrons to become positive. The device fabrication and structure are illustrated in Figure 7.7. By stacking a layer of nylon fabric, PI-cotton, Cu-cotton fabrics fabricated by PAMD as conducting electrodes and finally by sealing with PET laminating film (125 μm), a very simple textile triboelectric generator could be obtained (Figure 7.7, inset).

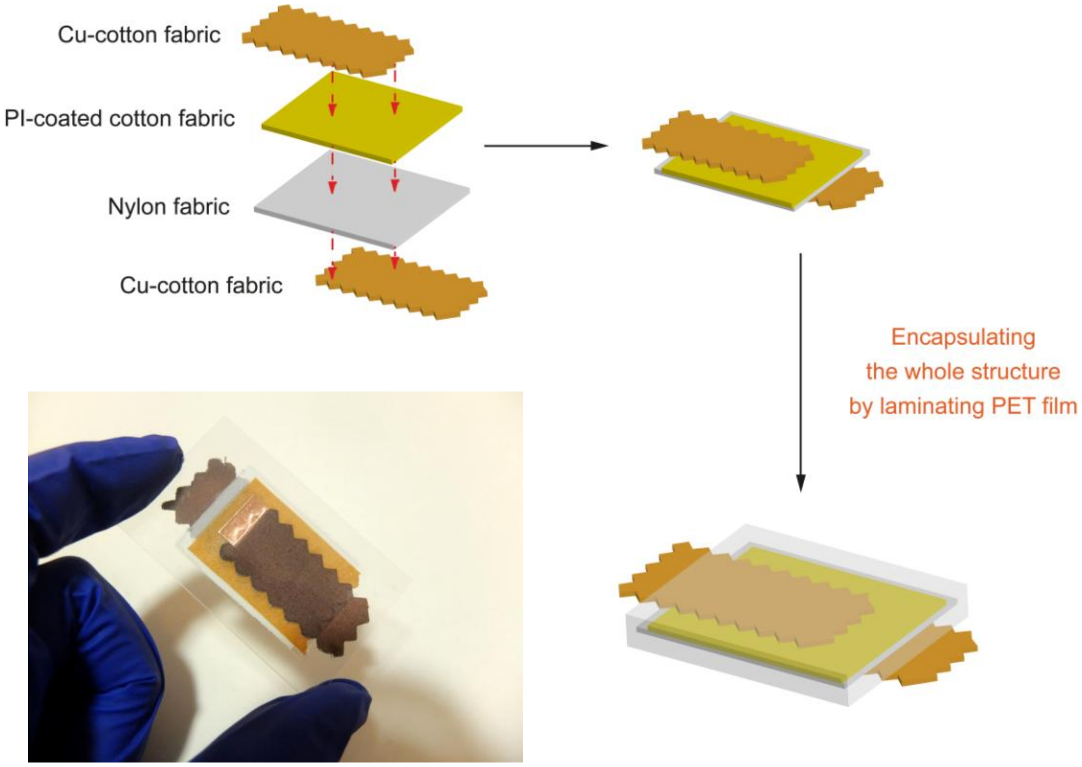

Figure 7.7 Schematic illustration showing the fabrication of the fabric-based triboelectric device and the as-made device (inset).

The performance of the triboelectric generator was evaluated. As shown in Figure 7.8, the maximum open circuit (OC) voltage of the fabric-based triboelectric generator is measured as ~4 V. It is observed that the voltage output is quite stable even though different acceleration values are applied to the sample. The maximum short-circuit (SC) current reaches ~30 nA, at an acceleration value of 6 m/s^2.

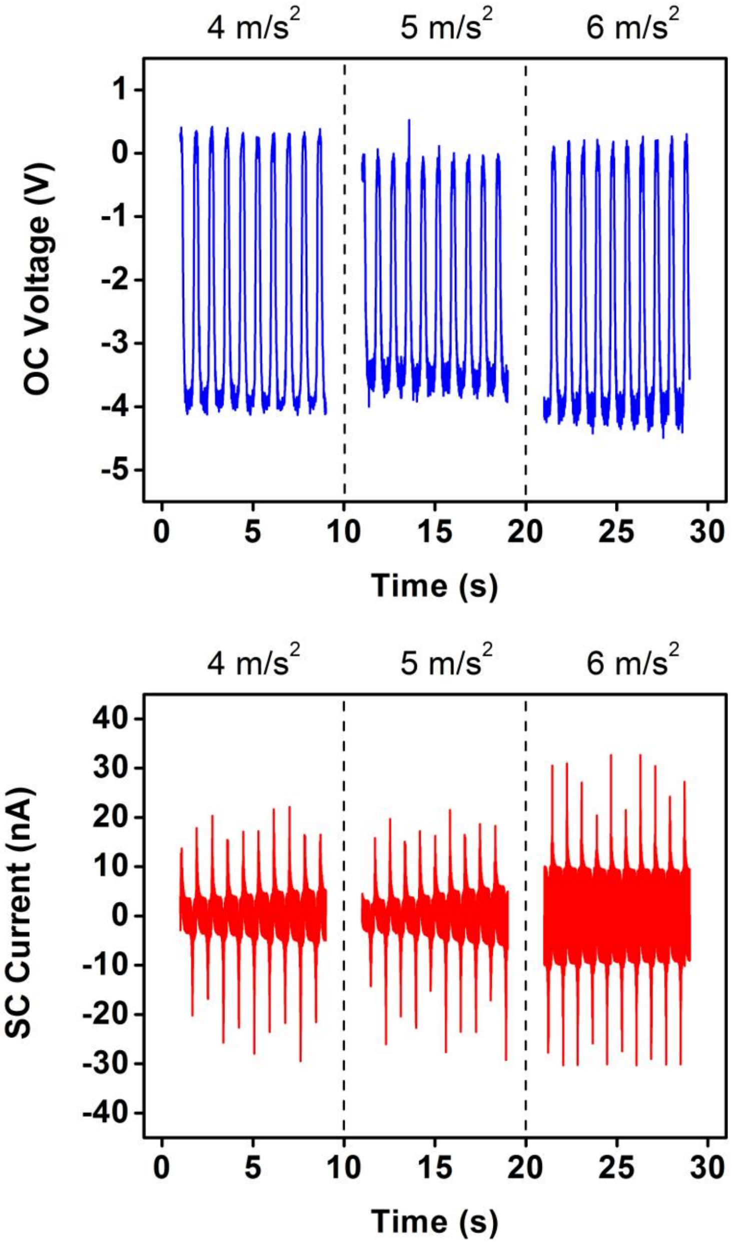

Figure 7.8 OC voltage (top) and SC current (bottom) of the cotton fabric-based triboelectric generator when bended under a fixed bending displacement of 46 mm at various acceleration values.

To simplify the device structure and to eliminate the high moisture regain cotton fabrics, a more practical design is proposed by using PET fabric as the fabric substrate. As shown in the schematic illustration, PET fabric was first coated with a layer of copper by PAMD to yield copper-coated PET fabric (Cu-PET). Then, the Cu-PET was coated with a layer of PI coating on top according to the optimized recipe to yield PI-coated Cu-PET. Another Cu-PET was then stacked onto the PI-coated Cu-PET (Figure 7.9). The triboelectric device was finally stitched at the four edges using polyester yarns to secure the whole device structure (Figure 7.10).

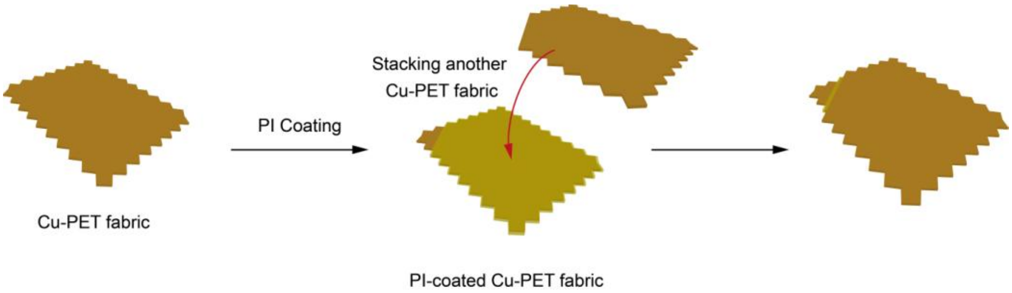

Figure 7.9 Fabrication of fabric-based triboelectric device.

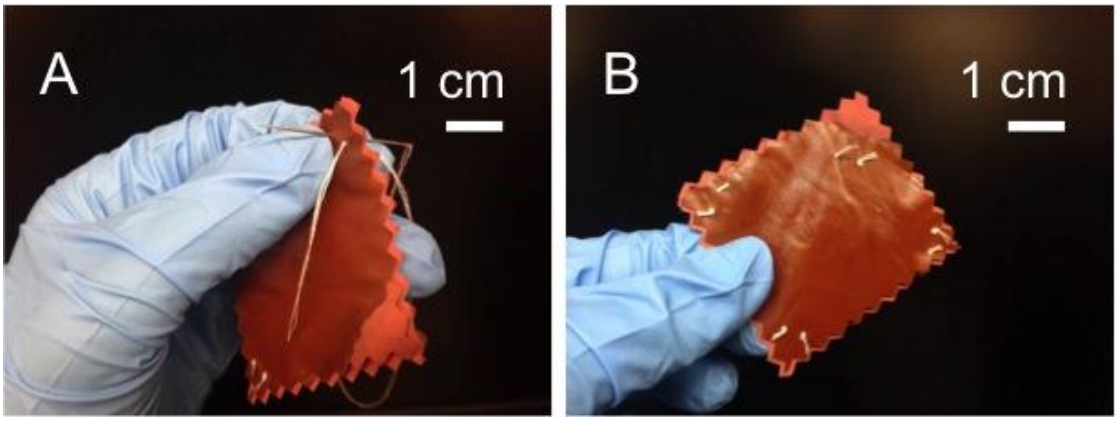

Figure 7.10 Making of the fabric-based triboelectric device. (A) Stitching the triboelectric device at the four edges using polyester yarns. (B) The finished triboelectric device.

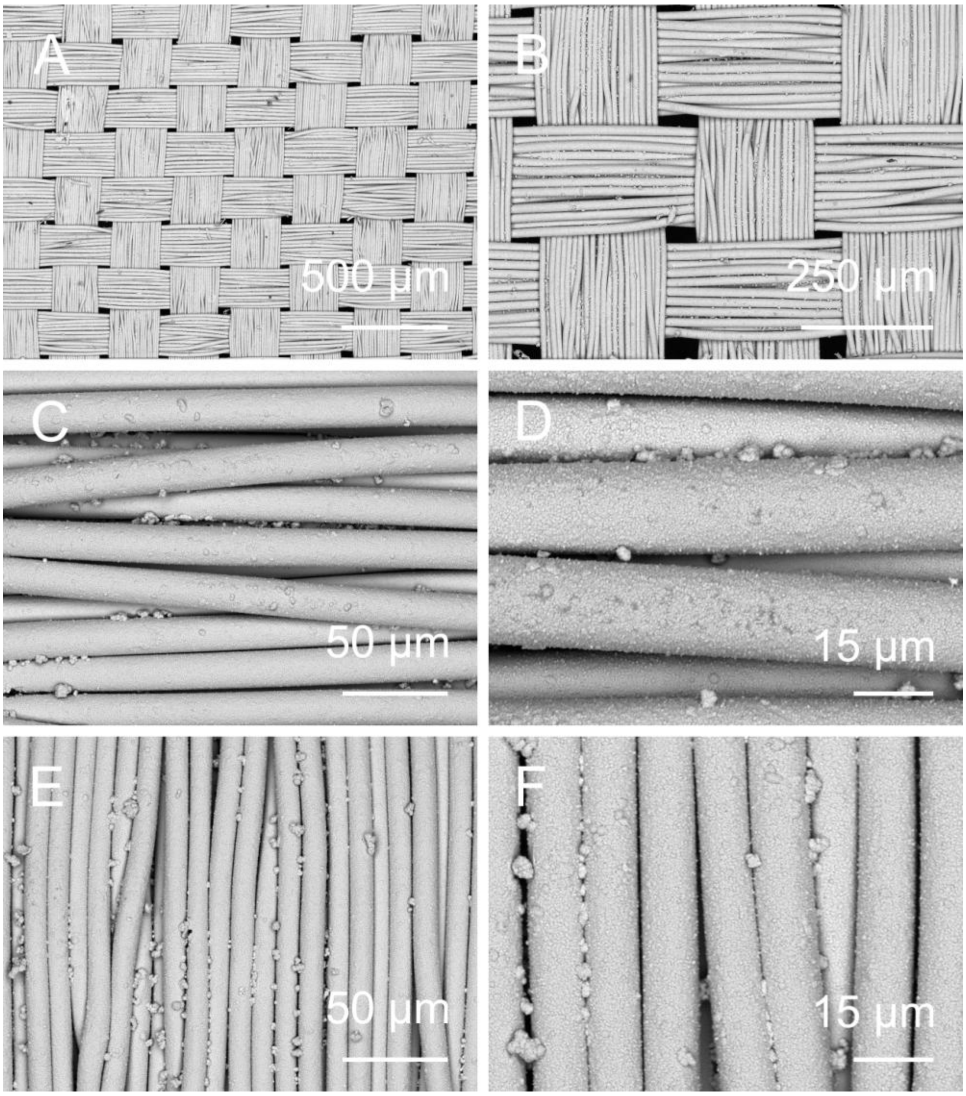

Figure 7.11 SEM images of Cu-PET fabric.

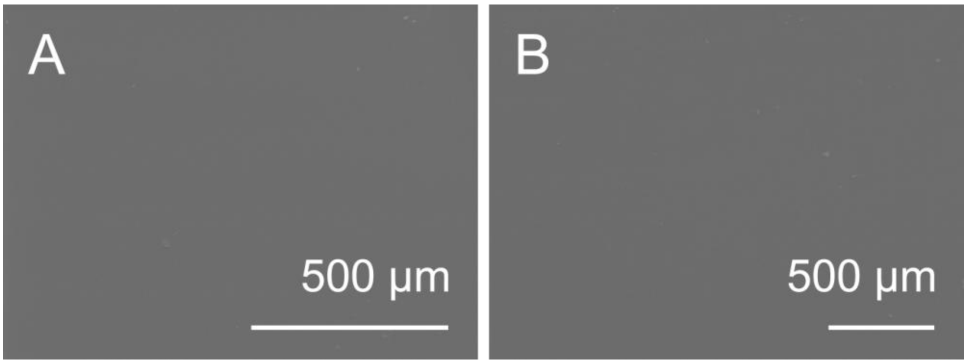

Figure 7.12 SEM images of Cu-PET fabric with PI coating.

The Cu-PET before and after coating of PI was characterized by SEM. As shown in Figure 7.11, the Cu-PET fibers are evenly deposited with a layer of copper. The bulk resistance of the Cu-PET (~4 cm x 4 cm) was measured as ~0.9 ohm. After PI coating, the typical woven structure of the PET disappeared, indicating a layer of PI coating on top covered the whole woven structure of the Cu-PET fabric (Figure 7.12). The successful deposition of PI on the Cu-PET was characterized by ATR-FTIR (Figure 7.13). After copper deposition, distinctive peaks of PET disappeared. Instead, a smooth spectrum was resulted which exhibited a typical spectrum of metal. The spectrum of PI-coated Cu-PET was in fact very similar to the spectrum of pure PI, showing distinctive peaks of C=O stretching and C-N stretching of imide ring at 1775 cm^{-1} and 1373 cm^{-1}, respectively, indicating that PI was successfully formed and wrapped around on the PET fabric surface.

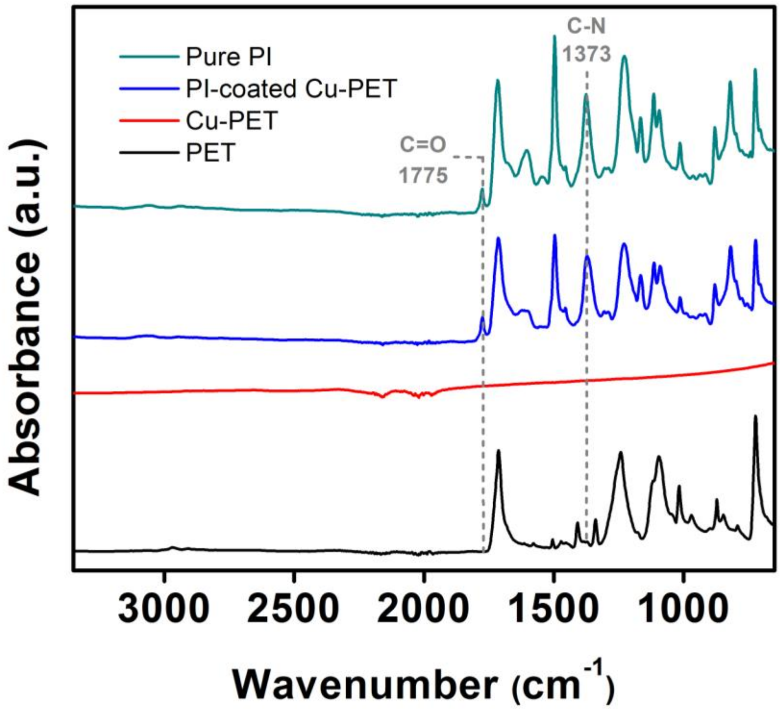

Figure 7.13 ATR-FTIR spectra of the modified PET fabric.

To better resemble the movement of the human body, the performance of the triboelectric device was evaluated by scratching the fabrics with each other. As shown in Figure 7.14, the OC voltage was measured as ~8 V while the SC current reached ~25 μA. Comparing to the fabric-based triboelectric generator made form cotton fabrics, the one using PET as the only substrate has a better performance, which is mainly contributed to the low moisture absorption of the PET. In fact, the pattern of the signal received is irregular, which is majorly caused by the uneven motion exerted by hands. However, the data collected by hand movement better resemble human movement, and gives a more realistic performance output of this fabric-based triboelectric generator.

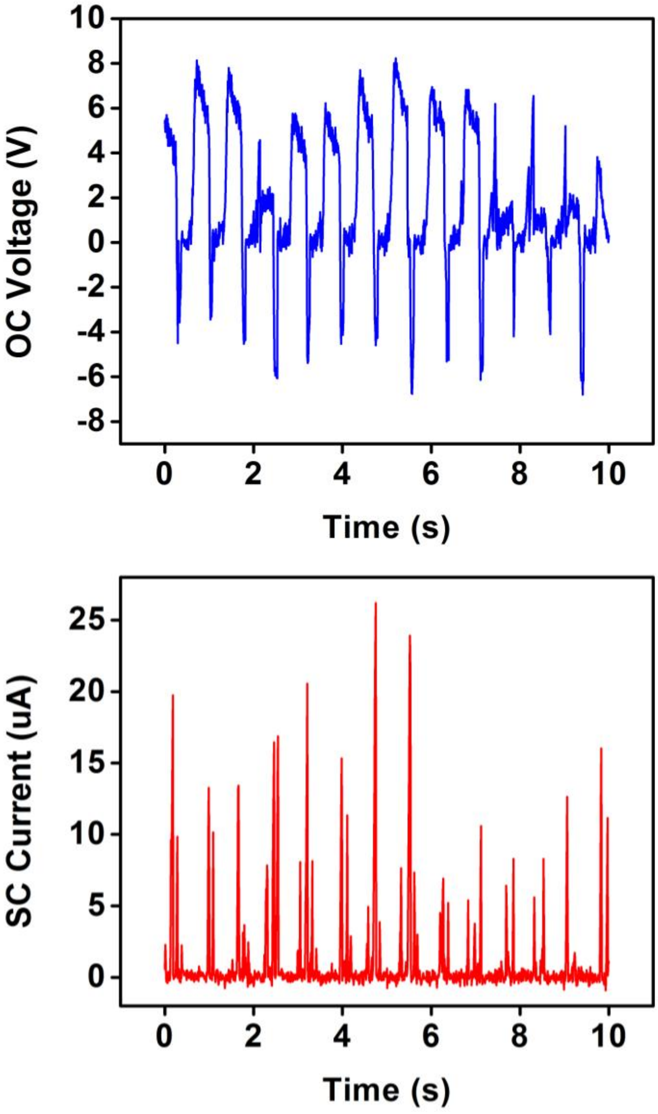

Figure 7.14 OC voltage (top) and SC current (bottom) of the PET fabric-based triboelectric generator when scratching separated fabric sheets with each other.

7.3.3 Fabrication and Performance Evaluation of Yarn-based Triboelectric Generator

To further increase the effective contact areas of the two triboelectric coupling surfaces, yarn-based triboelectric generator was developed. Fabrication of the yarn-based triboelectric generator involves only twisting a Cu-cotton yarn with a PI-coated Cu-cotton yarn as illustrated in Figure 7.15. The effective twisting length of the device is ~2 cm. The output performance of the triboelectric generator was evaluated and reported in Figure 7.16. It was found that the maximum OC voltage could reach ~4 V while the maximum SC current can reach ~200 nA, at an acceleration value of 8 m/s^2. It seems that the performance of the yarn-based triboelectric generator is more promising as comparing to the size of the fabric-based generator; yarn-based triboelectric generator in a smaller size exhibits a relatively greater output performance.

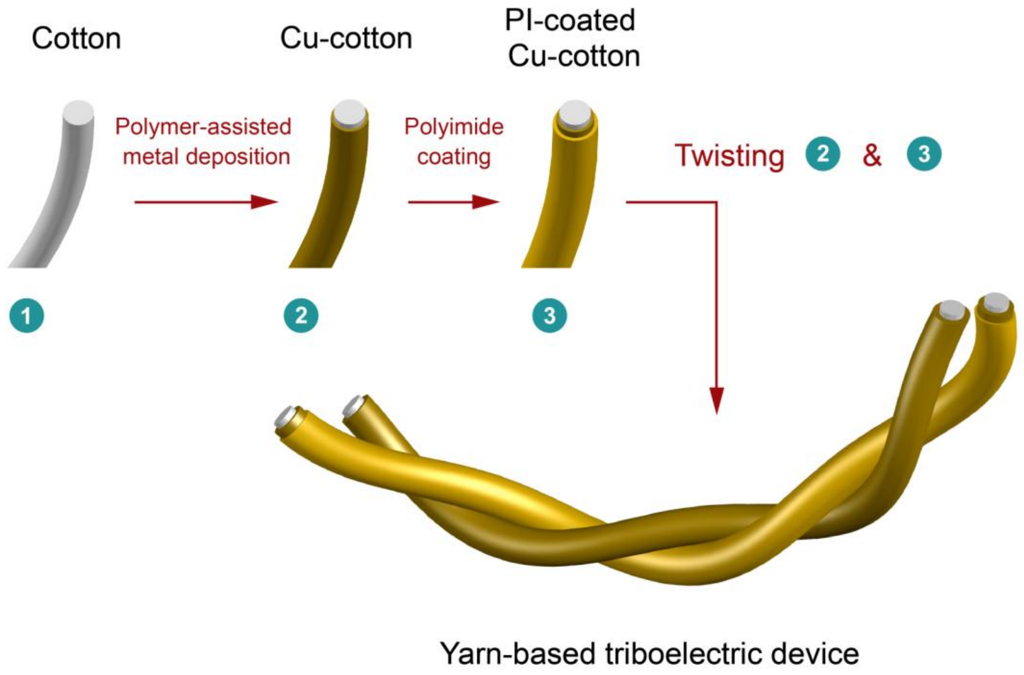

Figure 7.15 Fabrication scheme of the yarn-based triboelectric device.

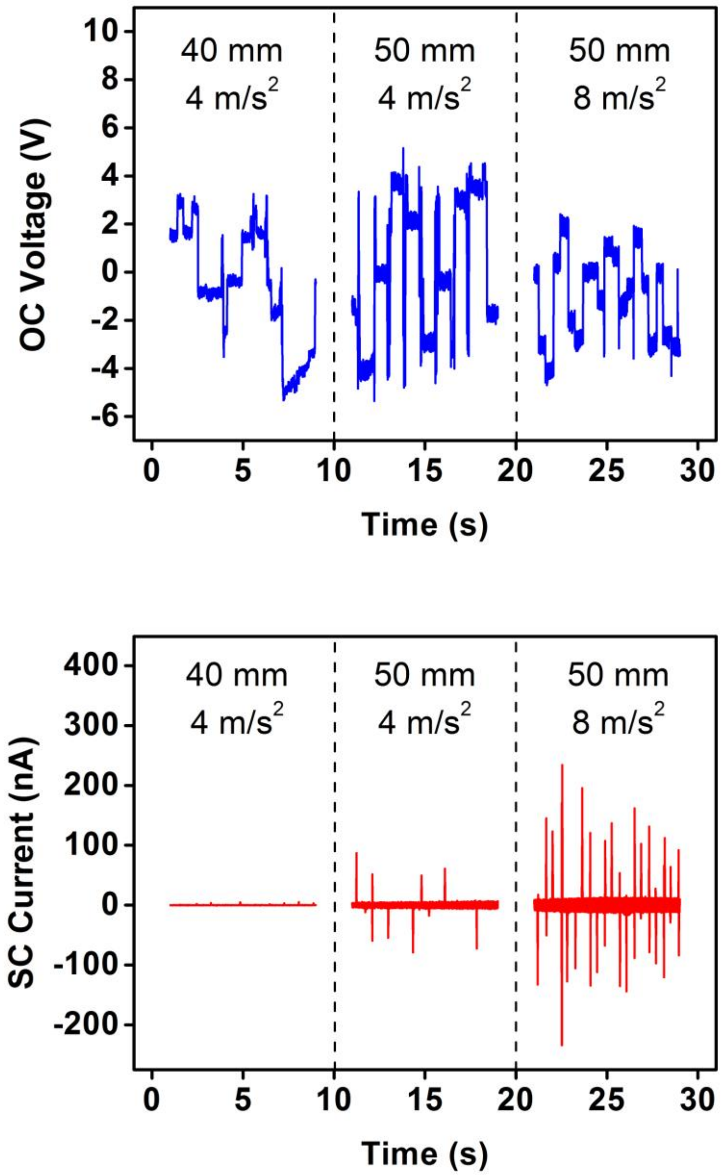

Figure 7.16 OC voltage (top) and SC current (bottom) of the PET fabric-based triboelectric generator when bended under various displacement and acceleration values.

7.3.4 Fabrication and Performance Evaluation of Woven-based Triboelectric Device

To further increase the effective contact areas of the two triboelectric coupling layers, a woven device structure consisting of warp and weft yarns is proposed. The fabrication of the weft and warp yarns is described as follows. PET yarns were first deposited with a layer of copper metal by PAMD. Two PET yarns were then twisted together to give a 2-ply Cu-PET yarn, which was the weft yarn in the woven fabric. The fabrication of warp yarn was one extra step to the weft yarn, by simply coating the 2-ply Cu-PET yarn with a layer of PI according to the previously optimized recipe. The structure of the warp yarn is shown in Figure 7.17.

The SEM image of a 2-ply Cu-PET yarn (weft) is shown in Figure 7.18 (top and middle). Twisting of two Cu-PET yarns gave a thicker 2-ply Cu-PET yarn. However, the linear resistance of the 2-ply Cu-PET yarn is almost halved when comparing to the single strand Cu-PET (Figure 7.20 and 7.21) due to more conductive pathways making up the yarn. SEM image (Figure 7.18, bottom) of the PI-coated Cu-PET yarn indicate that the yarn surface is fully covered with PI. The cross-section of the PI-coated Cu-PET yarn is showed in Figure 7.19. The yellow dashed line indicates the part of the 2-ply Cu-PET yarn while the white dashed line indicates the part of PI coating. The thickness of the PI coating was roughly estimated between ~20 to ~150 μm.

A triboelectric device was fabricated by weaving 6 2-ply PI-coated Cu-PET yarns as warp and 100 Cu-PET yarns as weft (Figure 7.22). To secure the whole woven structure, black cotton yarns were firstly woven and as well at the end. The output performance of the woven triboelectric generator was evaluated in which the SC current was ~0.15 uA and the OC voltage was as ~9 V when it was bent under a fixed bending displacement of 46 mm.

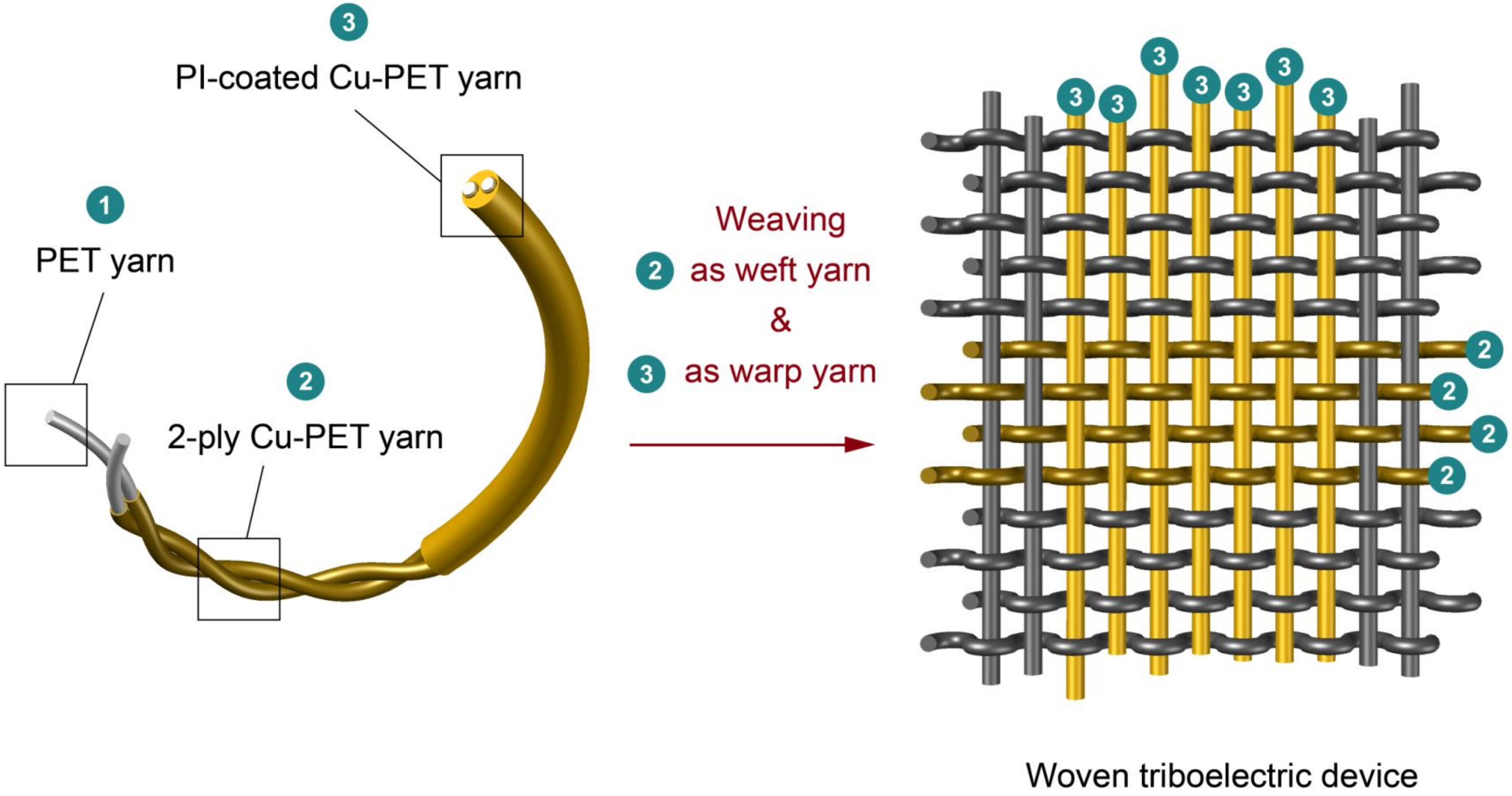

Figure 7.17 Illustration of the structures of PI-coated Cu-PET yarn and the woven triboelectric device.

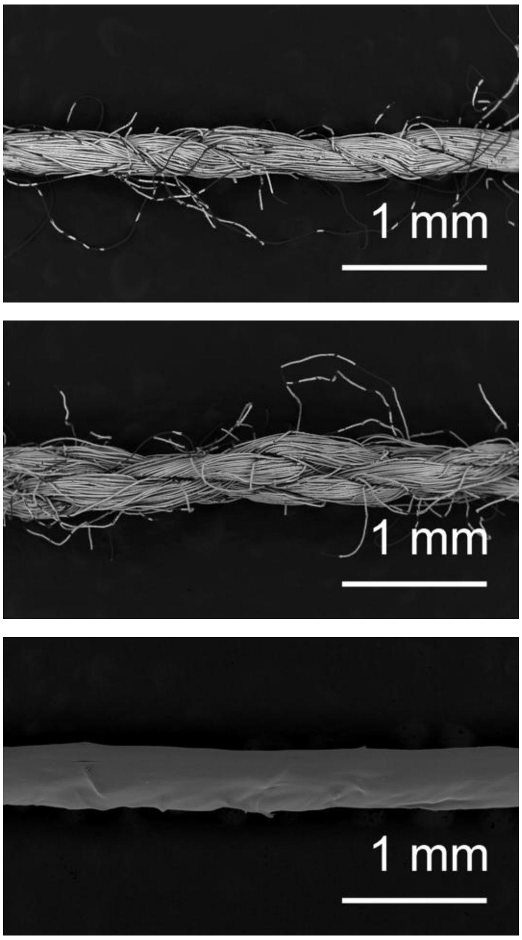

Figure 7.18 SEM images of the Cu-PET yarn (top), 2-ply Cu-PET yarn (middle) and PI-coated Cu-PET yarn (bottom).

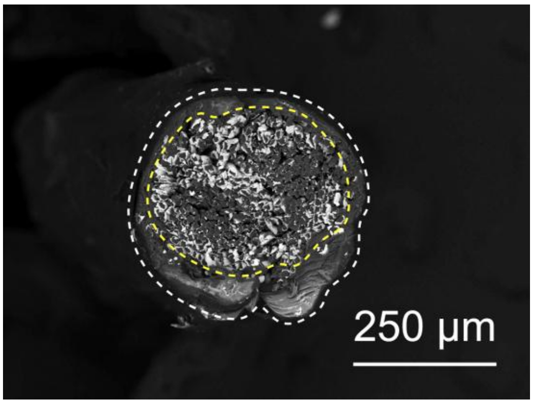

Figure 7.19 SEM images of the cross-section of the PI-coated Cu-PET yarn. The yellow dashed line indicates the cross-sectional part of the 2-ply Cu-PET yarn while the white dashed line indicates the cross-sectional part of the PI coating.

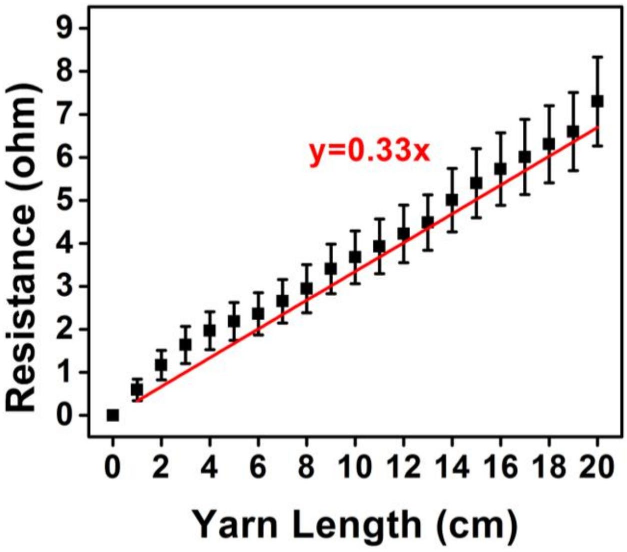

Figure 7.20 Linear resistance of a single strand Cu-PET yarn.

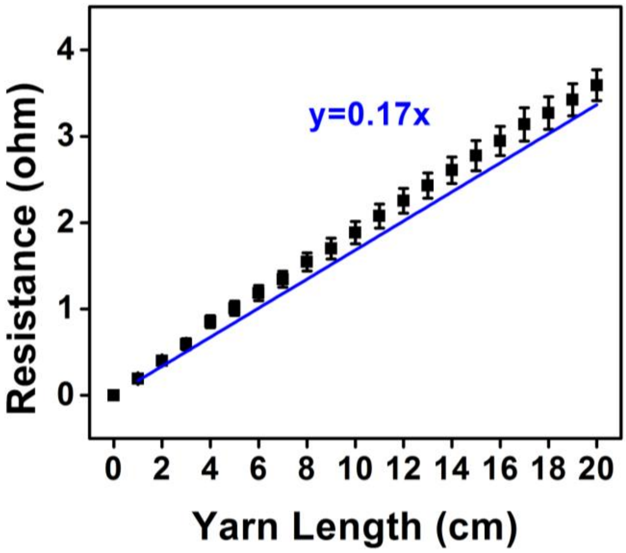

Figure 7.21 Linear resistance of a 2-ply Cu-PET yarn.

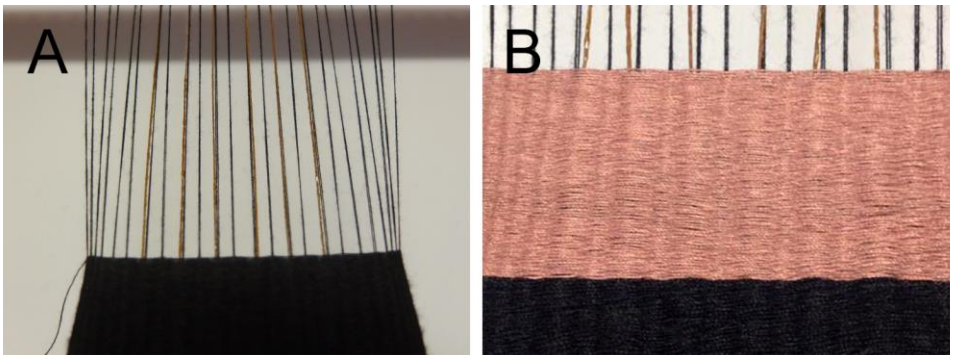

Figure 7.22 Weaving of the triboelectric device.

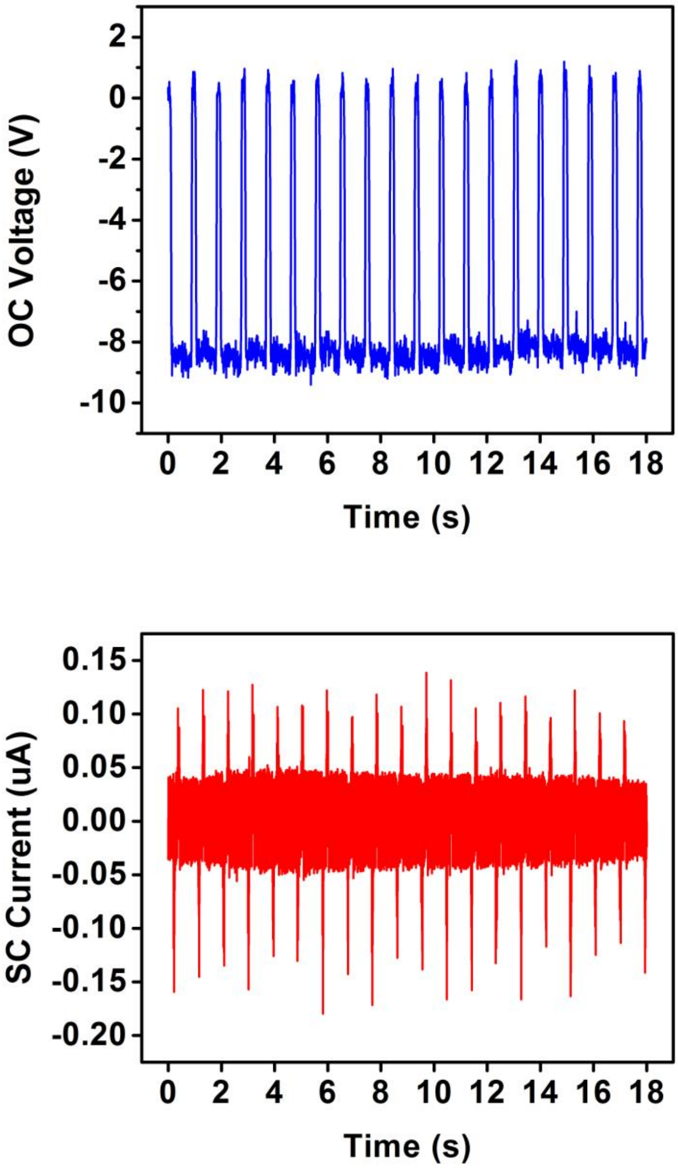

Figure 7.23 OC voltage (top) and SC current (bottom) of the woven-based triboelectric generator when bent under a fixed bending displacement of 46 mm.

7.4 Chapter Conclusion

In this chapter, preliminary results of fabrication of triboelectric generators using the metallic textiles synthesized by PAMD are reported. We have developed tree types of textile triboelectric generators, namely, fabric-based triboelectric generator, yarn-based triboelectric generator and woven triboelectric generator. In the fabrication of these devices, we incorporate the copper-coated textiles synthesized by PAMD. Their performances are summarized in Table 7.3

Type of textile triboelectric generator	Max. OC Voltage	Max. SC Current
Fabric-based	~4 V	~30 nA
Fabric-based	~8 V	~25 μA
Yarn-based	~5 V	~200 nA
Woven-based	~9 V	~0.15 μA

Table 7.3 Summary of the output performances of the demonstrated textile-based triboelectric generators.

CHAPTER 8: CONCLUSIONS AND DIRECTIONS IN FUTURE STUDIES

8.1 Conclusions

Considering the demand for flexible electronics and the market-driven wearable technology, durable, washable, and high-performance metallic textiles are of great potential in textile electronics in the foreseeable future. However, the metal adhesion and also the washing durability of these metal-coated textiles remain major challenges. Moreover, to date, there are still no practical strategies to fabricate high-performance, durable and washable metallic textiles in bulk. Addressing these challenges, this research mainly focuses on the fabrication of durable, washable, and high-performance metallic textiles via PAMD, and also the development of compatible technology for the textile industry to mass produce metallic textiles via the same strategy.

In this research, we have conducted thorough studies on three kinds of polymer brushes used in PAMD, namely in short: PMETAC, PMANa and PAANa. First, the fabrication of metallic textiles by grafting of a PMETAC brush layer on the textile surface is reported in Chapter 5. There are three remarkable points to be highlighted. First, free radical polymerization is found to be a suitable approach to graft the PMETAC brushes, to substitute SI-ATRP. Without using SI-ATRP, the whole fabrication process is high-throughput and can be carried out under ambient conditions. Second, the whole fabrication process is confirmed to be industry-compatible, where conventional textile finishing technologies such as pad-dry-cure and hank dyeing can be incorporated in the whole fabrication process. As-synthesized copper-coated cotton fabric has a very promising conductivity, with sheet resistance exhibited from 10^3 to 10^{-1} ohm/sq, depending on the ELD conditions. The as-synthesized Cu-cotton yarns also exhibited a very good conductivity with linear resistance measured as ~1.4 ohm/cm, with significant improvements on the yarn tensile properties due to the reinforcement by the as-deposited copper layer. Third, as PMETAC brush layer acts as an interfacial layer that bridges the copper metal and the textile fiber substrate, the copper layer on the textile surface exhibits remarkable adhesion, which can withstand repeated cycles of bending and machine washing up to 30 standard cycles.

To realize a true strategy for scale production in the industry, the use of expensive palladium-bearing catalyst in the ion exchange process for PMETAC polymer brushes should be eliminated. Chapter 6 reports the grafting of anionic PMANa or PAANa brushes on textile surface, which demonstrates an alternative approach to synthesizing metallic textiles. In the experiment, PMANa and PAANa brushes are successfully grafted on the cotton fabric surface by an in-situ free radical polymerization approach. Subsequently, by replacing the sodium ions with copper ions in PMANa or PAANa brushes, followed by reduction in sodium borohydride solution, a very thin copper seed layer is formed on the textile surface, which serves as nucleation site for the growth of copper metal layer in the electroless copper deposition. Comparing the associated cost of fabricating copper-coated yarns by grafting PMETAC and PMANa, grafting PMANa can have a cost reduction by ~30 %. The as-synthesized copper metal layer on the Cu-cotton also exhibits a remarkable adhesion and outstanding washing durability, proven that the anionic PMANa or PAANa brushes are of great potential to fabricate robust metallic textiles at relatively lower cost.

In Chapter 7, the fabrication of textile-based triboelectric generator is demonstrated using metallic textiles developed by PAMD in the previous chapters. Different structures and triboelectric coupling combinations of the triboelectric generators have been demonstrated, such as fabric-based triboelectric generators, yarn-based triboelectric generators and woven triboelectric generators. The output performances of these triboelectric generators are very promising. The woven triboelectric generators can have an output performance of maximum open circuit voltage of ~9 V while maximum short circuit voltage of ~0.15 μA.

8.2 Directions in Future Studies

1. The metallic textiles synthesized by PAMD having outstanding mechanical as well as washing durability are very suitable for further development of other wearable electronics such as wearable supercapacitors, solar cells and batteries.

2. The work reported in this thesis mainly focuses on the modification of fabric and yarn surface, and to deposit a layer of metal on top of the fabric and yarn surface. However, it is found that metal deposition is only restricted to the outermost layer of the fibers of the yarns. The reason for this is mainly due to the difficult penetration of the chemical species involved in the ELD process. As a result, lower resistance of the metal-coated textiles cannot be achieved further, unless all of the fibers making up the yarns are all coated with metal particles. Seeing this, surface modification of the fibers can be introduced in earlier stages (such as slivers and rovings) in the textile manufacturing process before they are spun into yarns.

3. As the results reported in Chapter 7 about textile triboelectric generators are preliminary, further investigation on the textile triboelectric generators is needed, particularly the woven structures as well as the PI coating on the yarns. Optimization of the device is also required in order to get a better overall performance.

APPENDIXES

Appendix 1: Table summary of all chemicals used for the fabrication of copper-coated textiles assisted with cationic poly{[2-(methacryloyloxy)ethyl]trimethyl-ammonium chloride} (PMETAC) brushes.

Procedure	**Chemical Name**	**CAS**
Silanization	Acetic acid (99+ %)	64-19-7
	Vinyltrimethoxysilane (98 %)	2768-02-7
Polymerization of METAC	Potassium persulphate (99+ %)	7727-21-1
	2-(methacryloyloxy)ethyl] trimethylammonium chloride, 80 wt. % solution in water	5039-78-1
Ion Exchange	Ammonium tetrachloropalladate(II) (97 %)	13820-40-1
Electroless Copper Deposition	Copper(II) sulphate pentahydrate (99+ %)	7758-99-8
	Sodium hydroxide pellet (ACS grade)	1310-73-2
	Potassium sodium tartrate tetrahydrate (ACS grade)	6381-59-5
	Formaldehyde, 37 wt.% solution in water	50-00-0

Appendix 2: Table summary of all chemicals used for the fabrication of copper-coated textiles assisted with anionic poly(methacrylic acid sodium salt) (PMANa) brushes.

Procedure	**Chemical Name**	**CAS**
Silanization	Acetic acid (99+ %)	64-19-7
	Vinyltrimethoxysilane (98 %)	2768-02-7
Polymerization of PMANa	Potassium persulphate (99+ %)	7727-21-1
	Sodium methacrylate (99 %)	5536-61-8
Ion Exchange	Copper(II) sulphate pentahydrate (99+ %)	7758-99-8
Ion Reduction	Sodium borohydride (96%)	16940-66-2
Electroless Copper Deposition	Copper(II) sulphate pentahydrate (99+ %)	7758-99-8
	Sodium hydroxide pellet (ACS grade)	1310-73-2
	Potassium sodium tartrate tetrahydrate (ACS grade)	6381-59-5
	Formaldehyde, 37 wt.% solution in water	50-00-0

Appendix 3: Table summary of all chemicals used for the fabrication of copper-coated textiles assisted with anionic poly(acrylic acid sodium salt) (PAANa) brushes.

Procedure	**Chemical Name**	**CAS**
Silanization	Acetic acid (99+ %)	64-19-7
	Vinyltrimethoxysilane (98 %)	2768-02-7
Polymerization of PAANa	Potassium persulphate (99+ %)	7727-21-1
	Sodium acrylate (97 %)	7446-81-3
Ion Exchange	Copper(II) sulphate pentahydrate (99+ %)	7758-99-8
Ion Reduction	Sodium borohydride (96%)	16940-66-2
Electroless Copper Deposition	Copper(II) sulphate pentahydrate (99+ %)	7758-99-8
	Sodium hydroxide pellet (ACS grade)	1310-73-2
	Potassium sodium tartrate tetrahydrate (ACS grade)	6381-59-5
	Formaldehyde, 37 wt.% solution in water	50-00-0

Appendix 4: Estimated price breakdown of making 10 kg of copper-coated cotton yarns via PMETAC-assisted copper deposition.

		CAS	Vendor	Unit Price (HKD)	Amount Used	HKD Estimated
Acetic acid (99+ %)		64-19-7	Acros	0.0104	160.2564	1.67
Vinyltrimethoxysilane (VTMS) (98 %)		2768-02-7	Aldrich	0.0949	4807.6923	456.25
Potassium persulphate (KPS) (99+ %)		7727-21-1	Acros	0.0234	28.8462	0.68
2-(methacryloyloxy)ethyl] trimethylammonium chloride, 80 wt. % solution in water (METAC) (20 % v/v)		5039-78-1	Aldrich	0.9481	9615.3846	9116.35
Ammonium tetrachloropalladate(II) (97 %)		13820-40-1	Acros	539.7000	13.8462	7472.77
ELD Part I:	Copper(II) sulphate pentahydrate (99+ %)	7758-99-8	UniChem	0.2000	33333.3333	6666.67
	Sodium hydroxide pellet (ACS grade)	1310-73-2	VWR	0.0078	30769.2308	240.00
	Potassium sodium tartrate tetrahydrate (ACS grade)	6381-59-5	VWR	0.0273	74358.9744	2030.00
ELD Part II:	Formaldehyde, 37 wt.% solution in water	50-00-0	VWR	0.0081	64102.5641	516.67
				Total Cost (HKD)		**26501.04**

Appendix 5: Detailed price breakdown of making 10 kg of copper-coated cotton yarns via PMANa-assisted copper deposition.

		CAS	**Vendor**	**Unit Price (HKD)**	**Amount Used**	**HKD Estimated**
Acetic acid (99+ %)		64-19-7	Acros	0.0104	160.2564	1.67
Vinyltrimethoxysilane (VTMS) (98 %)		2768-02-7	Aldrich	0.0949	4807.6923	456.25
Potassium persulphate (KPS) (99+ %)		7727-21-1	Acros	0.0234	36.1538	0.85
Sodium methacrylate (99.0 %)		5536-61-8	Accuchem	2.3200	3365.3846	7807.69
Copper(II) sulphate pentahydrate (99+ %)		7758-99-8	UniChem	0.2000	625.3846	125.08
Sodium borohydride (96%)		16940-66-2	Accuchem	3.8200	182.0000	695.24
ELD Part I:	Copper(II) sulphate pentahydrate (99+ %)	7758-99-8	UniChem	0.2000	33333.3333	6666.67
	Sodium hydroxide pellet (ACS grade)	1310-73-2	VWR	0.0078	30769.2308	240.00
	Potassium sodium tartrate tetrahydrate (ACS grade)	6381-59-5	VWR	0.0273	74358.9744	2030.00
ELD Part II:	Formaldehyde, 37 wt.% solution in water	50-00-0	VWR	0.0081	64102.5641	516.67
				Total Cost (HKD)		**18540.11**

REFERENCES

1. D. De Rossi, ‘Electronic Textiles: A Logical Step’, *Nat. Mater.* **2007**, *5*, 328.

2. S. Park, S. Jayaraman, ‘Smart Textiles: Wearable Electronic Systems’, *MRS Bull.* **2003**, *28*, 585.

3. J. A. Rogers, T. Someya, Y. Huang, ‘Materials and Mechanics for Stretchable Electronics’, *Science* **2010**, *327*, 1603.

4. H. R. Mattila, ‘Intelligent Textiles and Clothing’, Woodhead Publishing Limited, Cambridge, UK **2006**.

5. X. M. Tao, ‘Smart Fibres, Fabrics and Clothing: Fundamentals and Applications’, Woodhead, Cambridge, UK **2001**.

6. X. M. Tao, ‘Wearable Electronics and Photonics’, Woodhead Publishing Limited, Cambridge, UK **2005**.

7. J. R. Windmiller, J. Wang, ‘Wearable Electrochemical Sensors and Biosensors: A Review’, *Electroanalysis* **2013**, *25*, 29.

8. C. Pang, C. Lee, K. Y. Suh, ‘Recent Advances in Flexible Sensors for Wearable and Implantable Devices’, *J. Appl. Polym. Sci.* **2013**, *130*, 1429.

9. B. S. Shim, W. Chen, C. Doty, C. L. Xu, N. A. Kotov, ‘Smart Electronic Yarns and Wearable Fabrics for Human Biomonitoring made by Carbon Nanotube Coating with Polyelectrolytes’, *Nano Lett.* **2008**, *8*, 4151.

10. K. Cherenack, C. Zysset, T. Kinkeldei, N. Münzenrieder, G. Tröster, ‘Woven Electronic Fibers with Sensing and Display Functions for Smart Textiles’, *Adv. Mater.* **2010**, *22*, 5178.

11. C. A. Winterhalter, J. Tererovsky, P. Wilson, J. Slade, W. Horowitz, E. Tierney, V. Sharma, ‘Development of Electronic Textiles to Support Networks, Communications, and Medical Applications in Future U.S. Military Protective Clothing Systems’, *IEEE T Inf. Technol. B* **2005**, *9*, 402.

12. C. Yan, W. Kang, J. Wang, M. Cui, X. Wang, C. Y. Foo, K. J. Chee, P. S. Lee, ‘Stretchable and Wearable Electrochromic Devices ‘, *ACS Nano* **2014**, *8*, 316.

13. D. Schawaller, M. Voss, V. Bauch, E. Frank, M. R. Buchmeiser, ‘Flexible, Switchable Electrochromic Textiles’, *Macromol. Mater. Eng* **2014**, *299*, 330.

14. Y. Ding, M. A. Invernale, G. A. Sotzing, ‘Conductivity Trends of PEDOT-PSS Impregnated Fabric and the Effect of Conductivity on Electrochromic Textile’, *ACS Appl. Mater. Interfaces* **2010**, *2*, 1588.

15. L. Hu, M. Pasta, F. L. Mantia, L. Cui, S. Jeong, H. D. Deshazer, J. W. Choi, S. M. Han, Y. Cui, ‘Stretchable, Porous, and Conductive Energy Textiles’, *Nano Lett.* **2010**, *10*, 708.

16. Z. Gui, H. Zhu, E. Gillette, X. Han, G. W. Rubloff, L. Hu, S. B. Lee, ‘Natural Cellulose Fiber as Substrate for Supercapacitor’, *ACS Nano* **2013**, *7*, 6037.

17. K. Wang, Q. Meng, Y. Zhang, Z. Wei, M. Miao, ‘High-Performance Two-Ply Yarn Supercapacitors Based on Carbon Nanotubes and Polyaniline Nanowire Arrays’, *Adv. Mater.* **2013**, *25*, 1494.

18. D. Marculescu, R. Marculescu, N. H. Zamora, P. Stanley-Marbell, P. K. Khosla, S. Park, S. Jayaraman, S. Jung, C. Lauterbach, W. Weber, T. Kirstein, D. Cottet, J. Grzyb, G. Troster, M. Jones, T. Martin, Z. Nakad, 'Electronic Textiles: A Platform for Pervasive Computing', *Proc. IEEE* **2003**, *91*, 1995.

19. A. C. Siegel, S. T. Phillips, M. D. Dickey, N. Lu, Z. Suo, G. M. Whitesides, 'Foldable Printed Circuit Boards on Paper Substrates', *Adv. Funct. Mater.* **2010,** *20,* 28.

20. M. Hamedi, R. Forchheimer, O. Inganäs, 'Towards Woven Logic from Organic Electronic Fibers', *Nat. Mater.* **2007**, *6*, 357.

21. L. Bao, X. Li, 'Towards Textile Energy Storage from Cotton T-Shirts', *Adv. Mater.* **2012**, *24*, 3246.

22. A. M. Gaikwad, A. M. Zamarayeva, J. Rousseau, H. Chu, I. Derin,D. A. Steingart, 'Highly Stretchable Alkaline Batteries Based on an Embedded Conductive Fabric', *Adv. Mater.* **2012**, *24*, 5071.

23. S. Pan, Z. Yang, P. Chen, J. Deng, H. Li, H. Peng, 'Wearable Solar Cells by Stacking Textile Electrodes', *Angew. Chem. Int. Ed.* **2014**, *53*, 6110.

24. W. Zeng , L. Shu, Q. Li, S. Chen, F. Wang, X.M. Tao, 'Fiber-Based Wearable Electronics: A Review of Materials, Fabrication, Devices, and Applications', *Adv. Mater.* **2014**, *26*, 5310.

25. M. J. Yun, S. I. Cha, S. H. Seo, D. Y. Lee, 'Highly Flexible Dye-Sensitized Solar Cells Produced by Sewing Textile Electrodes on Cloth', *Sci. Rep.* **2014**, *4*, 5322.

26. M. J. Yun, S. I. Cha, S. H. Seo, H. S. Kim, D. Y. Lee, ‘Insertion of Dye-Sensitized Solar Cells in Textiles using a Conventional Weaving Process’, *Sci. Rep.* **2015**, *5*, 11022.

27. Y. Cheng , R. Wang, J. Sun, L. Gao, ‘Highly Conductive and Ultrastretchable Electric Circuits from Covered Yarns and Silver Nanowires’, *ACS Nano* **2015**, *9*, 3887.

28. A. F. Lotus, E. T. Bender, E. A. Evans, R. D. Ramsier, D. H. Reneker, G. G. Chase, ‘Electrical, Structural, and Chemical Properties of Semiconducting Metal Oxide Nanofiber Yarns ‘, *J. Appl. Phys.* **2008**, *103*, 024910.

29. C. Drew, X. Liu, D. Ziegler, X. Wang, F. F. Bruno, J. Whitten, L. A. Samuelson, J. Kumar, ‘Metal Oxide-Coated Polymer Nanofibers’, *Nano Lett.* **2003**, *3*, 143.

30. L. Frunza, N. Preda, E. Matei, S. Frunza, C. P. Ganea, A. M. Vlaicu, L. Diamandescu, A. Dorogan, ‘Synthetic Fabrics Coated with Zinc Oxide Nanoparticles by Electroless Deposition: Structural Characterization and Wetting Properties’, *J. Polym. Sci. Part B Polym. Phys.* **2013**, *51*, 1427.

31. L. Dall'Acqua, C. Tonin, R. Peila, F. Ferrero, M. Catellani, ‘Performances and Properties of Intrinsic Conductive Cellulose–Polypyrrole Textiles’, *Synth. Met.* **2004**, *146*, 213.

32. A. Kaynak, S. S. Najar, R. C. Foitzik, ‘Conducting Nylon, Cotton and Wool Yarns by Continuous Vapor Polymerization of Pyrrole’, *Synth. Met.* **2008**, *158*, 1.

33. B. Kim, V. Koncar, C. Dufour, ‘Polyaniline-Coated PET Conductive Yarns: Study of Electrical, Mechanical, and Electro-mechanical Properties’, *J. Appl. Polym. Sci.* **2006**, *101*, 1252.

34. N. V. Bhat, D. T. Seshadri, S. Radhakrishnan, ‘Preparation, Characterization, and Performance of Conductive Fabrics: Cotton + PANi’, *Text. Res. J.* **2004**, *74*, 155.

35. K. H. Hong, K. W. Oh, T. J. Kang, ‘Preparation and Properties of Electrically Conducting Textiles by In-Situ Polymerization of Poly(3,4-ethylenedioxythiophene)’, *J. Appl. Polym. Sci.* **2005**, *97*, 1326.

36. M. Zhang, K. R. Atkinson, R. H. Baughman, ‘Multifunctional Carbon Nanotube Yarns by Downsizing an Ancient Technology’, *Science* **2004**, *306*, 1358.

37. M. D. Lima, S. Fang, X. Lepró, C. Lewis, R. Ovalle-Robles, J. Carretero-González, E Castillo-Martínez, M. E. Kozlov, J. Oh, N. Rawat, C. S. Haines, M. H. Haque, V. Aare, S. Stoughton, A. A. Zakhidov, R. H. Baughman, ‘Biscrolling Nanotube Sheets and Functional Guests into Yarns’, *Science* **2011**, *331*, 51.

38. K. Jiang, Q. Li, S. Fan, ‘Nanotechnology: Spinning Continuous Carbon Nanotube Yarns’, *Nature* **2002**, *419*, 801.

39. F. Ko, Y. Gogotsi, A. Ali, N. Naguib, H. Ye, G. L. Yang, C. Li, P. Willis, ‘Electrospinning of Continuous Carbon Nanotube-Filled Nanofiber Yarns’, *Adv. Mater.* **2003**, *15*, 1161.

40. Y. Shang, Y. Li, X. He, S. Du, L. Zhang, E. Shi, S. Wu, Z. Li, P. Li, J. Wei, K. Wang, H. Zhu, D. Wu, A. Cao, ‘Highly Twisted Double-Helix Carbon Nanotube Yarns’, *ACS Nano* **2013**, *7*, 1446.

41. J. S. Jur, J. C. Spagnola, K. Lee, B. Gong, Q. Peng, G. N. Parsons, ‘Temperature-Dependent Subsurface Growth during Atomic Layer Deposition on Polypropylene and Cellulose Fibers’, *Langmuir* **2010**, *26*, 8239.

42. G. K. Hyde, K. J. Park, S. M. Stewart, J. P. Hinestroza, G. N. Parsons, ‘Atomic Layer Deposition of Conformal Inorganic Nanoscale Coatings on Three-Dimensional Natural Fiber Systems: Effect of Surface Topology on Film Growth Characteristics’, *Langmuir* **2007**, *23*, 9844.

43. T. Yuranova, A. G. Rincon, A. Bozzi, S. Parra, C. Pulgarin, P. Albers, J. Kiwi, ‘Antibacterial Textiles Prepared by RF-Plasma and Vacuum-UV Mediated Deposition of Silver’, *J. Photochem. Photobiol. A* **2003**, *161*, 27.

44. K. W. Oh, K. H. Hong, S. H. Kim, ‘Electrically Conductive Textiles by In-Situ Polymerization of Aniline’, *J. Appl. Polym. Sci.* **1999**, *74*, 2094.

45. R. Hirase, M. Hasegawa, M. Shirai, ‘Conductive Fibers Based on Poly(ethylene terephthalate)–Polyaniline Composites Manufactured by Electrochemical Polymerization’, *J. Appl. Polym. Sci.* **2003**, *87*, 1073.

46. J. Slade, M. Agpaoa-Kraus, J. Bowman, A. Riecker, T. Tiano, C. Carey, P. Wilson, ‘Washing of Electrotextiles’, *MRS Proceedings* **2002**, *736*, D3.1.

47. K. W. Oh, S. H. Kim, E. A. Kim, ‘Improved Surface Characteristics and the Conductivity of Polyaniline–Nylon 6 Fabrics by Plasma Treatment’, *J. Appl. Poly. Sci.* **2001**, *81*, 684.

48. R. Guo, Y. Yu, J. Zeng, X. Liu, X. Zhou, L. Niu, T. Gao, K. Li, Y. Yang, F. Zhou, Z. J. Zheng, ‘Bio-Mimicking Topographic Elastomeric Petals (E-Petals) for Omnidirectional Sstretchable and Printable Electronics’, *Adv. Sci.* **2015**, *2*, 1400021.

49. C. Chen, X. Zhou, Z. Xie, T. Gao, Z. J. Zheng, ‘Construction of 3D Polymer Brushes by Dip-Pen Nanodisplacement Lithography: Understanding the Molecular Displacement for Ultrafine and High-Speed Patterning’, *Small* **2015**, *11*, 613.

50. K. Li, H. Zhen, L. Niu, X. Fang, Y. Zhang, R. Guo, Y. Yu, F. Yan, H. Li, Z. J. Zheng, ‘Full-Solution Processed Flexible Organic Solar Cells Using Low-Cost Printable Copper Electrodes’, *Adv. Mater.* **2014**, *26*, 7271.

51. Y. Yu, J. Zeng, C. Chen, Z. Xie, R. Guo, Z. Liu, X. Zhou, Y. Yang, Z. J. Zheng, ‘Three-Dimensional Compressible and Stretchable Conductive Composites’, *Adv. Mater.* **2014**, *26*, 810.

52. R. Guo, Y. Yu, Z. Xie, X. Q. Liu, X. C. Zhou, Y. F. Gao, Z. L. Liu, F. Zhou, Y. Yang, Z. J. Zheng, ‘Matrix-Assisted Catalytic Printing for the Fabrication of Multiscale, Flexible, Foldable, and Stretchable Metal Conductors’, *Adv. Mater.* **2013**, *25*, 3343.

53. X. Ma, Z. Xie, Z. L. Liu, X. Q. Liu, T. Cao, Z. J. Zheng, ‘Polymer Brush Electrets’, *Adv. Funct. Mater.* **2013**, *23*, 3239.

54. X. C. Zhou, Z. L. Liu, Z. Xie, X. Q. Liu, Z. J. Zheng, ‘High-Resolution, Large-Area, Serial Fabrication of 3D Polymer Brush Structures by Parallel Dip-Pen Nanodisplacement Lithography’, *Small* **2012**, *8*, 3568.

55. X. Q. Liu, X. C. Zhou, Y. Li, Z. J. Zheng, ‘Surface-Grafted Polymer-Assisted Electroless Deposition of Metals for Flexible and Stretchable Electronics’, *Chem. –Asian J.* **2012**, *7*, 862.

56. X. C. Zhou, X. Q. Liu, Z. Xie, Z. J. Zheng, ‘3D-Patterned Polymer Brush Surfaces’, *Nanoscale* **2011**, *3*, 4929.

57. X. Wang, H. Hu, Y. Shen, X. C. Zhou, Z. J. Zheng, ‘Stretchable Conductors with Ultrahigh Tensile Strain and Stable Metallic Conductance Enabled by Prestrained Polyelectrolyte Nanoplatforms’, *Adv. Mater.* **2011**, *23*, 3090.

58. Z. L. Liu, H. Y. Hu, B. Yu, M. A. Chen, Z. J. Zheng, F. Zhou, ‘Binary Oppositely Charged Polyelectrolyte Brushes for Highly Selective Electroless Deposition of Bimetallic Patterns’, *Electrochem. Commun.* **2009**, *11*, 492.

59. F. Zhou, Z. J. Zheng, B. Yu, W. Liu, W. T. S. Huck, ‘Multicomponent Polymer Brushes’, *J. Am. Chem. Soc.* **2006**, *128*, 16253.

60. O. Azzaroni, Z. J. Zheng, Z. Q. Yang, W. T. S. Huck, ‘Polyelectrolyte Brushes as Efficient Ultrathin Platforms for Site-Selective Copper Electroless Deposition’, *Langmuir* **2006**, *22*, 6730.

61. X. Q. Liu, H. Chang, W. T. S. Huck, Z. J. Zheng, ‘Polyelectrolyte-Bridged Metal/Cotton Hierarchical Structures for Highly Durable Conductive Yarns’, *ACS Appl. Mater. Interfaces* **2010**, *2*, 529.

62. K. Matyjaszewski, J. Xia, ‘Atom Transfer Radical Polymerization’, *Chem. Rev.* **2001***, 101,* 2921.

63. T. E. Patten, K. Matyjaszewski, ‘Atom Transfer Radical Polymerization and the Synthesis of Polymeric Materials’, *Adv. Mater.* **1998**, *10*, 901.

64. K. Matyjaszewski, T. P. Davis, ‘Handbook of Radical Polymerization’, Wiley-VCH, New York, **2002**.

65. J. Brandrup, D. H. Immergut, ‘Polymer Handbook’, Wiley-VCH, New York, **1989**.

66. G. Moad, D. H. Solomon, ‘The Chemistry of Free Radical Polymerization’, Pergamon, Oxford, **1995**.

67. V. V. Choogin, P. Bandara, E. V. Chepelyuk, ‘Mechanisms of Flat Weaving Technology’, Woodhead Publishing Limited, Cambridge, UK **2013**.

68. B. K. Behera, P. K. Hari, ‘Woven Textile Structure: Theory and Applications’, Woodhead Publishing Limited, Cambridge, UK **2010**.

69. K. L. Gandhi, ‘Woven Textiles: Principles, Developments and Applications’, Woodhead Publishing Limited, Cambridge, UK **2012**.

70. S. C. Ray, ‘Fundamentals and Advances in Knitting Technology’, Woodhead Publishing Limited, Cambridge, UK **2012**.

71. S. J. Russell, ‘Handbook of Nonwovens’, Woodhead Publishing Limited, Cambridge, UK **2007**.

72. A. R. Horrocks, S. C. Anand, ‘Handbook of Technical Textiles’, Woodhead Publishing Limited, Cambridge, UK **2000**.

73. B. J. McCarthy, ‘Textiles for Hygiene and Infection Control’, Woodhead Publishing Limited, Cambridge, UK **2011**.

74. V. T. Bartels, ‘Handbook of Medical Textiles’, Woodhead Publishing Limited, Cambridge, UK **2011**.

75. S. C. Anand, J. F. Kennedy, M. Miraftab, S. Rajendran, ‘Medical and Healthcare Textiles’, Woodhead Publishing Limited, Cambridge, UK **2010**.

76. E. Wilusz, ‘Military Textiles’, Woodhead Publishing Limited, Cambridge, UK **2008**.

77. E. Sparks, ‘Advances in Military Textiles and Personal Equipment’, Woodhead Publishing Limited, Cambridge, UK **2012**.

78. D. I. Fotiadis, C. Glaros, A. Likas, ‘Wearable Medical Devices*,* Wiley Encyclopedia of Biomedical Engineering’*,* Wiley-VCH, NY, **2006**.

79. R. F. Service, ‘Electronic Textiles Charge Ahead ‘, *Science* **2003**, *301*, 909.

80. K. Cherenack, L. V. Pieterson, ‘Smart Textiles: Challenges and Opportunities’, *J. Appl. Phys.* **2012**, *112*, 091301.

81. E. R. Post, M. Orth, P. R. Russo, N. Gershenfeld, ‘E-broidery: Design and Fabrication of Textile-Based Computing’, *IBM Syst. J.* **2000**, *39*, 840.

82. C. Gopalsamy, S. Park, R. Rajamanickam, S. Jayaraman, ‘The Wearable Motherboard™: The first generation of adaptive and responsive textile structures (ARTS) for medical applications’, *Virtual Reality* **1999**, *4*, 152.

83. S. Park, K. Mackenzie, S. Jayaraman, ‘The Wearable Motherboard: A Framework for Personalized Mobile Information Processing (PMIP)’, Proceeding DAC '02 Proceedings of the 39th annual Design Automation Conference, 170.

84. F. Carpi, D. De Rossi, ‘Electroactive Polymer-Based Devices for E-Textiles in Biomedicine’, *IEEE Trans. Inform. Technol. Biomed.* **2005**, *9*, 295.

85. D. Tao, Q. Feng, D. Gao, L. Pan, Q. Wei, D. Wang, ‘Surface Functionalization of Polypropylene Nonwovens by Metallic Deposition’, *J. Appl. Polym. Sci.* **2010**, *117*, 1624.

86. S. Park, Y. Lee, B. S. Kim, I. S. Kim, ‘Thermal Insulation Property of Cu-Metallized Nanofibers’, *Adv. Polym. Technol.* **2012**, *31*, 1.

87. R. H. Guo, S. X. Jiang, Y. D. Zheng, J. W. Lan, ‘Electroless Nickel Deposition of A Palladium-Activated Self-Assembled Monolayer on Polyester Fabric’, *J. Appl. Polym. Sci.* **2013**, *127*, 4186.

88. T. Yuranova, A. G. Rincon, A. Bozzi, S. Parra, C. Pulgarin, P. Albers, J. Kiwi, ‘Antibacterial Textiles Prepared by RF-Plasma and Vacuum-UV Mediated Deposition of Silver’, *J. Photochem. Photobiol. A* **2003**, *161*, 27.

89. H. Zhang, X. Zou, J. Liang, X. Ma, Z. Tang, J. Sun, ‘Development of Electroless Silver Plating on Para-Aramid Fibers and Growth Morphology of Silver Deposits’, *J. Appl. Polym. Sci.* **2012**, *124*, 3363.

90. L. Li, D. Yu, L. Wang, W. Wang, ‘Electroless Silver Plating on the PET Fabrics Modified with 3-Mercaptopropyltriethoxysilane’, *J. Appl. Polym. Sci.* **2012**, *124*, 1912.

91. N. A. Clayton, K. S. Kappagantula, M. L. Pantoya, S. C. Kettwich, S. T. Iacono, ‘Fabrication, Characterization, and Energetic Properties of Metallized Fibers *‘, ACS Appl. Mater. Interfaces* **2014***, 6, 6049.*

92. E. Han, Y. Wang, X. Chen, G. Shang, W. Yu, H. Niu, S. Qi, D. Wu, R. Jin, ‘Consecutive Large-Scale Fabrication of Surface-Silvered Polyimide Fibers via an Integrated Direct Ion-Exchange Self-Metallization Strategy’, *ACS Appl. Mater. Interfaces* **2013**, *5*, 4293.

93. B. K. Little, Y. Li, V. Cammarata, R. Broughton, G. Mills, ‘Metallization of Kevlar Fibers with Gold’, *ACS Appl. Mater. Interfaces* **2011**, *3*, 1965.

94. K Lai, R. Sun, M. Chen, H. Wu, A. Zha, ‘Electromagnetic Shielding Effectiveness of Fabrics with Metallized Polyester Filaments’, *Text. Res. J.* **2007**, *77*, 242.

95. D. Depla, S. Segers, W. Leroy, T. V. Hove, M. V. Parys, ‘Smart Textiles: An Explorative Study of the Use of Magnetron Sputter Deposition’, *Text. Res. J.* **2011**, *81*, 1808.

96. Q. Wei, L. Yu, N. Wu, S. Hong, ’Preparation and Characterization of Copper Nanocomposite Textiles’, *J. Ind. Text.* **2008**, *37*, 275.

97. B. Kalanyan, C. J. Oldham, W. J. Sweet III, G. N. Parsons, ‘Highly Conductive and Flexible Nylon-6 Nonwoven Fiber Mats Formed using Tungsten Atomic Layer Deposition’, *ACS Appl. Mater. Interfaces* **2013**, *5*, 5253.

98. J. S. Jur, W. J. Sweet III, C. J. Oldham, G. N. Parsons, ‘Atomic Layer Deposition of Conductive Coatings on Cotton, Paper, and Synthetic Fibers: Conductivity Analysis and Functional Chemical Sensing Using “All-Fiber” Capacitors’, *Adv. Funct. Mater.* **2011**, *21*, 1993.

99. W. J. Sweet III, C. J. Oldham, G. N. Parsons, ‘Atomic Layer Deposition of Metal Oxide Patterns on Nonwoven Fiber Mats using Localized Physical Compression’, *ACS Appl. Mater. Interfaces* **2014**, *6*, 9280.

100. R. Schumacher, J. J. Pesek, O. R. Melroy,’ Kinetic Analysis of Electroless Deposition of Copper’, *J. Phys. Chem.* **1985**, *89*, 4338.

101. G. O. Mallory, J. B. Hajdu, ‘Electroless Plating: Fundamentals and Applications’, American Electroplaters and Surface Finishers Society, Orlando, FL **1990**.

102. M. Schlesinger, M. Paunovic, ‘Modern Electroplating’, Wiley-VCH, NY **2011**.

103. Y. Lu, Q. Liang, L. Xue, ‘Palladium-free Catalytic Electroless Copper Deposition on Bamboo Fabric: Preparation, Morphology and Electromagnetic Properties’, *Appl. Surf. Sci.* **2012**, *258*, 4782.

104. H. M. Lee, S. Y. Choi, A. Jung, S. H. Ko, ‘Highly Conductive Aluminum Textile and Paper for Flexible and Wearable Electronics’, *Angew. Chem. Int. Ed.* **2013**, *52*, 7718.

105. M. Montazer, V. Allahyarzadeh, ‘Electroless Plating of Silver Nanoparticles/Nanolayer on Polyester Fabric using $AgNO_3$/NaOH and Ammonia’, *Ind. Eng. Chem. Res.* **2013**, *52*, 8436.

106. W. Wang, R. Li, M. Tian, L. Liu, H. Zou, X. Zhao, L. Zhang, ‘Surface Silverized Meta-Aramid Fibers Prepared by Bio-inspired Poly(dopamine) Functionalization’, *ACS Appl. Mater. Interfaces* **2013**, *5*, 2062.

107. B. Hu, D. Li, O. Ala, P. Manandhar, Q. Fan, D. Kasilingam, P. D. Calvert, ‘Textile-based Flexible Electroluminescent Devices’, *Adv. Funct. Mater.* **2011**, *21*, 305.

108. S. H. Aboutalebi, R. Jalili, D. Esrafilzadeh, M. Salari, Z. Gholamvand, S. A. Yamini, K. Konstantinov, R. L. Shepherd, J. Chen, S. E. Moulton, P. C. Innis, A. I. Minett, J. M. Razal, G. G. Wallace, ‘High-Performance Multifunctional Graphene Yarns: Toward Wearable All-Carbon Energy Storage Textiles’, *ACS Nano* **2014**, *8*, 2456.

109. J. B. Lee and V. Subramanian, *Electron Devices Meeting* **2003**, IEDM '03 Technical Digest, IEEE International, 8.3.1.

110. M. Hamedi, L. Herlogsson, X. Crispin, R. Marcilla, M. Berggren, O. Inganäs, 'Fiber-embedded Electrolyte-gated Field-effect Transistors for E-Textiles', *Adv. Mater.* **2009**, *21*, 573.

111. C. Müller*,* M. Hamedi*,* R. Karlsson*,* R. Jansson*,* R. Marcilla*,* M. Hedhammar*,* O. Inganäs*, ' Woven Electrochemical Transistors on Silk Fibers', Adv. Mater.* **2011***, 23, 898.*

112. K. Malzahn, J. R. Windmiller, G. Valdes-Ramirez, M. J. Shoning, J. Wang, 'Wearable Electrochemical Sensors for in-situ Analysis in Marine Environments', *Analyst* **2011**, *136*, 2912.

113. J. R. Windmiller, A. J. Bandodkar, S. Parkhomovsky, J. Wang, 'Stamp Transfer Electrodes for Electrochemical Sensing on Non-planar and Oversized Surfaces', *Analyst* **2012**, *137*, 1570.

114. L. Viry, A. Levi, M. Totaro, A. Mondini, V. Mattoli, B. Mazzolai, L. Beccai, 'Flexible Three-Axial Force Sensor for Soft and Highly Sensitive Artificial Touch', *Adv. Mater.* **2014**, *26*, 2659.

115. J. Lee, H. Kwon, J. Seo, S. Shin, J. H. Koo, C. Pang, S. Son, J. H. Kim, Y. H. Jang, D. E. Kim, T. Lee, 'Conductive Fiber-Based Ultrasensitive Textile Pressure Sensor for Wearable Electronics', *Adv. Mater.* **2015**, *27*, 2433.

116. Y. Meng, Y. Zhao, C. Hu, H. Cheng, Y. Hu, Z. Zhang, G. Shi, L. Qu, 'All-Graphene Core-Sheath Microfibers for All-Solid-State, Stretchable Fibriform Supercapacitors and Wearable Electronic Textiles', *Adv. Mater.* **2013**, *25*, 2326.

117. Y. H. Lee, J. S. Kim, J. Noh, I. Lee, H. J. Kim, S. Choi, J. Seo, S. Jeon, T. S. Kim , J. Y. Lee, J. W. Choi, 'Wearable Textile Battery Rechargeable by Solar Energy', *Nano Lett.* **2013**, *13*, 5753.

118. L. Liu, Y. Yu, C. Yan, K. Li, Z. Zheng, ‘Wearable Energy-dense and Power-dense Supercapacitor Yarns Enabled by Scalable Graphene-Metallic Textile Composite Electrodes’, *Nature Communications* **2015**, *6*, 7260.

119. F. Fan, Z. Tian, Z. L. Wang, ‘Flexible Triboelectric Generator’, *Nano Energy* **2012**, *1*, 328.

120. J. Zhong, Y. Zhang, Q. Zhong, Q. Hu, B. Hu, Z. L. Wang, J. Zhou, ‘Fiber-Based Generator for Wearable Electronics and Mobile Medication’, *ACS Nano* **2014**, *8*, 6273.

121. A. Ulman, ‘Formation and Structure of Self-Assembled Monolayers’, *Chem. Rev.* **1996**, *96*, 1533.

122. W. C. Bigelow, D. L. Pickett, W. A. Zisman, ‘Oleophobic Monolayers: I. Films Adsorbed from Solution in Non-polar Liquids’, *J. Colloid Interface Sci.* **1946**, *1*, 513.

123. R. G. Nuzzo and D. L. Allara, ‘Adsorption of Bifunctional Organic Disulfides on Gold Surfaces’, *J. Am. Chem. Soc.* **1983**, *105*, 4481.

124. P. Silberzan, L. Leger, D. Ausserre, J. J. Benattar, ‘Silanation of Silica Surfaces. A New Method of Constructing Pure or Mixed Monolayers’, *Langmuir* **1991**, *7*, 1647.

125. J. B. Brzoska, I. Benazouz, F. Rondelez, ‘Silanization of Solid Substrates: A Step toward Reproducibility’ *Langmuir* **1994**, *10*, 4367.

126. M. E. McGovern, K. M. R. Kallury, M. Thompson, ‘Role of Solvent on the Silanization of Glass with Octadecyltrichlorosilane’, *Langmuir* **1994**, *10*, 3607.

127. M. L. Hair, C. P. Tripp, ‘Alkylchlorosilane Reactions at the Silica Surface’, *Colloids Surf. A* **1995**, *105*, 95.

128. B. Lee, Y. Chen, F. Duerr, D. Mastrogiovanni, E. Garfunkel, E. Y. Andrei, V. Podzorov, ‘Modification of Electronic Properties of Graphene with Self-Assembled Monolayers’, *Nano Lett.* **2010**, *10*, 2427.

129. S. A. DiBenedetto, A. Facchetti, M. A. Ratner, T. J. Marks, ‘Molecular Self-Assembled Monolayers and Multilayers for Organic and Unconventional Inorganic Thin-Film Transistor Applications’, *Adv. Mater.* **2009**, *21*, 1407.

130. S. Kobayashi, T. Nishikawa, T. Takenobu, S. Mori, T. Shimoda, T. Mitani, H. Shimotani, N. Yoshimoto, S. Ogawa, Y. Iwasa, ‘Control of Carrier Density by Self-Assembled Monolayers in Organic Field-Effect Transistors’, *Nat. Mater.* **2004**, *3*, 317.

131. J. Takeya, T. Nishikawa, T. Takenobu, S. Kobayashi, Y. Iwasa, T. Mitani, C. Goldmann, C. Krellner, B. Batlogg, ‘Effects of Polarized Organosilane Self-Assembled Monolayers on Organic Single-Crystal Field-Effect Transistors’, *Appl. Phys. Lett.* **2004**, *85*, 5078.

132. I. H. Campbell, J. D. Kress, R. L. Martin, D. L. Smith, N. N. Barashkov, J. P. Ferraris, ‘Controlling Charge Injection in Organic Electronic Devices Using Self-Assembled Monolayers’, *Appl. Phys. Lett.* **1997**, *71*, 3528.

133. S. Li, S. Zhang, X. Wang, ‘Fabrication of Superhydrophobic Cellulose-Based Materials through a Solution-Immersion Process’ *Langmuir*, **2008**, *24*, 5585.

134. R. Guo, Y. Li, J. Lan, S. Jiang, T. Liu, W. Yan, ‘Microwave-Assisted Synthesis of Silver Nanoparticles on Cotton Fabric Modified with 3-Aminopropyltrimethoxysilane’, *J. Appl. Polym. Sci.* **2013**, *130*, 3862.

135. R. Barbey, L. Lavanant, D. Paripovic, N. Schüwer, C. Sugnaux, S. Tugulu, H. A. Klok, ‘Polymer Brushes via Surface-Initiated Controlled Radical Polymerization: Synthesis, Characterization, Properties, and Applications’, *Chem. Rev.* **2009**, *109*, 5437.

136. S. T. Milner, ‘Polymer Brushes’, *Science* **1991**, *251*, 905.

137. W. J. Brittain, S. Minko, ‘A Structural Definition of Polymer Brushes’, *J. Polym. Sci. A Polym. Chem.* **2007**, *45*, 3505.

138. X. Huang and M. J. Wirth, ‘Surface-Initiated Radical Polymerization on Porous Silica’, *Anal. Chem.* **1997**, *69*, 4577.

139. M. Ejaz, S. Yamamoto, K. Ohno, Y. Tsujii, T. Fukuda, ‘Controlled Graft Polymerization of Methyl Methacrylate on Silicon Substrate by the Combined Use of the Langmuir−Blodgett and Atom Transfer Radical Polymerization Techniques’, *Macromolecules* **1998**, *31*, 5934.

140. O. Prucker and J. Rühe, ‘Polymer Layers through Self-Assembled Monolayers of Initiators’, *Langmuir* **1998**, *14*, 6893.

141. M. Biesalski and J. Rühe, ‘Preparation and Characterization of a Polyelectrolyte Monolayer Covalently Attached to a Planar Solid Surface’, *Macromolecules* **1999**, *32*, 2309.

142. B. Peng, D. Johannsmann, J. Rühe, ‘Polymer Brushes with Liquid Crystalline Side Chains’, *Macromolecules* **1999**, *32*, 6759.

143. W. X. Huang, G. Skanth, G. L. Baker, M. L. Bruening, ‘Surface-Initiated Thermal Radical Polymerization on Gold’, *Langmuir* **2001**, *17*, 1731.

144. W. Cui, D. Wu, W. C. Wang , L. Zhang, B. Cao, R. Jin, ‘Surface-Silvered Polyimide Films Prepared by Plasma-Induced Grafting of Viologen and Electroless Plating’, *Surf. Coat. Technol.* **2009**, *203*, 1885.

145. A. Garcia, T. Berthelot, P. Viel, J. Polesel-Maris, S. Palacin, ‘Microscopic Study of a Ligand Induced Electroless Plating Process onto Polymers’, *ACS Appl. Mater. Interfaces* **2010**, *2*, 3043.

146. A. Garcia, J. Polesel-Maris, P. Viel, S. Palacin, T. Berthelot, ‘Localized Ligand Induced Electroless Plating (LIEP) Process for the Fabrication of Copper Patterns Onto Flexible Polymer Substrates’, *Adv. Funct. Mater.* **2011**, *21*, 2096.

147. B. Zdyrko and I. Luzinov, ‘Polymer Brushes by the “Grafting To” Method’, *Macromol. Rapid Commun.* **2011**, *32*, 859.

148. S. Edmondson, V. L. Osborne, W. T. S. Huck, ‘Polymer Brushes via Surface-Initiated Polymerizations’, *Chem. Soc. Rev.* **2004**, *33*, 14.

149. W. Sun, S. Zhou, B. You, L. Wu, ‘Polymer Brush-Functionalized Surfaces with Reversible, Precisely Controllable Two-Way Responsive Wettability’, *Macromolecules* **2013**, *46*, 7018.

150. T. Masuda, M. Hidaka, Y. Murase, A. M. Akimoto, K. Nagase, T. Okano, R. Yoshida, ‘Self-Oscillating Polymer Brushes’, *Angew. Chem.* **2013**, *125*, 7616.

151. A. Carlmark and E. Malmström, ‘Atom Transfer Radical Polymerization from Cellulose Fibers at Ambient Temperature’, *J. Am. Chem. Soc.* **2002**, *124*, 900.

152. C. H. Xue, X. J. Guo, J. Z. Ma, S. T. Jia, ‘Fabrication of Robust and Antifouling Superhydrophobic Surfaces via Surface-Initiated Atom Transfer Radical Polymerization’, *ACS Appl. Mater. Interfaces* **2015**, *7*, 8251.

153. S. Jung, J. Lee, T. Hyeon, M. Lee, D. H. Kim, ‘Fabric-Based Integrated Energy Devices for Wearable Activity Monitors’, *Adv. Mater.* **2014**, *26*, 6329.

154. S. Wang, L. Lin, Z. L. Wang, ‘Nanoscale Triboelectric-Effect-Enabled Energy Conversion for Sustainably Powering Portable Electronics’, *Nano Lett.* **2012**, *12*, 6339.

155. P. Bai, G. Zhu, X. H. Lin, Q. Jing, J. Chen, G. Zhang, J. Ma, Z. L. Wang, ‘Integrated Multilayered Triboelectric Nanogenerator for Harvesting Biomechanical Energy from Human Motions’, *ACS Nano* **2013**, *7*, 3713.

156. F. R. Fan, J. Luo, W. Tang, C. Li, C. Zhang, Z. Tian, Z. L. Wang, ‘Highly Transparent and Flexible Triboelectric Nanogenerators: Performance Improvements and Fundamental Mechanisms’, *J. Mater. Chem. A* **2014**, *2*, 13219.

157. H. Zhang, Y. Yang, T. C. Hou, Y. Su, C. Hu, Z. L. Wang, ‘Triboelectric Nanogenerator Built Inside Clothes for Self-Powered Glucose Biosensors’, *Nano Energy* **2013**, *2*, 1019.

158. S. Wang, Y. Xie, S. Niu, L. Lin, Z. L. Wang, ‘Freestanding Triboelectric-Layer-Based Nanogenerators for Harvesting Energy from a Moving Object or Human Motion in Contact and Non-Contact Modes’, *Adv. Mater.* **2014**, *26*, 2818.

159. Y. Xie, S. Wang, S. Niu, L. Lin, Q. Jing, J. Yang, Z. Wu, Z. L. Wang, ‘Grating-Structured Freestanding Triboelectric-Layer Nanogenerator for Harvesting Mechanical Energy at 85% Total Conversion Efficiency’, *Adv. Mater.* **2014**, *26*, 6599.

160. Q. Jing, G. Zhu, P. Bai, Y. Xie, J. Chen, R. P. S. Han, Z. L. Wang, ‘Case-Encapsulated Triboelectric Nanogenerator for Harvesting Energy from Reciprocating Sliding Motion’, *ACS Nano* **2014**, *8*, 3836.

161. S. Kim, M. K. Gupta, K. Y. Lee, A. Sohn, T. Y. Kim, K. S. Shin, D. Kim, S. K. Kim, K. H. Lee, H. J. Shin, D. W. Kim, S. W. Kim, ‘Transparent Flexible Graphene Triboelectric Nanogenerators’, *Adv. Mater.* **2014**, *26*, 3918.

162. K. Y. Lee, J. Chun, J. H. Lee, K. N. Kim, N. R. Kang, J. Y. Kim, M. H. Kim, K. S. Shin, M. J. Gupta, J. M. Baik, S. W. Kim, ‘Hydrophobic Sponge Structure-Based Triboelectric Nanogenerator’, *Adv. Mater.* **2014**, *26*, 5037.

163. H. Zhang, Y. Yang, Y. Su, J. Chen, K. Adams, S. Lee, C. Hu, Z. L. Wang, ‘Triboelectric Nanogenerator for Harvesting Vibration Energy in Full Space and as Self-Powered Acceleration Sensor’, *Adv. Mater.* **2014**, *24*, 1401.

164. S. Lee, W. Ko, Y. Oh, J. Lee, G. Baek, Y. Lee, J. Sohn, S. Cha, J. Kim, J. Park, J. Hong, ‘Triboelectric Energy Harvester Based on Wearable Textile Platforms Employing Various Surface Morphologies’, *Nano Energy* **2015**, *12*, 410.

165. M. Ha, J. Park, Y. Lee, H. Ko, ‘Triboelectric Generators and Sensors for Self-Powered Wearable Electronics’, *ACS Nano* **2015**, *9*, 3421.

166. X. Pu, L. Li, H. Song, C. Du, Z. Zhao, C. Jiang, G. Cao, W. Hu, Z. L. Wang, ‘A Self-Charging Power Unit by Integration of a Textile Triboelectric Nanogenerator and a Flexible Lithium-Ion Battery for Wearable Electronics’, *Adv. Mater.* **2015**, *27*, 2472.

167. A. F. Diaz, R. M. Felix-Navarro, ‘A Semi-Quantitative Tribo-Electric Series for Polymeric Materials: The Influence of Chemical Structure and Properties’, *J. Electrostat.* **2004**, *62*, 277.

168. E. Pyun, R. J. Mathisen, C. S. P. Sung, ‘Kinetics and Mechanisms of Thermal Imidization of A Polyamic Acid Studied by Ultraviolet-Visible Spectroscopy’, *Macromolecules* **1989**, *22*, 1174.

169. S. Y. Zhang, G. Guan, S. Jiang, H. Guo, J. Xia, M. D. Regulacio, M. Wu, K. W. Shah, Z. Dong, J. Zhang, M. Y. Han, ‘Rapid Copper Metallization of Textile Materials: A Controlled Two-Step Route to Achieve User-Defined Patterns under Ambient Conditions’, *ACS Appl. Mater. Interfaces* **2015**, *7*, 21545.

170. D. Zabetakis, M. Dinderman, P. Schoen, ‘Metal-Coated Cellulose Fibers for Use in Composites Applicable to Microwave Technology’, *Adv. Mater.* **2005**, *17*, 734.

171. S. Ma, L. Liu, V. Bromberg, T. J. Singler, ‘Electroless Copper Plating of Inkjet-Printed Polydopamine Nanoparticles: A Facile Method to Fabricate Highly Conductive Patterns at Near Room Temperature’, *ACS Appl. Mater. Interfaces* **2014**, *6*, 19494.

172. Y. C. Liao and Z. K. Kao, ‘Direct Writing Patterns for Electroless Plated Copper Thin Film on Plastic Substrates’, *ACS Appl. Mater. Interfaces* **2012**, *4*, 5109.

173. D. Zabetakis and W. J. Dressick, ‘Statistical Analysis of Plating Variable Effects on the Electrical Conductivity of Electroless Copper Patterns on Paper’, *ACS Appl. Mater. Interfaces* **2012**, *4*, 2358.

174. S. Han, S. Hong, J. Yeo, D. Kim, B. Kang, M. Y. Yang, S. H. Ko, ‘Nanorecycling: Monolithic Integration of Copper and Copper Oxide Nanowire Network Electrode through Selective Reversible Photothermochemical Reduction’, *Adv. Mater.* **2015**, DOI: 10.1002/adma.201503244.

175. R. C. Advincula, W. J. Brittain, K. C. Caster, J. Rühe, ‘Polymer Brushes’, Wiley-VCH, Germany **2004**.

176. J. Pyun, T. Kowalewski and K. Matyjaszewski, ‘Synthesis of Polymer Brushes Using Atom Transfer Radical Polymerization’, *Macromol. Rapid Commun.* **2003**, *24*, 1043.

177. W. Senaratne, L. Andruzzi, C. K. Ober, ‘Self-Assembled Monolayers and Polymer Brushes in Biotechnology: Current Applications and Future Perspectives’, *Biomacromolecules* **2005**, *6*, 2427.

178. S. Minko, S. Patil, V, Datsyuk, F. Simon, K. J. Eichhorn, M. Motornov, D. Usov, I. Tokarev, M. Stamm, ‘Synthesis of Adaptive Polymer Brushes via “Grafting To” Approach from Melt’, *Langmuir* **2002**, *18*, 289.

179. O Azzaroni, ‘Polymer Brushes Here, There, and Everywhere: Recent Advances in their Practical Applications and Emerging Opportunities in Multiple Research Fields’, *J. Polym. Sci. A Polym. Chem.* **2012**, *50*, 3225.

180. W. Seung, M. K. Gupta, K. Y. Lee, K. S. Shin, J. H. Lee, T. Y. Kim, S. Kim, J. Lin, J. H. Kim, S. W. Kim, 'Nanopatterned Textile-Based Wearable Triboelectric Nanogenerator', *ACS Nano* **2015**, *9*, 3501.

181. T. Zhou, C. Zhang, C. B. Han, F. R. Fan, W. Tang, Z. L. Wang, 'Woven Structured Triboelectric Nanogenerator for Wearable Devices', *ACS Appl. Mater. Interfaces* **2014**, *6*, 14695.

182. A. M. Hussain, F. A. Ghaffar, S. I. Park, J. A. Rogers, A. Shamim, M. M. Hussain, 'Metal/Polymer Based Stretchable Antenna for Constant Frequency Far-Field Communication in Wearable Electronics', *Adv. Funct. Mater.* **2015**, DOI: 10.1002/adfm.201503277.